Alma Mater Studiorum – Università di Bologna

DOTTORATO DI RICERCA IN

SCIENZE CHIMICHE

Ciclo XXV

Settore Concorsuale di afferenza: 03/B1

Settore Scientifico disciplinare: CHIM/03

BIODEGRADABLE SYSTEMS FOR THE DEVELOPMENT OF FUNCTIONAL MATERIALS

Presentata da: Michela Gioffrè

Coordinatore Dottorato **Relatore**

Chiar.ma Prof.ssa Adriana Bigi **Chiar.ma Prof.ssa Adriana Bigi**

Esame finale anno 2013

Table of contents

Abstract

This PhD work was aimed to design, develop, and characterize gelatin-based scaffolds, for the repair of defects in the muscle-skeletal system.
Gelatin is a biopolymer widely used for pharmaceutical and medical applications, thanks to its biodegradability and biocompatibility. It is obtained from collagen via thermal denaturation or chemical-physical degradation. Despite its high potential as biomaterial, gelatin exhibits poor mechanical properties and a low resistance in aqueous environment. Crosslinking treatment and enrichment with reinforcement materials are thus required for biomedical applications.
In this work, gelatin based scaffolds were prepared following three different strategies: films were prepared through the *solvent casting method, electrospinning* technique was applied for the preparation of porous mats, and 3D porous scaffolds were prepared through *freeze-drying*.
The results obtained on films put into evidence the influence of pH, crosslinking and reinforcement with montmorillonite (MMT), on the structure, stability and mechanical properties of gelatin and MMT/gelatin composites. The information acquired on the effect of crosslinking in different conditions was utilized to optimize the preparation procedure of electrospun and freeze-dried scaffolds.
A successful method was developed to prepare gelatin nanofibrous scaffolds electrospun from acetic acid/water solution and stabilized with a non-toxic crosslinking agent, genipin, able to preserve their original morphology after exposure to water. Moreover, the *co-electrospinning* technique was used to prepare nanofibrous scaffolds at variable content of gelatin and polylactic acid. Preliminary *in vitro* tests indicated that the scaffolds are suitable for cartilage tissue engineering, and that their potential applications can be extended to cartilage-bone interface tissue engineering.
Finally, 3D porous gelatin scaffolds, enriched with calcium phosphate, were prepared with the *freeze-drying* method. The results indicated that the crystallinity of the inorganic phase influences porosity, interconnectivity and mechanical properties. Preliminary *in vitro* tests show good osteoblast response in terms of proliferation and adhesion on all the scaffolds.

Chapter I

Introduction

1.1 Tissue engineering and regenerative medicine in muscle-skeletal tissue

Tissue engineering (TE) is an interdisciplinary science that applies the principles of engineering and life sciences towards the design and construction, in the laboratory, of functional tissues intended for the maintenance, regeneration or replacement of malfunctioning organs (Langer et al., 1993; Nerem et al., 1992).
TE involves the development of a well-defined three-dimensional (3D) scaffold, the seeding of appropriate cells into it and the culturing of the resulting construct in a bioreactor under conditions that promote cell and tissue growth (Guillot et al., 2007). Tissue-engineered constructs should be designed properly to interface with natural tissues from a structural, mechanical, and bio-functional point of view. They must provide a suitable surface chemistry for cell attachment, proliferation and differentiation, and, once implanted, they must support the tissue regeneration process. The term "regenerative medicine" (RM) came into vogue in the mid 1990s, with the development of stem cells technology. Regenerative medicine is aimed to repair, replace, or regenerate tissues and organs damaged by injury or disease. It involves cell therapy, whose main strategy is focused on the extraordinary potential of the stem cells, and tissue engineering. TE and RM are widely applied to the muscle-skeletal system, which can be affected by several problems, including degenerative, surgical, and traumatic processes (Cancedda et al., 2007; Sundelacruz and Kaplan, 2009; Temenoff and Mikos, 2000).
Both cartilage and bone are highly structured and hierarchically organized tissues, but they exhibit quite different properties. Cartilage is an avascular tissue with a very low capacity for repair, whereas bone is a highly vascularized tissue with high rate of remodelling.
The reconstruction of bone tissue is necessary in the case of extensive bone loss due to pathological events such as trauma, inflammation, and surgical treatment of tumors. In order to obtain optimal bone regeneration, engineered scaffold structure must have pores, interconnections and a suitable morphology to allow functions and vitality of bone and vascular cells. Moreover, the scaffold must be biodegradable *in situ* in parallel to bone regeneration.
Degeneration of the joint's cartilage can be due to primary osteoarthritis or from trauma causing loss of tissue. Cartilage shows very little tendency for self-repair, its injuries are maintained for years and can eventually lead to further degeneration. Some forms of arthritis and cartilage damage from sports injury are also common.

1.2 Bone and cartilage

Bone

Bone, the structural component of human body, is a composite material constituted of an inorganic (a basic calcium phosphate assimilated to hydroxyapatite) and an organic (collagen) phase. There are two main types of bone, cortical (or compact) and cancellous (trabecular or porous), with quite different shapes and inner structures, depending on their respective functions. The diversity of morphology in bone tissues reflects the fine-tuning and the adaptation of the structure to its function.
Cortical bone is found in long bones (femur, tibia, fibula, etc.) and is usually fairly dense with porosity of the order of 6%, mainly due to the presence of blood vessels. Cancellous bone is definitely more porous with a percentage of porosity of about 80%: it can be considered as a foam-like network of trabecular bone. It is found in the core of bones and in flat bones. The typical thickness of the trabecular bone is about 200 μm (Figure 1).

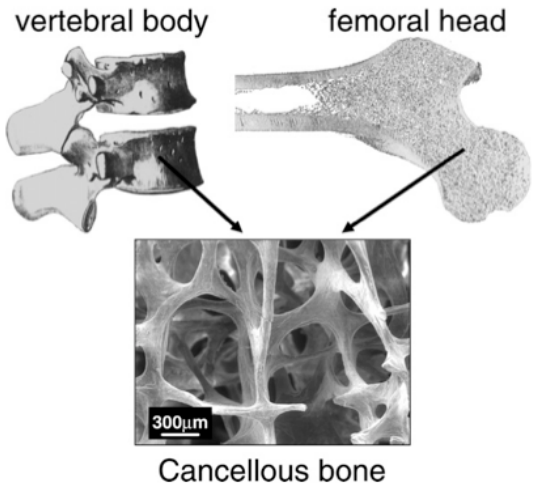

Figure 1. *Spongy structure of some bones or part of them, called trabecular bone (Fratzl et al., 2007).*

The structure of a long bone (Figure 2a) and a cross section of a deer antler (b), are showed in Figure 2. The outer regions consist of cortical bone whilst cancellous bone constitutes the inner regions. The presence of porosity allows to reduce the weight of the bone and antler, even if reduces too their strength. Bones are shaped in such a manner that strength is provided only where it is needed. The mechanical strength is generally determined by the relative amount of cortical and cancellous bone tissue. Porosity and pore distribution modulate the mechanical properties (Meyers et al., 2008).

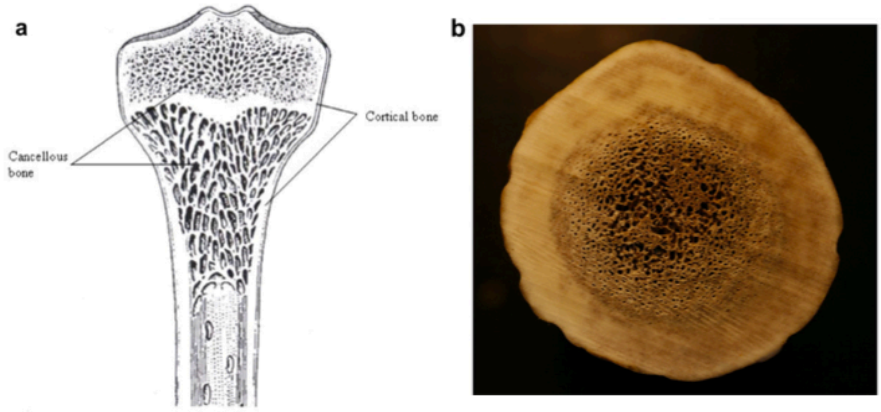

Figure 2. *Structure of a long bone (a) and cross section of a deer antler (b) (Meyers et al., 2008).*

The mechanical properties of bone materials reflect many different variables such as the diversity in structures, the orientation of the specimens and, as mentioned before, the porosity (Weiner and Wagner, 2008).
Bone is a composite of the fibrous protein collagen type I, also present in skin, tendon, and a variety of other soft tissues, and mineral nanoparticles made of carbonated hydroxyapatite. The third major component is water.
These components are intimately associated into an ordered structure, the mineralized collagen fibril, which is the basic building block of bone. Collagen fibril consists of an assembly of 300 nm long and 1.5 nm thick collagen molecules, which are deposited by the osteoblasts (bone forming cells) into the extracellular space and then self-assembled. These collagen fibrils are filled and coated by tiny carbonated hydroxyapatite crystals, mostly arranged parallel to each other and to the long axis of the fibrils. Crystal deposits occur at regular intervals along the fibrils, with an approximate repeat distance of 67 nm, corresponding to the distance by which adjacent collagen molecules are staggered (Figure 3).

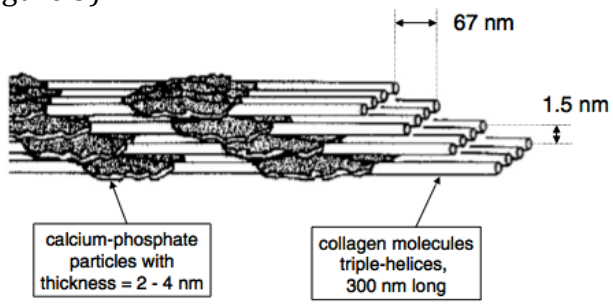

Figure 3. *Structure of collagen fibrils, filled and coated by tiny mineral crystals (Fratzl et al., 2007).*

The relative amounts of organic matrix, inorganic phase and water, as well as the manner in which the building blocks are organized into higher order structures can vary considerably among bone family members.
Figure 4 illustrates the hierarchical organization of bone tissue, which ranges in scale from nanometers to millimeters, and then centimeters (the whole bone). At the first level, hydroxyapatite crystals and non-mineralized collagen fibril are present. Level 2 consists in mineralized collagen fibril whilst level 3 is the fibrils assembly in a superior ordered structure. Bone

tissues display several array patterns of organization, which influence mechanical properties and function (level 4). At level 5, we found the osteons, or Haversian system, which are roughly cylindrical structures. Each osteon is composed of concentric layers of compact bone tissue that surround the central canal (Haversian canal). This canal contains nerve and blood vessels.
Level 6 includes compact and cancellous bone; level 7 is the whole bone (Weiner and Wagner, 2008).

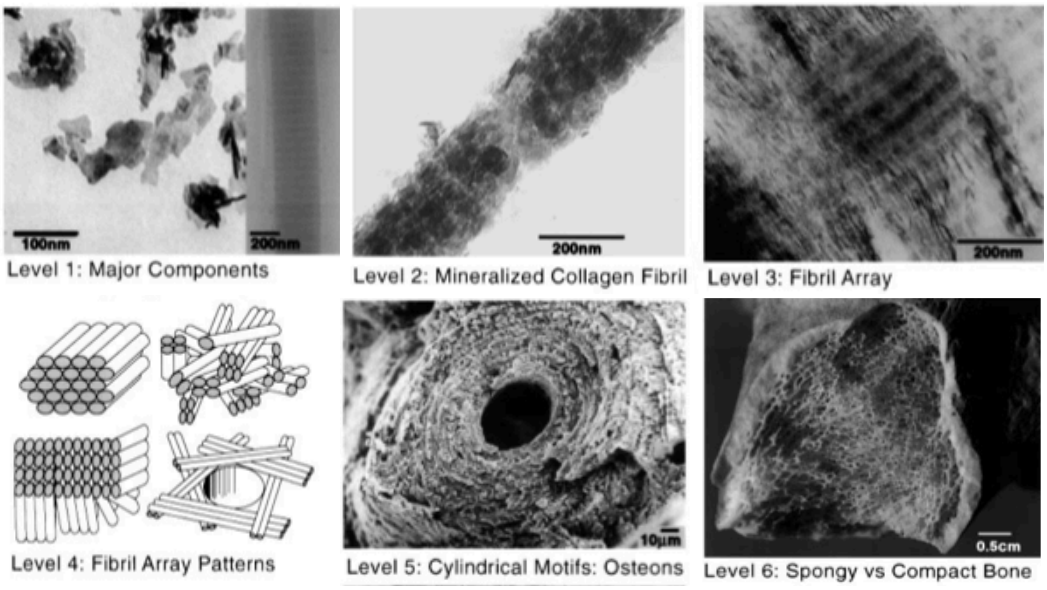

Figure 4. *Hierarchical organization of bone (Weiner and Wagner, 2008).*

Cartilage

Cartilage is a flexible material, belonging to connective tissues, which is found in several areas of the body, including joints, ear, nose and rib cage. Its main function is of support and protection.
Cartilage is composed of cells called chondrocytes, which produce the extracellular matrix macromolecules (ECM), constituted of collagen (that will be further treated in the next section), elastin and proteoglycans.
There are three kinds of cartilage tissue, *fibro-*, *elastic* and *hyaline cartilage*, classified in function of the relative amounts of the protein and non-protein components in ECM. Hyaline cartilage is the only one found in the knee and has a white, glassy appearance, with no macroscopic evidence of fibers, at variance with fibrocartilage. Bones such as femur and tibia are protected with a layer of hyaline cartilage at the joint surface (Figure 1).

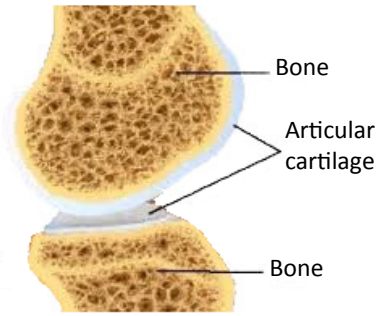

Figure 1. *Layer of hyaline cartilage at the joint surface.*

The synovial membrane surrounds the joint and forms a barrier to retain the synovial fluid in the knee. This fluid provides lubrication and nutrients for the cartilage since no blood vessel penetrates into the tissue from the subchondral bone. For this reason, cartilage grows and repairs more slowly than the other connective tissues. Elastic cartilage is present in the ear and nose and is characterized by the presence of elastin in the extracellular matrix (ECM). Fibrocartilage contains a higher proportion of collagen than hyaline cartilage and it is found at the ends of tendons and ligaments in apposition to bone.

Although chondrocytes represent only a very low percentage of the volume of cartilage (Temenoff et al., 2000), they are essential for the replacement of degraded matrix molecules in order to maintain the correct size and mechanical properties of the tissue. Chondrocytes are believed to modify matrix properties in response to loading. In this way, they play a role in sensing the mechanical environment of the cell.

Proteoglycans are composed of about 95% polysaccharides and about 5% protein, consisting in a protein core to which are attached, through covalent bonds at a serine residue, more varieties of glycosaminoglycan (GAG) chains. The vast majority of proteoglycans found in articular cartilage are known as aggrecans, which bind with hyaluronan to form a large proteoglycan aggregate.

The aggrecans form a strong, porous-permeable, fiber-reinforced composite material with collagen. There are no chemical bonds between the proteoglycans and collagen fibers. The aggregation prevents diffusion of the proteoglycans out of the matrix during joint loading (Figure 2).

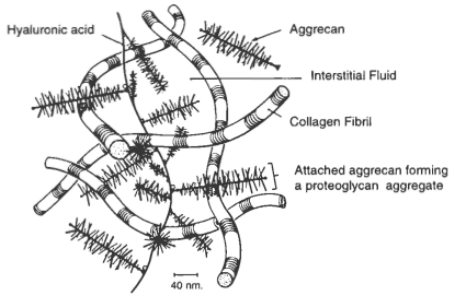

Figure 2. *Articular cartilage extracellular matrix that shows how the collagen network traps the proteoglycan aggregate to form a fiber-reinforced composite (Cohen et al., 1998).*

Proteoglycans contain repeating sulfate and carboxylate groups along their chains, which become negatively charged when placed in an aqueous solution and tend to repel each other and other anions, while attracting cations and facilitating interaction with water. Because of the ability to attract water, aggregans are thought to be responsible for much of the resilience and stress distribution in articular cartilage.
In addition to water, tissue fluid is an essential part of hyaline cartilage, comprising up to 80% of the wet weight of the tissue. In this fluid, gases, metabolites and a large amount of cations are present to balance the negatively charged macromolecules in the ECM. The entrapment of this fluid through interactions with the components of ECM makes the cartilage tissue able to resist compression and return to normal shape after deformation. Moreover, the exchange of this fluid with the synovial fluid provides nutrients and oxygen to the avascular cartilage.
In articular cartilage, a viscoelastic behavior observed. When it is loaded under compression, articular cartilage undergoes a volumetric change, causing a pressure change in the tissue and results in the flow of interstitial fluid through the porous extracellular matrix. The flow causes the generation of a significant frictional resistance within the tissue, which is the primary determinant of the viscoelastic behavior seen in cartilage.
Three distinct zones are individuated in articular cartilage tissue, in which collagen present different orientations: the superficial zone, the transitional or middle zone and the deep zone.

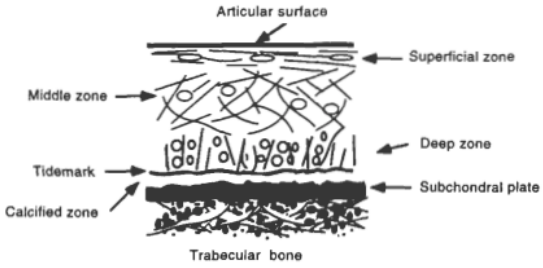

Figure 3. *Organization of articular cartilage (Cohen et al., 1998).*

As showed in Figure 3, in the superficial zone, the collagen fibrils are arranged in a parallel way to the surface. In the deep zone, on the contrary, the fibrils are perpendicular to the surface of the joint. In the middle zone, the collagen fibril orientation is generally less organized. The tidemark delineates the boundary between the deep zone and the zone of calcified cartilage, which is the closer to bone tissue (Cohen et al., 1998).
The most common injuries in articular cartilage involve matrix disruption and partial or full thickness defects. The first case usually occurs from a blunt trauma and implies damage of the ECM. If the injury is not extreme, the chondrocytes that are still viable increase their synthetic activity to repair the damaged tissue. Full thickness defects arise from damage that transverses the entire cartilage tissue and penetrates until the subchondral bone. In this case, the defect is filled with a fibrin clot and a classic wound healing response ensues. When an only partially damage occurs, defects demonstrate disruption of the cartilage surface but this does not extend to the subchondral bone.

1.2.1 Collagen

Collagen is one of the most abundant protein components present in living organisms and it is principally located in connective tissues such as skin, tendons, bones, cartilage, blood vessels, and ligaments (Malafaya et al., 2007; Kretlow and Mikos, 2008; Ma, 2008; Chen et al., 2006; Sung et al., 1999; Tiktopulo and Kajava, 1998). This protein is regarded as an ideal scaffold or matrix for tissue engineering thanks to its natural abundance and properties such as high mechanical strength, good biocompatibility and tailored biodegradation. Collagen is composed by structural macromolecules that include one or several domains having a characteristic triple helical conformation (Sionkowska and Kaminska, 1999). Twenty-seven types of collagens have been identified to date (Malafaya et al., 2007).
Fibrillar collagens (type I, II, III, V and XI) are the most abundant in vertebrate organisms. In particular, type I is present in skin, cornea and it is the main component of tendons and bones. Type V is less abundant than type I but exhibits a similar distribution. Types II and XI are principally located in cartilage and in vitreous humor of eyes, whilst type III is present, often associated to type I, in many tissues such as skin and walls of blood vessels. All tissues mentioned above own evidently different mechanical properties because of the collagen fibrils orientation and the dissimilar chemical composition. The different collagens are first synthesized as large precursor molecules known as procollagens (Kivirikko, 1998). Collagen molecules consist of three polypeptide left-handed chains of glycine-X-Y (Gly-X-Y) amino acid repeats thrown into a right-handed superhelix (Berisio et al., 2002; Pezron et al., 1990). Every chain is composed by about one thousand amino acid residues, where an unusual high percentage, 30%, consists of glycine (Gly). Great amount of proline (Pro) and 4-hydroxyproline (Hyp) are present too. The periodic sequence Gly-X-Y, where X and Y are often Pro and Hyp (Mann, 2001) greatly influences collagen structure. The single polypeptide chain exhibits a left-handed helical conformation (α-helix chain), because of steric hindrance of proline and hydroxyproline rings (Figure 1).

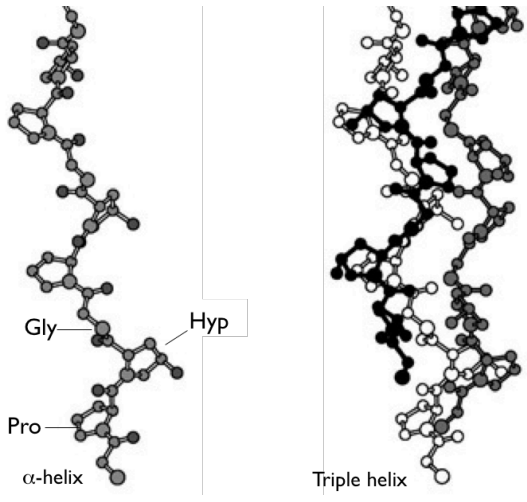

Figure 1. *Left-handed helical conformation of glycine-X-Y chain (α-helix chain). Three polypeptide left-handed chains of Gly-X-Y twined around one another to form triple helices (Triple helix chain).*

Furthermore, the presence of a hydrogen atom as lateral group in glycine residue permits an efficient interaction among chains because of the low steric hindrance. Hydrogen bonds are observed between amino group of glycine and carboxylic groups of Pro and Hyp residues (Shanmugam et al., 2009) (Figure 2).

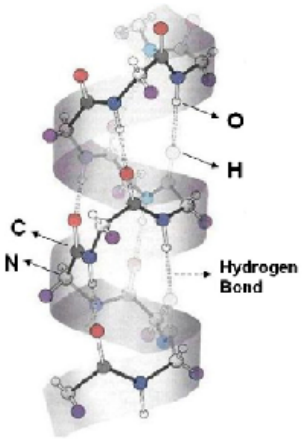

Figure 2. *Hydrogen bonds (dashed line) between amino groups of glycine and carboxylic groups of Pro and Hyp residues (Meyers et al., 2008).*

Hydrogen bonds, both intra and inter molecular, allow the formation of a stable coiled-coil triple helix structure. Moreover, interactions established between OH- group of Hyp and water molecules are fundamental to maintain the natural collagen structure (Bear, 1942; Ellis and Gavin, 1970). At the ends of triple helix, there are two zones known as *telopeptides* in which the sequence Gly-X-Y is no longer respected and no periodic ordered structure is observed. Generally, collagen molecule has a length of about 300 nm and its diameter is about 1.15 nm (Mann, 2001). Collagen molecules assemble in microfibrils and then in fibrils.

Collagen structure

Collagen fibrils have been widely studied by X-ray diffraction technique (Veis, 1964). Wide-angle X-ray diffraction (WXRD) analysis permits a characterization at the level of the molecular structure, while small-angle X-ray diffraction (SXRD) allows studying the structural organization of collagen fibrils (Stainsby, 1958). Wide-angle diffraction pattern of type I collagen exhibits a very clear meridional reflection at a spacing of about 0.29 nm, which is associated to distance among residues along helical chains. The equatorial reflection, at a spacing of 1.45 nm for native fibers and 1.06 nm for dried samples, is related to molecular diameter (Figure 3). Diffraction pattern is in agreement with a pitch of the left-handed helices of about 0.95 nm and the presence of about ten residues per three turns (Miller, 1976).

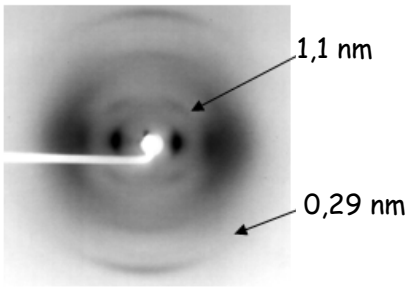

Figure 3. *WXRD pattern of type I collagen. Meridian reflection at 0.29 nm is associated to distance among residues along helical chains and the equatorial reflection (1.45 nm for native fibers and 1.06 nm for dried samples) is related to molecular diameter.*

The structural organization of fibrillar collagen has been described on the basis of small-angle X-ray diffraction analysis and transmission electron microscopy (TEM), carried out on rat tendon. SAXD patterns show several meridian reflections related to D-axial periodicity of collagen fibrils. This periodicity is of about 64 nm, for dry samples, and of about 67 nm, for native samples, and it is due to the peculiar arrangement of collagen molecules. Every molecule, in fact, has a length of approximately 300 nm, corresponding to 4.4D and it is staggered a distance D from its neighbors. In this way, number of intermolecular bonds is optimized and structure stability is reached (Mann, 2001) (Figure 4).

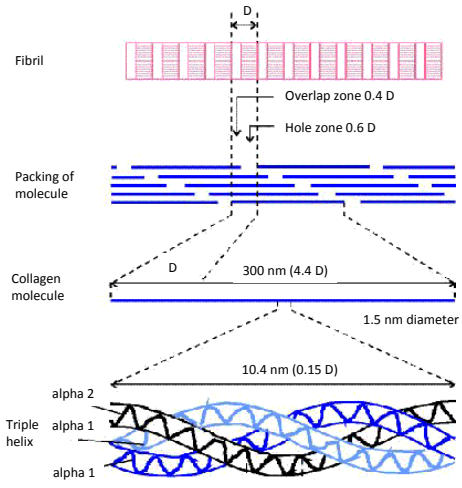

Figure 4. *Collagen molecules are long about 300 nm, defined as well as 4.4D, and staggered of D-distance from each other. The molecules pack in ordered structures (microfibrils) and then in fibrils.*

On TEM image of negatively stained collagen fibrils, this particular structural organization results in the characteristic alternation of dark zones, 0.6D long, and light zones, 0.4D long, which correspond to zones of minor (gap) and major (overlap) electronic density (Viidik and Vuust., 1990) (Figure 5).

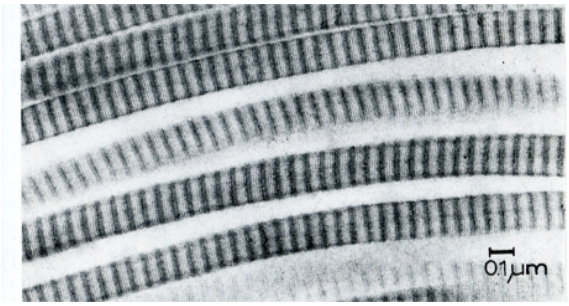

Figure 5. *TEM image of negatively stained collagen fibrils. The fibrils are tightly packed in a parallel array (Viidik and Vuust., 1990).*

Collagen fibrils show a melting point of 60°C. Beyond this temperature, removal of structural water provokes a dramatic contraction of D-periodic distance.
Denaturation of collagen through thermal treatment or chemical process, leads to the destruction of the triple helix into random coiled chain segments. The material with this disordered structure, obtained from collagen denaturation is known as *gelatin*.

1.3 Scaffolds for muscle-skeletal tissue repair

The success of the tissue engineering strategy is principally related to the development of suitable scaffolds that provide the necessary support for cell attachment, mimicking the main features and structure of the extracellular matrix (ECM). Scaffolds should be designed to address the specific functions of ECM, such as acting as cell substrate, supplying nutrition and delivering bioactive molecules (Willie et al., 2010; Panzavolta et al. – *in press*). Hierarchical porous architectures define the mechanical properties of the scaffold as well as the void space that is available for regenerating cells to form new tissues (including new blood vessels) and the pathways for mass transport (Owen and Shoichet, 2010; Mano et al., 2007; Malafaya et al., 2007). Several fabrication methods have been developed to prepare pure or inorganic/organic composite scaffolds, including solvent/solution casting method, electrospinning techniques and thermally induced phase separation (freeze-drying method) (Sun et al., 2011).

Biocompatibility and biodegradability are only two of the main features that engineered scaffolds must have to fulfill biological requirements. The general criteria for selecting suitable materials for scaffolds are to mimic the chemical and mechanical features of ECM, such as the time of degradation, to the needs of the application. The biomaterial must be metabolized in the body after fulfilling its purpose without leaving any trace; it must be non-mutagenic, non-antigenic, non-carcinogenic, non-toxic and non-teratogenic. Scaffolds for application in the skeletal muscle system must allow cartilaginous and bone integration without causing an adverse immunological reaction (Place et al., 2009). The combination of synthetic and natural polymers in a single scaffold is a strategy that allows improving mechanical and degradation properties, as well as biological properties of the scaffold, in comparison with individual components. Synthetic bioresorbable polymers provide structural functionalities to the scaffold, whereas natural polymers display unique bioactive properties and excellent cellular affinity (Torricelli et al. - in press).

Taking into account bone composition, a number of biodegradable polymers – calcium phosphate composite materials have been proposed to develop porous 3D scaffolds. To this aim a number of fabrication techniques, such as porogen leaching, gas foaming, phase separation, fibre meshing, supercritical fluid processing, microsphere sintering, 3D printing, freeze-drying, have been employed (Panzavolta et al. – *in press*).

1.3.1 Gelatin

Gelatin is a natural polymer derived from collagen and consists in amino acidic chains, containing a large number of glycine, proline and 4-hydroxyproline residues (Malafaya et al., 2007). It is commonly used for pharmaceutical and medical applications because of its biodegradability and biocompatibility in physiological environments. At variance with collagen, which shows antigenicity because of its animal origin, gelatin is a denatured material, which does not show antigenicity in physiological environment.

Gelatin is obtained via thermal denaturation or chemical-physical degradation of collagen. These treatments lead to destruction of third,

secondary and, to some degree, primary structure of native collagen macromolecules. This phenomenon mostly concerns breaking non-covalent bonds (van den Bosch and Gielens, 2003). Gelatin can be obtained from collagen extracted from pig or bovine skins, and bones. In recent years, fishes are also used as a good alternative source for collagen (Yang et al., 2008; Muyonga et al., 2004; Gilsenan and Ross-Murphy, 2006; Aewsiri et al., 2008; Badii and Howell, 2006). Different types of gelatin can be produced depending on source and method of extraction.
Key parameters are pH, temperature and time of extraction process. Chemical degradation, for example, provides gelatins with different characteristics as a function of the treatment conditions. Gelatin extracted with acid treatment, Type A gelatin, shows an isoelectric point (IEP) at a pH value in the range 7-9. On the other hand, alkaline-extracted gelatin, Type B gelatin, has an IEP at pH about 5 (Djagny et al., 2001). These differences can be justified on the basis of the hydrolysis process of amino acid groups of collagen chains, which under alkaline treatment leads to a high concentration of carboxylic groups, and to a consequent increase of negative electric net charge in gelatin chains and reduction of IEP. Conversely, acidic treatment is less invasive and hardly influences the electrostatic nature of protein. In this case gelatin shows an IEP closer to that of the original collagen (Tabata and Ikada, 1998; Young et al., 2005) (Figure 1).

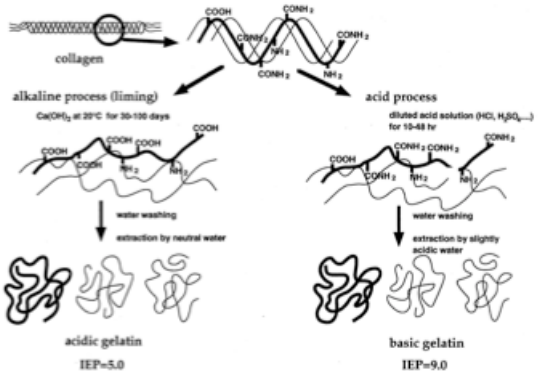

Figure 1. *Preparative process for acidic and basic gelatins from collagen (Tabata and Ikada, 1998).*

Consequences for the acidic or alkaline extracted-gelatins are the differen dispersion and gelling capabilities, which are directly related to IEP value. These parameters are fundamental for a classification of gelatin material, especially in food industry.
Intrinsic viscosity of acidic-extracted gelatin is slightly greater than that of Type B; no differences are observed in melting point whereas viscosity influences gelling process and gel stability. These properties are expressed through the *Bloom index*, which is directly related to stiffness and strength of a gel (Bigi et al., 2007). In these regards, thermal denaturation of collagen yields to a variety of gelatin samples with different chemical and physical properties. For example, treatment of collagen at low temperatures results in stronger gelatins with a relatively higher Bloom index than gelatins extracted at high temperature.
In aqueous solution and at a temperature beyond 40°C, gelatin chains assume the configuration of statistic random coil. This and other characteristics (Veis,

1964) make gelatin a substance comparable to linear-chain synthetic polymers, with a rather wide molecular weight distribution and high flexibility of chains. It has been observed that under specific condition of temperature, pH and solvent, gelatin macromolecules show sufficient flexibility to assume a variety of conformation, which is not noticed, for example, in native collagen (Malafaya et al., 2007). Furthermore, gelatin is able to organize in different supra-molecular structures, from the simplest globular one, typical of amorphous polymers, up to the more ordered triple-helix structure, observed in native collagen. The kind of structure notably influences the physical and mechanical properties of gelatin-based materials.
Beyond these characteristics, gelatin is also a substance of natural origin and shows the typical features of biopolymers, not observable in the synthetic ones. Its macromolecules contain both acidic and alkaline functional groups, which confer to gelatin the characteristics of a polyelectrolyte. Furthermore, the interaction between water and gelatin chains is different respect to that observed with hydrophilic polymers. The presence of molecules of water in gelatin-based material, in fact, greatly affects the structural and mechanical properties, both in solid and gel state (Kozlov, 1983).
Gelling process usually takes place by cooling down a gelatin solution. Gelatin macromolecules undergo a conformational change from a random coil to a more ordered helical disposition which leads to a partial regain of the characteristic triple-helix structure (renatured gelatin). This is a thermo-reversible process whose rate depends from several variables such as molecular weight, presence of intermolecular covalent bonds and concentration. It has been observed that the ordered structure of renatured gelatin shows a similar conformation of native collagen (Guo et al., 2003; Mackie et al., 1998) with main differences in the length and in the orientation of triple-helix segments, since gelling never yields a complete renaturation (Veis, 1964). From the structural point of view, gelatin in gel state can be described as a tree-dimensional network composed by peptides residues chains in a disordered state and junction zones, constituted by short segments of randomly oriented triple-helices (Mackie et al., 1998). There are great structural differences between dry and hydrated state of the gelatin materials. During drying part of the triple-helix segments align parallel one each other whilst this disposition is lost in presence of water molecules. Moreover, lack of order favors swelling of fibers. Renaturation level depends from several factors such as origin of gelatin, solvent, temperature and aging time, and it strongly influences gelatin properties both in gel state and in the form of film (Gornall and Terentjev, 2008; Dai and Liu, 2006).
Gelatin-based materials find definitely wide applications in several fields thanks to its good workability, possibility of tunable chemical and physical properties, stability both in gel and solid state. In food industry, clarification and stabilization are regarded as the major classical uses of gelatin. In the former case, gelatin is employed to obtain clearness of beverages containing tannins, for example wine and beer, by lessening bitter-tasting perception and, as a consequence, improving the flavor. In the latter, several foods such as meat or fruit are stored in gelatin to preserve freshness and goodness. Moreover, the foaming ability of gelatin helps in producing stable foams that gives light and airy texture to mousse and cream for dessert or cakes (Djagny et al., 2001).

Photographic industry sees gelatin as a good chemical binder for the photosensitive silver salts and for photographic paper. The ink-jet printer paper, in fact, when coated with gelatin, guarantees brilliant colors and clear shapes (http://www.gelatine.org).
An unusual application of gelatin is in the ballistic fields. In fact, thanks to its capability to closely simulate the density and viscosity of human and animal muscle tissue, it is used for testing the effect of firearms ammunition on human tissues (http://en.wikipedia.org/wiki/Ballistic_gelatin).
Gelatin-based materials find great interest as well in the pharmaceutical and biomedical fields, whose applications are the major matter of this PhD work. Gelatin is used for several applications such as the preparation of hard and soft capsules for the controlled release of biologically active proteins or drugs (Malafaya et al., 2007). In surgery, it is used like injectable hydrogels or sealant for vascular prostheses, or as foamed or nanofibrous scaffolds to support tissue engineering development (Mano et al., 2007). In spite of all the advantages that gelatin could offer, insufficient mechanical properties due to its poorly crystalline inner structure represent a remarkable obstacle. Moreover, the high solubility of this biopolymer in physiological environment could greatly restrict its application in the field of tissue engineering. Enhancements in mechanical properties are observed by increasing the renaturation level of drawn gelatin film through uniaxial deformation (Bigi et al., 1998), or by enriching the biopolymer with inorganic phase (Martucci et al., 2007; Zheng et al., 2002; Li et al., 2003; Panzavolta et al., 2009; Panzavolta et al. – *in press*).
Solubility in aqueous environment is decisively reduced thanks to crosslinking treatment that fix gelatin macromolecules through both inter and intra molecular bonds, guaranteeing improvement of mechanical properties and thermic stability of the biopolymer.

Crosslinking methods for gelatin

There are several chemical and physical crosslinking methods able to fix gelatin-based materials. Physical methods offer the great advantage to not release substances that might be minor (gap) toxic, even if it the possibility of side effects provoked by the process cannot be excluded. Moreover, treatment with physical methods does not guarantee a good efficacy of crosslinking and it is difficult to modulate the crosslinking degree of the fixed material, which is possible instead with chemical ones (Yao et al., 2004). Physical methods include thermic treatment (Weadock et al., 1995; Wang et al., 1994), radiation with microwaves and exposition to γ ultra-violet rays (Visser et al., 1992).
Chemical methods generally employ reagents that possess, at least, two functional groups and are able to react with two different parts of gelatin macromolecules to fix them. Usually the reaction involves functional groups of the crosslinking agent and amino acidic residues of the gelatin chains, such as ε-amino group of lysine and hydroxylysine as well as carboxylic groups of aspartic and glutamic acids. Chemical crosslinking most often proceeds through soaking the materials in the crosslinking agent solution. Gelatin, in particular, can be crosslinked both in solution and in gel or solid state. Concentration of reagents, time and temperature of crosslinking process are

fundamental variables for the success of the reaction. Concentration of gelatin in aqueous solution is of great importance because the distance between gelatin macromolecules definitely establishes type of new forming bonds. As a matter of fact, intermolecular bonds are easier to form in concentrated solutions whilst intramolecular bonds are more common in diluted solutions. Thickness is a further variable that could influence crosslinking process when it is performed on gelatin films.
The most used chemical crosslinking agents include aldehydes, polyepoxides, acyl azides, carbodiimides and esametilen diisocyanate. Among them, glutaraldehyde (GTA) is by far the most widely used, due to its high efficiency in collagenous materials stabilization. Crosslinking of collagenous samples with GTA involves the reaction of free amino groups of lysine or hydroxylysine amino acid residues of the polypeptide chains with the aldehyde groups of GTA. By varying GTA concentration in solution, it is possible to obtain tunable physical chemical properties of gelatin-based materials. Common values of GTA concentration range from 2 to 5 % w/v (Bigi et al., 2001).
One of the most important problems to use GTA as crosslinking agent, such as most reagents mentioned above, is the grade of toxicity. In the particular case of glutaraldehyde, for example, a gradual release of molecules in physiological environment is observed. This aspect could seem another obstacle for the application of gelatin as a biopolymer for a biomedical use, but recent works demonstrated the possibility to use naturally occurring agents for this purpose. The fundamental aspect is in the comparable efficiency of crosslinking of these natural agents respect to that of the synthetic ones.
Genipin is an organic molecule by far less cytotoxic than GTA (Sung et al., 1999; Tsai et al., 2000). It has been widely used in herbal medicine (Akao et al., 1994), and the dark blue pigments obtained by its spontaneous reaction with amino acids or proteins have been used in the fabrication of food dyes (Paik et al., 2001). Other applications involve the preparation of gelatin capsules and the immobilization of enzymes (Fujikawa et al., 1987). Further studies demonstrated that genipin fixed tissue has a resistance against enzymatic degradation comparable to the GTA fixed tissue (Sung et al., 1998; Huang et al., 1998).

Genipin

Genipin is a naturally occurring molecule, widely used to crosslink biopolymer such as chitosan or gelatin derivatives (Bigi et al., 2002; Yao et al., 2004; Chen et al., 2006; Mi, 2005; Mi et al., 2003). Genipin can be obtained through the hydrolysis of the enzyme β-glucosidase on the iridoid glucoside, geniposide (Figure 2), abundantly present in the fruit of *Gardenia Jasminoides Ellis* (Park et al., 2002; Lee et al., 2003) and *Genipa americana* (Jagua) (U.N.C.O.T.A.D. 2005). Genipa americana is widely distributed throughout the tropical and parts of the subtropical areas of Latin America. Areas where it grows naturally range from Mexico to Argentina and include the Caribbean as well. Gardenia is grown in East Asia, including Japan and Chorea.

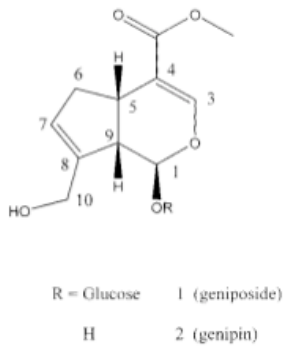

Figure 2. *Chemical structures of geniposide 1 and genipin 2 (Paik et al., 2001).*

In the sixties, Carl Djerassi and co-workers (Djerassi et al., 1960 and 1961) have been the first who investigated the molecular structure and chemical physical properties of genipin, but this molecule were already well known in Eastern medicine thanks to its anti-inflammatory, diuretic and hemostatic properties.

Genipin reacts with materials containing primary amine groups, such as chitosan and some peptides and polypeptides, to form covalently crosslinked networks (Butler et al., 2003). As mentioned before, reaction between genipin and amino groups gives rise to not toxic dark blue pigments, which are widely employed in food industry (Park et al., 2002; Paik et al., 2001). Moreover, genipin is used in forensic field as fingerprint sampler, in replacement of ninhydrin (Lee et al., 2003).

The reaction leading to the formation of dark blue pigments was deeply investigated (Touyama et al., I and II, 1994) and it has been demonstrated that interaction between genipin and methylamine, in presence of oxygen, gives rise to a dark blue material constituted of long polymeric chains with high molecular weight (about 40-44 monomeric unit per chain). On the contrary, in inert atmosphere this kind of reaction yields to formation of a brownish-red mixture at low molecular weight, which changes color to dark blue as soon as it comes into contact with the oxygen.

On this basis, it is possible to suppose that beyond the reaction with primary amine, genipin is subject to polymerization, which happens only in presence of oxygen, exhibiting the dark blue color. The common hypothesis about genipin polymerization is a radical mechanism (Butler et al., 2003; Touyama et al., II, 1994).

The change of color is clearly observable during crosslinking process of film-shaped gelatin with genipin (Gioffrè et al., 2011). In fact, gelatin color changes from the typical amber-yellow, through green until the dark blue.

It has been supposed that crosslinks form via two reactions involving different sites on the genipin molecule. The two steps of the reaction involving genipin that are believed to result in crosslinking of polymers containing primary amine groups are shown in Figure 3. The first step consists in an initial nucleophilic attack from a primary amine group to C3 carbon atom of genipin, forming an intermediate aldehyde group (Figure 3 a and b).

Opening of the dihydropyran ring is then followed by the attack on the resulting aldehyde group by the secondary amine formed in this step of the reaction, with the formation of a pyridine-like ring (Figure 3 c and d).

The second step of crosslinking reaction is an S_N2 nucleophilic substitution reaction that involves the replacement of the ester group on the genipin molecule by a secondary amide linkage. Polymerization of genipin molecules occurs at the second stage, probably by radical reaction (Touyama et al., II, 1994; Chang et al., 2003).

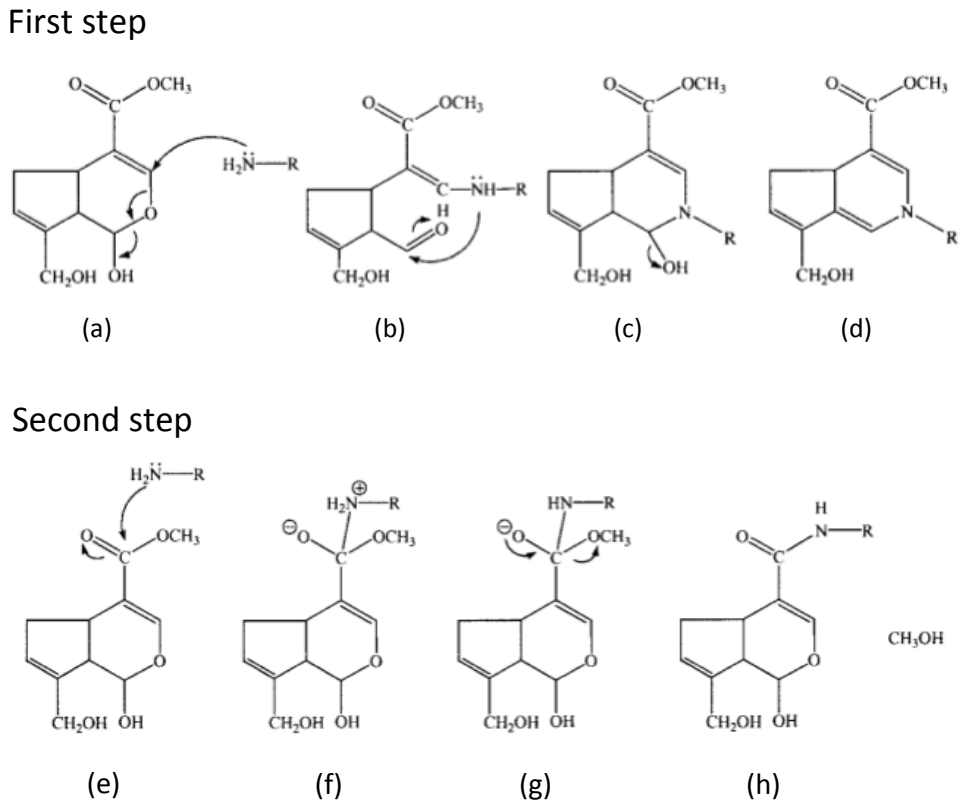

Figure 3. *Crosslinking reaction that involves genipin and a primary ammine (Butler et al., 2003).*

The two steps of crosslinking process have been investigated through UV/Vis spectroscopy. UV/vis spectra showed that the λ_{max} of genipin at 240 nm decreased during the transformation of the blue pigments, while an intermediate peak at about 290 nm, relative to the absorption of pyridine-like ring, appeared and increased rapidly. After that, the 290 nm peak gradually decreases, and finally the λ_{max} of blue pigment polymers at about 580 nm appeared.

Several studies on this pigment showed that it is soluble in water, in methanol and in ethanol but insoluble in the organic solvent such as chloroform (Touyama et al., II, 1994). In literature, comparisons of gelatin treated with several types of crosslinking agents are reported (Sung et al., 1999; Chang et al., 2003). In particular, it has been observed that swelling properties, extensibility as well as the enthalpy of denaturation of gelatin films crosslinked with genipin, are quite close to those treated with GTA although the formers show a lower crosslinking degree.

In surgery, it has been reported that the degree of inflammatory reaction observed for wounds treated with genipin-crosslinked dressing was less severe than that covered with GTA treated dressing (Chang et al., 2003). All these studies demonstrate that this naturally occurring crosslinking agent,

which was proved to be remarkably less cytotoxic than GTA, can be considered a very good alternative as fixative for gelatin based materials for biomedical applications.

1.3.2 Poly-Lactic Acid

Poly-lactic acid (PLA) is a thermoplastic, high-strength and high-modulus synthetic polymer, which belongs to the family of aliphatic polyesters, in particular of α-hydroxy acids.
It is a polymer with a very broad range of applications, especially in industrial packaging and biocompatible/bioabsorbable medical device market. Generally, all the aliphatic polyesters, included PLA are biodegradable and compostable. Moreover, poly-lactic acid has excellent organoleptic characteristics for food contact and related packaging applications. The widespread use of this polymer is mainly due to its easy processability in most standard plastics equipment to yield transparent films, fibers or blow-moldable preforms for bottles. It shows a broad range of thermal and mechanical properties thanks to its good ability to be stress crystallized, thermally crystallized, impact modified, filled and copolymerized. PLA is produced from renewable resources and it is nontoxic to the environment and the human body (Inkinen et al., 2011). Moreover, PLA is degraded by simple hydrolysis of the ester bond and does not require the presence of enzymes to catalyze this hydrolysis. The rate of degradation depends on the size and shape of the article, the isomer ratio, and the temperature of hydrolysis (Garlotta, 2001).
As the name suggests, PLA derives from the *lactic acid* monomer, also known as 2-hydroxy propionic acid. This highly water-soluble molecule is the simplest hydroxy acid with an asymmetric carbon atom, and it exists in two optically active configurations, as showed in Figure 1 (Lunt, 1998).

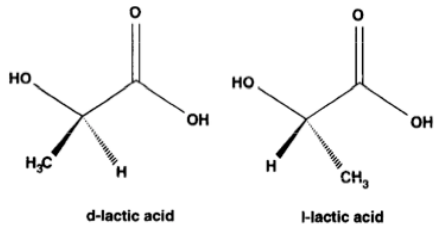

Figure 1. *Lactic acid stereoisomers (Lunt, 1998).*

The L(+)-isomer is produced in mammals, included humans, and both D(-)- and L(+)enantiomers are produced by microorganisms. The majority of the world's commercially produced lactic acid is made by the bacterial fermentation of carbohydrates, using homolactic organisms such as various optimized or modified strains of the genus *Lactobacilli*, which exclusively forms lactic acid (Garlotta, 2001). Synthesis of PLA can proceed through a direct condensation reaction of the lactic acid, or through the ring-opening polymerization of the cyclic lactide dimer (Figure 2). Lactide is the cyclic dimer of lactic acid, which exists as well in the two optical isomers D and L.

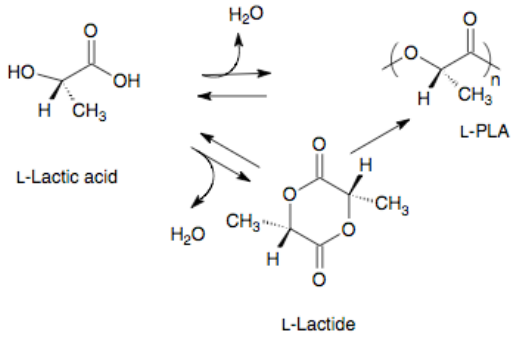

Figure 2. *Polymerization routes to poly-lactic acid (Henton et al., 2005).*

Many catalyst systems, such as complexes of aluminum, zinc, tin, and lanthanides, have been evaluated for the polymerization by the ring-opening process. Strong bases as well, such as metal alkoxides, have been used with some success. In Figure 3 a coordination-insertion mechanism with ring opening of the lactide using tin octoate is showed (Henton et al., 2005).

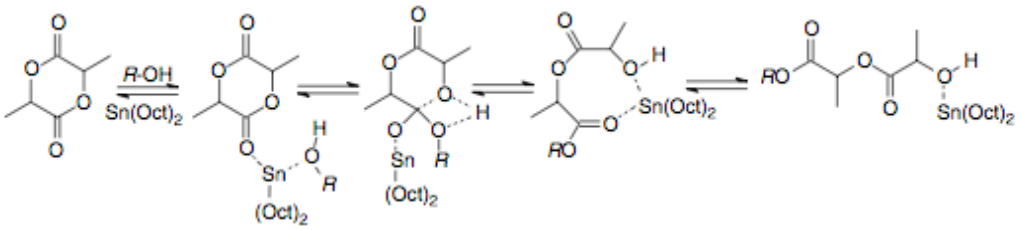

Figure 3. *Synthesis of PLA through a coordination-insertion mechanism with ring opening of the lactide using tin octoate.*

Tin compounds are usually preferred for the bulk polymerization of lactide due to their solubility in molten lactide, high catalytic activity, and low rate of racemization of the polymer. As a function of catalysts systems and conditions of the whole process, several mechanisms have been proposed to explain the kinetics and nature of the end groups observed in lactide polymerization (Henton et al., 2005).

Polymerizing a controlled mixture of the L- or D-isomers, it is easy to modify the stereochemical structure of the resulting polyester and yield high-molecular-weight amorphous or crystalline polymers. Obviously, the properties of the resulting polymers are strictly dependent on the morphological structure and nature of precursors. For example, the naturally occurring isomer L-lactide yields a semi-crystalline homopolymer (LPLA). On the contrary poly(DL-lactic acid), obtained from DL-lactide, the synthetic blend of D-lactide and L-lactide, is an amorphous polymer with a random distribution of both isomeric forms of lactic acid, unable to arrange into a crystalline organized structure.

Morphological differences greatly influence thermal and mechanical properties of the two polymeric materials and, as a consequence the final application. LPLA displays high tensile strength and short elongation with a consequently high modulus and it is more suitable than the amorphous polymers for load-bearing applications, such as in orthopedic fixation and sutures. On the contrary, DLPLA is more attractive as a drug delivery system because of its lower tensile strength and higher elongation, and its greater

degradation rate than LPLA. Copolymers are commonly used to disrupt the L-lactide crystallinity in order to accelerate the degradation process of LPLA (Middleton and Tipton, 2000).
In the biomedical and pharmaceutical fields, the aliphatic polyester PLA is regarded as one of the most common applied synthetic material to replace and support damaged tissues, such as skin recovery, vascular grafts, bone fixation devices, tissue engineering matrices and so forth. Moreover, it is widely used in blends with natural polymer, such as collagen and gelatin (Sionkowska, 2011). Natural polymers are usually biocompatible and display excellent cellular affinity. On the other hand, synthetic polymers have good mechanical properties and thermal stability, much better than several naturally occurring polymers. The research focused on development of synthetic and natural polymers composites leads to new materials with improved mechanical properties and biocompatibility, compared with those of the single components.

1.3.3 Polyacrylic Acid

Poly(acrylic acid) (PAA) is a synthetic high molecular weight polymer whose monomeric unit derives from acrylic acid (Figure 1a). Polymerization process involves the vinyl group and gives rise to long aliphatic chains with carboxyl side groups (Figure 1b).

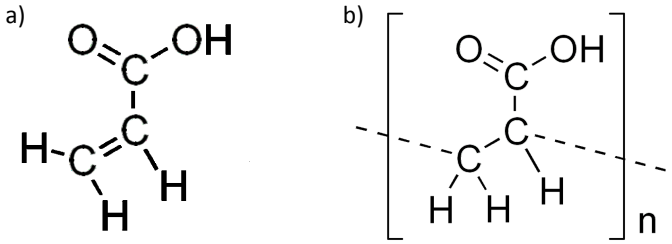

Figure 1. *a) Acrylic acid molecule; b) monomeric unit of poly(acrylic acid).*

PAA is a water soluble polymer and is essentially non ionic in neutral solutions; whereas carboxyl side groups undergo ionization to carboxylate anions at basic pHs. This property is widely exploited in the biomedical field, in which production of hydroxyapatite/polymer composite materials are of great interest for the development of biomaterials suitable to repair the skeletal system (Liu et al., 1997). One of the main advantages of inorganic phase/polymer composites is the possibility to modulate biodegradability, bioactivity and mechanical properties through variations in composition. Furthermore, the presence of the polymer could improve the interfacial bonding of the composite with bone tissue.
Poly(acrylic acid) is easily and irreversibly adsorbed on hydroxyapatite through a process that has been ascribed to electrostatic interactions and/or hydrogen bonds. The enrichment with PAA reduces the crystallinity and the crystal dimensions of the inorganic phase leading apatitic crystals with dimensions comparable to those characteristics of biological apatites (Bertoni et al., 1999).

1.3.4 Montmorillonite

Montmorillonite (MMT) is a clay mineral, belonging to phyllosilicate group of minerals, and it is the major constituent of the deposit of volcanic ashes, *bentonite*.
The classification of silicate minerals is based on the structure of their silicate group, which contains different ratios of silicon and oxygen. Usually, clay minerals are composed of layers of tetrahedral and octahedral sheets. If there is only one tetrahedral and one octahedral layer in each sheet the clay is known as 1:1. The alternative 2:1 clay, as montmorillonite, has two tetrahedral layers sandwiching a central octahedral one. The octahedral layer is constituted by aluminum and/or magnesium surrounded by six oxygen atoms whilst the tetrahedral one is composed of SiO_4^{4-}. Oxygen atoms that are not shared with other metal ions are bonded to hydrogen atoms. The whole crystal structure of clay mineral is formed from a stack of negatively charged layers, with cations such as Na^+ or K^+ and water molecules in the interlayer spaces (Figure 1).

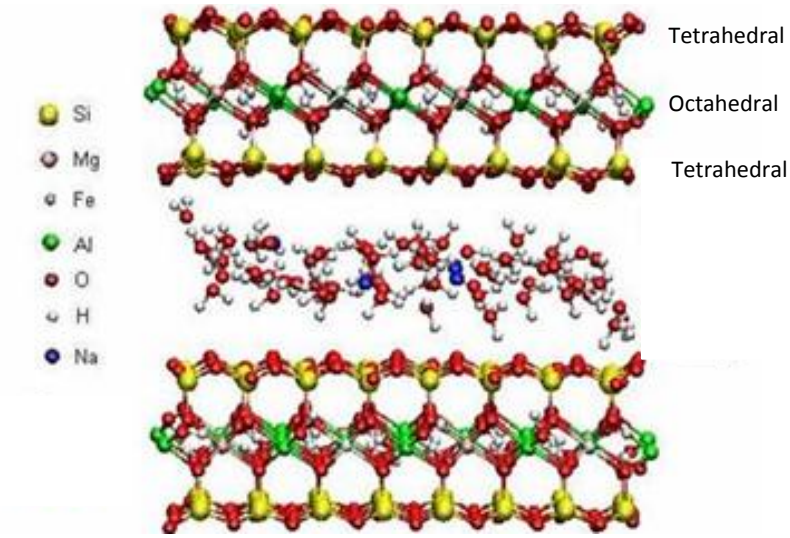

Figure 1. *Example of a sodium montmorillonite structure.*

Water content of montmorillonite is variable and it affects the interlayer distance, which greatly increases along the c-axis, perpendicular to the (001) plane, as a function of hydration degree (Talibudeen, 1950; Katti and Katti, 2006).
Montmorillonites have a sheet-type structure characterized by high surface/volume ratio: layer dimensions in the length and width directions can be measured in hundreds of nanometers, whereas thickness amounts to just about one nanometer.
Chemically, MMT is a hydrated sodium calcium aluminum magnesium silicate hydroxide. In particular, in this PhD work, montmorillonite known as Nanofil 116, Southern Clay Products, has been used.
Crystallographic data of montomorillonite are showed in Table 1.

Table 1. Crystallographic data of sodium calcium montmorillonite.

Category	Phyllosilicate
Formula	$(Na,Ca)_{0.33}(Al,Mg)_2(Si_4O_{10})(OH)_2 \cdot nH_2O$
Crystal symmetry	Monoclinic prismatic
Unit cell	a = 5.17 Å, b = 8.94 Å, c = 9.95 Å; β = 99.54°

The possibility to interchange the ions present in the interlayer space with other kind of molecules, polymeric macromolecules included, provides a wide range of possible applications (Yao et al., 2010; Ray and Bousmina, 2005; Bonderer et al., 2008; Xu et al., 2006; Shchipunov et al., 2006; Darder et al., 2003). In the first nineties, one of the first hybrid nanocomposite materials, constituted of nylon-6 and montmorillonite, was developed by Toyota Central Research & Development Labs (Usuki et al., 1993).
Nanocomposites are a new class of materials which have attracted industrial and research attention because of the material improved properties, even at very low filler content, due to the high aspect ratio of the filler and the nano–level interactions with the polymer matrix.
A composite is usually classified among *nanoclass* materials if the dimension of at least one of its phases is less than 100 nm. It is possible to distinguish three types of nanocomposites, depending on how many dimensions of the dispersed particles are in the nanometer range. If the three dimensions are in the order of nanometers, isodimensional nanoparticles, such as spherical silica nanoparticles or semiconductor nanoclusters are involved. Two dimensions in the nanometer scale with a third larger one form an elongated structure, such as nanotubes, which are studied as reinforcing nanofillers yielding materials with exceptional properties. The third type of nanocomposites is known as polymer-layered crystal nanocomposites and is characterized by only one dimension in the nanometer range. The filler, in this case, is present in the form of sheets, from one to a few nanometers thick and hundreds to thousands of nanometers long (Alexandre and Dubois, 2000).
It is supposed that atomic and molecular interactions can have a significant influence on the macroscopic material properties, when the domain size is comparable to the size of a molecule. As a consequence, superior property enhancements can be achieved (Bae et al., 2009). Montmorillonite is a promising reinforcing material thanks to its great ability to intercalate a wide variety of materials. Just a little amount of MMT could clearly enhance thermal and mechanical properties, as well as swelling behavior, of clay/polymer nanocomposites (Li et al., 2003).

1.3.5 Calcium phosphates

Calcium (ortho)phosphates (CaPs) are the most important inorganic constituents of vertebrates hard tissues such as bones and teeth, where they occur as poorly crystalline, non-stoichiometric and ion-substituted minerals (Mann, 2001). CaPs present in biological environment are commonly referred to as biological apatites (Vallet-Regí and González-Calbet, 2004) and their main function is to provide stability, hardness and function. The mineral phase of bone and teeth is indeed a basic calcium phosphate, which is assimilated to synthetic hydroxyapatite (HA), $Ca_{10}(PO_4)_6(OH)_2$, even if

biological apatites differ from stoichiometric HA in several aspects, including non-stoichiometry, small crystal dimensions and poor crystallinity.
In particular biological apatites are described as carbonated-apatites. Non-stoichiometry is due to the presence of significant amounts of further foreign ions, either incorporated in the apatite crystal lattice or just adsorbed on the crystal surface.
Further calcium phosphates occur in biological tissues, usually in pathological calcifications, such as amorphous calcium phosphate (ACP), dicalcium phosphate dihydrate (DCPD), octacalcium phosphate (OCP) and Mg-substituted β-tricalcium phosphate (β-TCMP) (Boanini et al., 2010).
Thanks to the closer chemical and structural similarity of hydroxyapatite to the mineral component of bone, it is the most used calcium phosphate in the preparation of biomaterials. HA is the most stable and the most insoluble of the CaPs, and exhibits excellent biocompatibility, bioactivity, osteoconductivity, direct bonding to bone, etc.
HA can be easily prepared in aqueous solution. Notwithstanding the several methods described to prepare hydroxyapatite, the syntheses follow two main routes. The first is a stoichiometric titration of a calcium hydroxide slurry with phosphoric acid up to neutrality, whilst the second is a precipitation method, consisting in dropwise addition of a solution of ammonium or sodium monohydrogen phosphate to a calcium solution (generally calcium nitrate or acetate) or vice versa (Boanini et al., 2010). Alternative methods to obtain apatites, as well as other CaPs, include the transformation of more soluble, metastable phosphates in a wet environment (Tadic et al., 2002).
Crystallinity of the resulting mineral depends on several factors such as temperature and reaction time. In fact, short reaction times provide nanocrystals and/or amorphous products, whereas crystal dimensions and crystallinity increase with increasing reaction time. Incorporation of carbonate ions in the reaction products usually occurs if synthesis is carried out in air.
In biomineralized tissues, calcium orthophosphates (biological apatite) are always nanodimensional and nanocrystalline, and are formed in vivo under mild conditions under the control of organic macromolecules, which regulate nucleation, growth, morphology, and assembly of inorganic crystals. Nanostructured minerals provide a better capability for specific interaction with proteins. Furthermore, nanodimensional apatite has a crucial role for a wide variety of metabolic functions in organisms as a reservoir of calcium and orthophosphate ions. On this basis, the development of nanodimensional and nanocrystalline calcium orthophosphates, with optimized structure and properties mimicking bone minerals, is of relevant interest for the preparation of biomaterials for hard tissues repair (Dorozhkin, 2012).

Chapter II

Films

Materials and Methods

2.1 Materials

2.1.1 Preparation of gelatin films

All the films were prepared using type A gelatin (280 Bloom, Italgelatine S.p.A.) from pigskin. Gelatin films were prepared from 5% (w/v) aqueous gelatin solutions. About 10 mg of sodium azide were added to prevent bacteriological degradation. The films were obtained by pouring 10 mL of gelatin solution on the bottom of Petri dishes (diameter of 6 cm) and air-drying at room temperature (Bigi et al., 1998).

Gelatin films at different pH values

Gelatin films were prepared from 5% (w/v) aqueous gelatin solutions at specific pH values, from 2 to 12. The pH adjustments were made with 2M NaOH or HCl solutions. No pH adjustment was necessary to obtain gelatin film at pH 5.
Samples were labelled GX, where X is the pH of the gelatin solution used to prepare films. Sample at pH 5 was labelled Gel.

Gelatin films containing montmorillonite (MMT)

Clay montmorillonite Nanofil 116 (Southern Clay Products, Inc.) was used. A 5% (w/v) aqueous gelatin solution was mixed with aqueous suspensions at different MMT content (5%, 15% or 20% w/w with respect to gelatin) under stirring. Before mixing, clay suspensions were submitted to ultrasonication for 20 min.
The composite films were obtained from 10 mL of the clay-gelatin suspension on the bottom of Petri dishes (diameter of 6 cm) after water evaporation, at room temperature. Samples were labelled FAGY, where Y is the concentration of clay.

2.1.2 Crosslinking of gelatin films with genipin

Some gelatin and gelatin-MMT films were crosslinked with the naturally occurring agent genipin (Wako, Japan). A volume of 10 mL of genipin in

phosphate buffered saline solution (PBS) 0.1M at pH 7.4, was poured onto the dried films in the Petri dishes (Bigi et al., 2002). Crosslinking was performed using different genipin concentrations (0.67%, 0.15% or 0.07% w/v) either for 1h or for 24h at 25°C. After this period, the genipin solution was removed and substituted with an equal volume of 0.1M glycine for an hour, to remove the excess of genipin. Finally, the films were repeatedly washed with double distilled water and air-dried at room temperature. Crosslinked samples were labelled GXGZ, FAGY GZ. As described above, X and Y are respectively the pH of the gelatin solution used to prepare films and the concentration of clay in gelatin-MMT composite films, whereas Z is the concentration of genipin used to crosslink films. The duration time of crosslinking process is also indicated (1h or 24h). Non crosslinked gelatin film was labelled Gel.
In order to investigate the effect of a different crosslinking procedure, some films were crosslinked by adding genipin (3% w/w with respect to gelatin) to a 5% (w/v) aqueous gelatin solution containing 10mL of PBS solution 0.1M at pH7.4 and 90mL of distilled water. Films were prepared at the bottom of Petri dishes and air-dried as described above, and labelled GelG0.15in.

2.2 Methods

2.2.1 X-ray diffraction analysis

High-angle X-ray diffraction patterns were recorded on a flat camera with a sample-to-film distance of 60 mm using Ni-filtered CuK radiation.
XRD analysis was carried out by means of a PANalytical X'Celerator powder diffractometer using CuKa radiation (40 mA, 40 KV). Gelatin films were analysed in the 2θ range from 3° to 14° in transmission mode whilst the range for gelatin-MMT composite films was from 3° to 40°, analysed in reflection mode. Both analyses were performed in a continuous scanning mode. The area under the diffraction peak at 2θ=7.7° was evaluated using the program X'Pert High Score.
The gelling process of gelatin in presence of the crosslinking agent and salts was investigated by means of X-ray diffraction: patterns were recorded overnight from 5% (w/v) gelatin solutions in the 2θ range from 3° to 14°, in reflection mode. Temperature and relative humidity were recorded by means of a data logger ESCORT RH iLog.

2.2.2 Mechanical tests

Stress-strain curves were recorded using an INSTRON Testing Machine 4465 and the Series IX software package. Strip-shaped samples (3x30 mm, thickness around 0.12 mm) of air-dried films were stretched using a crosshead speed of 5 mm/min. Samples were tested in wet conditions too: strip-shaped films were immersed in a mixture of water and ethanol in a 2:3 ratio (constant relative humidity of 75%) for 72h and stretched in the mixture with the same crosshead speed. The thickness of the samples was determined using a Leitz SM-LUX-POL microscope. Young's modulus, E, the stress at break, σ_b, and the strain at break, ε_b, were measured in a static mode. Single factor analysis of variance (ANOVA) was employed to assess

statistical significance of the results. A value of $P<0.001$ was considered statistically significant.

2.2.3 Thermal analyses

Calorimetric measurements were performed using a Perkin Elmer Pyris Diamond DSC equipped with a model ULSP intracooler. Temperature and enthalpy calibration were performed using high-purity standards (*n*-decane and indium). Samples were examined under both air-dried and wet conditions. The measurements in wet conditions were carried out on known amounts of gelatin films (3-4 mg), which had been stored in a mixture of water/ethanol in the ratio 2:3 for 72h (constant relative humidity of 75%). The wet samples were wiped with filter paper to remove excess of liquid and hermetically sealed in aluminium pans (to prevent any loss of liquid during measurements). Heating was carried out at 5°C/min from 0° to 60°C for the wet samples and from 40°C to 130°C for the dry samples. Denaturation temperature (T_D) was determined as the peak value of the corresponding endothermic event. The value of denaturation enthalpy was calculated with respect to the weight of air-dried gelatin. Water content of the gelatin films was determined through thermogravimetric analysis, which was carried out using a Perkin Elmer TGA-7. Heating was performed in a platinum crucible in air flow (20 mL/min) at a rate of 10°C/min up to 800°C. The samples weights were in the range 5-10 mg.

2.2.4 Crosslinking degree

The extent of crosslinking of gelatin and gelatin-MMT films was determined by an UV assay of the non-crosslinked ε-amino groups before and after reaction with genipin (Bubnis and Ofner, 1992). After reaction with 0.5% trinitrobenzensulfonic acid (TNBS), gelatin was hydrolysed with 6M HCl. A volume of 5mL of the hydrolyzate was diluted with 5mL of water and then extracted with ethyl ether. A 5mL aliquot of the aqueous phase was removed from each sample and heated for 15 min in a hot water bath, cooled at room temperature and diluted with 15mL of water. The absorbance of the diluted solution was measured at 346 nm in a Kontron Uvikon 931 spectrophotometer against a blank. The relationship between absorbance and moles of ε-amino groups per gram of gelatin was:

$$moles\ \varepsilon - amino\ groups/_{g\ gelatin} = \frac{2 \cdot Absorbance \cdot 0.02\ L}{1.46 \cdot 10^4 \cdot b \cdot x}$$

where $1.46 \cdot 10^4$ L/mol·cm is the molar absorptivity of TNP-lys, b is the cell path length in centimeter and x is the sample weight in grams.

2.2.5 Swelling

Swelling of gelatin and gelatin-MMT films was measured on samples, about 40 mg, weighted in air-dried conditions. Then, the air-dried samples were immersed in PBS solution 0.1M at pH7.4 for different periods of time. Wet samples were wiped with filter paper to remove excess liquid and weighted.

The amount of adsorbed water was calculated as:

$$W\% = \frac{(W_w - W_d) \cdot 100}{W_d}$$

where W_w and W_d are respectively the weights of the wet and the air-dried samples.

2.2.6 Release of gelatin

50 mg of gelatin or gelatin-MMT films were immersed in 5mL of a phosphate buffered saline solution 0.1M at pH 7.4, at 37°C. Gelatin concentration in the release solution was determined by a colorimetric assay using a bicinchoninic acid protein assay kit (Sigma Chemical Co., St. Louis, MO, USA): a 4% copper (II) sulphate penthahydrate solution was mixed with an excess of bicinchoninic acid at a final ratio of 1:50 v/v. A 300μL aliquot of the release solution was added to 2mL of the assay solution in a test tube. Phosphate buffer solution was then added up to a final volume of 5mL. Solutions were stored at 37°C for 30 min and then the absorbance of each solution at 562nm was measured using a Kontron Uvikon 931 spectrophotometer (Hakata et al., 1994). The gelatin concentration in the release solution was determined through a calibration curve.

2.2.7 Wettability

In order to investigate the relative hydrophilicity of gelatin and gelatin-MMT composite films, water contact angle (WCA) measurements were performed. It is pointed out that the surface wettability reflects surface hydrophilicity (Gualandi et al., 2012). Samples were analysed with CAM 200 (KSV Instruments Ltd., Finland).

2.2.8 Scanning electron microscopy

Morphological investigation of fracture surfaces of the dried of gelatin-MMT composite films was performed using a Philips XL-20 scanning electron microscope operating at 15 kV. The samples were sputter-coated with gold prior to examination.

2.2.9 Cytotoxicity in vitro tests

L929 fibroblasts were used to evaluate cytotoxicity of some selected crosslinked films. Samples were sterilized with gamma rays (Cobalt-60) at a dose of 25 kGy. The cells were cultured in Dulbecco's Modified Eagle Medium (DMEM) (Sigma, UK) supplemented with 10% Fetal Calf Serum (FCS), and 1% antibiotics (100 U/mL penicillin and 100 μg/mL streptomycin), detached from culture flasks by trypsinization, and centrifuged. The cell number and viability were checked with trypan blue dye exclusion test.
Sterile samples were positioned to cover the bottom of eight wells in a 24-well plate. Fibroblast cells were plated at a density of 5×10^4 cells/mL in wells containing films. The same concentration of cells was seeded in empty wells

as the control (CTR(−)) and in a 0.5% DMEM phenol solution that is recognized to be toxic for cell culture as positive control (CTR(+)). The plate was cultured in standard conditions, at 37°C ± 0.5 with 95% humidity and 5% CO_2 for 48h.
The cytotoxicity was evaluated by measuring cell proliferation, lactate dehydrogenase enzyme (LDH) release, and cell morphology after 48h of culture.
Cell proliferation and viability were assessed by WST1 (Roche Diagnostics GmbH, Manheim, Germany) colorimetric reagent test. WST1 solution (50µL) and 450µL of medium (final dilution: 1:10) were added to the cell monolayer, and the multiwell plates were incubated at 37°C for 4h. The supernatants were quantified spectrophotometrically at 450nm with 625nm as the reference wavelength. The WST1 was recorded as optical density (OD) and correlated with the cell number. The proliferation percent relative to CTR(−) was also reported.
At the end of experimental times, the supernatant was collected from all wells and centrifuged to remove any particulates for LDH measure. A biochemical test (LDH, MeDia IVD s.r.l, Forlì, Italy, lotto F13H) was performed. A 0.033% solution of Neutral Red stain (Sigma, UK) in culture medium was added to two wells for each group for 90 min at the end of experimental times. Only viable cells were stained in cytoplasm, while dead cells did not. The cultures were examined by microscopy for a qualitative evaluation of cell morphology, and explanatory images were selected.

Statistical analysis

Statistical evaluation of data was performed using the software package SPSS/PC+ StatisticsTM 10.1 (SPSS Inc., Chicago, IL USA). The data represented the mean of six replicates and were reported as the mean ± SD at a significance level of $p<0.05$. After having verified normal distribution and homogeneity of variance, a one-way ANOVA was performed for comparison between the groups.
In addition, Scheffé's post hoc multiple comparison tests were performed to detect significant differences between groups.

Results

2.3 Gelatin films

2.3.1 X-ray diffraction analysis

Gelatin films were investigated by wide-angle X-ray diffraction (WXRD) analysis to examine the renaturation level (relative triple-helix content) of the protein, and its modifications due to pH and crosslinking. The characteristic collagen WXRD pattern includes two diffraction reflections: one, at about 1.1nm, related to the diameter of the triple helix and the other, at about 0.29nm, related to the distance between amino acidic residues along the helix (Pezron et al., 1990). These reflections disappear after collagen denaturation, whereas they can be observed in the WXRD pattern of partially renaturated gelatin as shown in Figure 1(a).

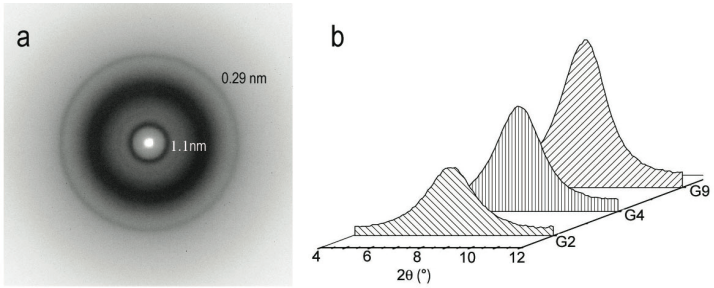

Figure 1. *(a) High-angle X-ray diffraction pattern of a gelatin film. (b) Integrated intensity of the 1.1nm reflection obtained from the diffraction patterns of samples: G2, G4, and G9.*

The integrated intensity of the 1.1nm reflection can be used as a measure of the triple-helix content of gelatin films (Bigi et al., 2000 and 2004; Boanini et al. 2010). The 1.1nm reflections present in the X-ray diffraction patterns of gelatin films prepared from solutions at different pHs are shown in Figure 1(b). It can be observed that the integrated area of the reflection varied with pH: the integrated intensity increased (Table 1) as a function of raising pH up to 5, it remained nearly constant in the pH range 5–9, and then it decreased as pH increased up to 12.

Table 1. Integrated intensity of the 1.1nm reflection obtained from the diffraction patterns of gelatin films prepared at different pHs.

Sample	*Integrated Intensity ± St dev (%)*
G2	20680 ± 5
G3	28509 ± 7
G4	36314 ± 6
Gel	42507 ± 7
G6	40434 ± 5
G7	41709 ± 2
G8	43933 ± 5
G9	44843 ± 2
G10	36068 ± 6
G11	33989 ± 3
G12	25413 ± 10

The gelling process of gelatin in presence of the crosslinking agent and/or PBS was investigated by means of X-ray diffraction analysis during cooling of solutions prepared at 50°C. During cooling down to r.t. gelatin passed through the gel state and dried. The integrated intensity of 1.1nm reflection in function of the time is reported in Figure 2.

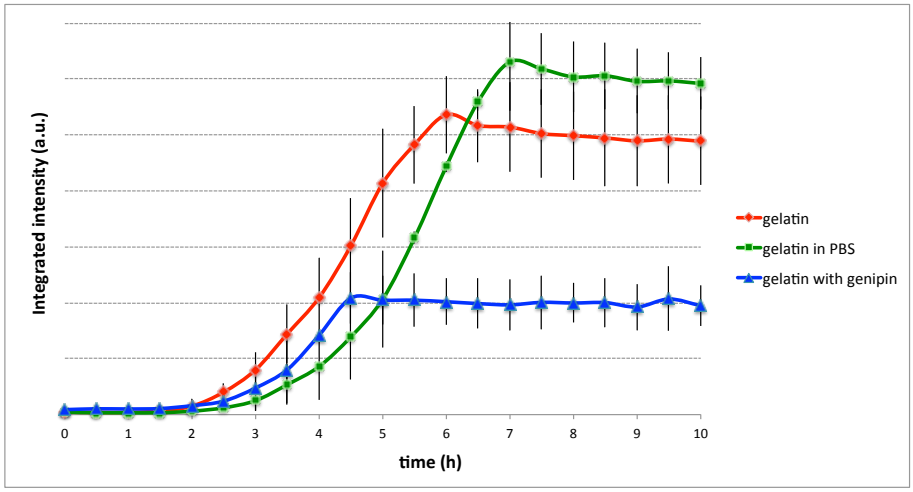

Figure 2. *Integrated intensity of the 1.1nm reflection in function of time, obtained from gelatin (red line), gelatin dissolved in PBS (green line) and gelatin dissolved in presence of genipin (blue line).*

Increase of the integrated intensity of 1.1nm reflection (restoration of triple helix) from gelatin solution (red line) started after about three hours, with the beginning of drying. The process ended when gelatin is completely dried (plateau). The presence of PBS (green line) did not influence significantly the intensity of the dried sample, and therefore its triple helix content, but slightly slowed down the renaturation process.

The great difference between the intensities of blue and green plateaus revealed that genipin (blue line) prevented the formation of the triple helix.
The results of WAXD investigation carried out on gelatine films treated with genipin solutions at increasing concentration confirmed the results of the gelling experiment. The data reported in Figure 3 show that the integrated intensity of the reflection, and as a consequence the relative triple helix content, decreased with genipin concentration and with crosslinking time. Sample treated with the highest genipin concentration, for 24h, exhibited the lowest value of integrated intensity of 1.1nm reflection (Figure 3). Moreover, all crosslinked films exhibited an integrated intensity of 1.1nm reflection lower than that of pure gelatin.

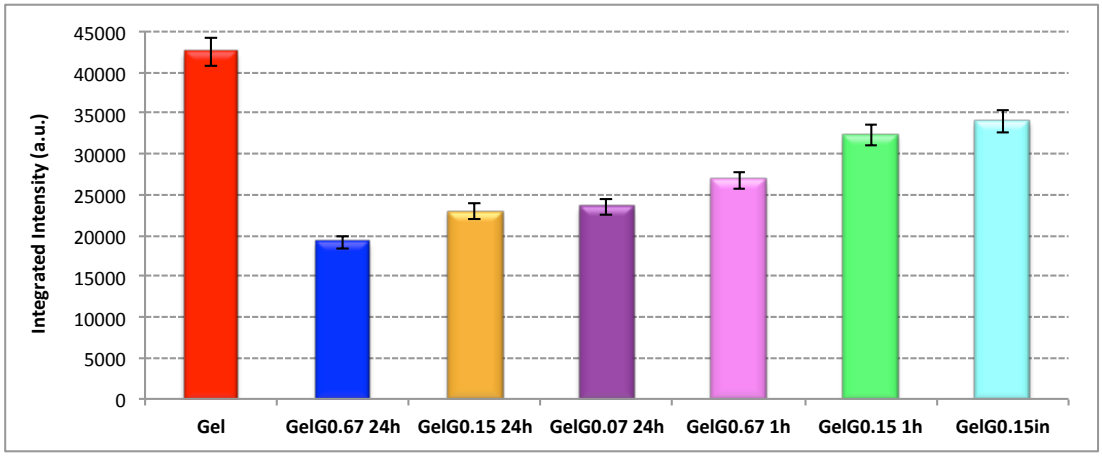

Figure 3. *Integrated intensity of the 1.1nm reflection obtained from the diffraction patterns of gelatin films crosslinked for 1h and 24h at different concentrations of genipin.*

2.3.2 Differential Scanning Calorimetry (DSC)

The DSC thermograms of the films prepared at different pHs were characterized by an endothermic peak associated with the helix–coil transition (Figure 4). The denaturation enthalpy associated with this peak is related to the relative amount of triple helical structure in the samples, and it is significantly lower for gelatin than collagen (Bigi et al. 2000; Achet et al. 2005).

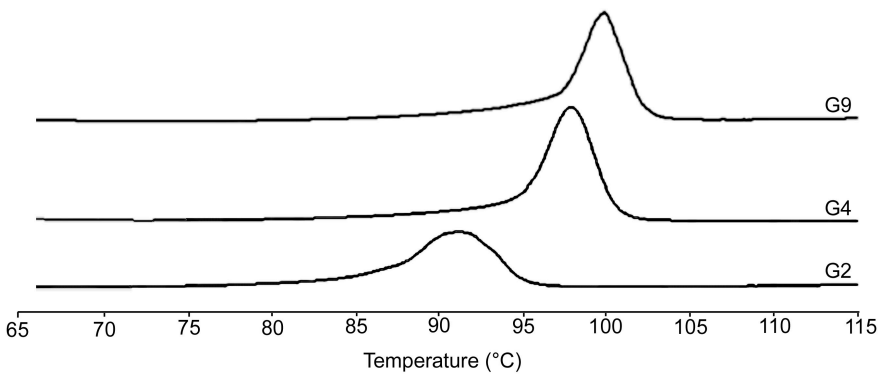

Figure 4. *DSC thermograms recorded for samples G2, G4, and G9.*

The denaturation temperature, T_D, and denaturation enthalpy, ΔH_D, of gelatin films prepared at different pHs are reported in Table 2.

Table 2. Denaturation temperature, T_D, and denaturation enthalpy, ΔH_D, of gelatin films examined in wet and air-dried conditions as a function of pH.

	Dried samples		Wet samples	
Sample	***T_D (°C)***	***ΔH_D (J/g)***	***T_D (°C)***	***ΔH_D (J/g)***
G2	91 ± 1	16 ± 1	n.d.	n.d.
G3	92 ± 1	20 ± 1	n.d.	n.d.
G4	97 ± 1	26 ± 1	34 ± 1	25 ± 1
Gel	98 ± 1	28 ± 1	36 ± 1	25 ± 1
G6	96 ± 1	28 ± 1	37 ± 1	25 ± 1
G7	95 ± 1	26 ± 1	37 ± 1	25 ± 1
G8	104 ± 1	28 ± 1	37 ± 1	27 ± 1
G9	103 ± 1	27 ± 1	36 ± 1	24 ± 1
G10	99 ± 1	23 ± 1	36 ± 1	21 ± 1
G11	97 ± 1	24 ± 1	34 ± 1	19 ± 1
G12	89 ± 1	16 ± 1	n.d.	n.d.

n.d. not determined

In dry state, ΔH_D exhibited an average value of 27±1 J/g in the central region of pH, which decreased to ~16±1 J/g in extreme acidic and basic conditions, indicating a reduction of the triple-helix content. Moreover, the films prepared at relatively high and low pHs displayed a reduced thermal stability, in agreement with the observed decrease of the denaturation temperature.
The variation of ΔH_D values with pH of rehydrated films (RH at 75%) was similar to those of the dry films, and the significant reduction of triple-helix content at extreme pHs was further confirmed by the fact that samples prepared at very high and low pH dissolved on rehydration. Analysis of rehydrated samples was possible, in fact, only for G4–G11. The T_D values of the rehydrated films did not show any significant modification in this pH range.

2.3.3 Termogravimetric Analysis (TGA)

Termogravimetric analysis (TGA) has been performed on gelatin film to evaluate structural water content, just after preparation of film and six months later (Figure 5).
Mass loss due to the production of aqueous vapor is revealed in both curves below 200°C. The second, greater, losses are ascribable to structural water.
After six months from film preparation, structural water percentage was lower (about 10%) than that of gelatin film analyzed just after preparation (about 13%). This indicates that, during time, a slow gradual release of humidity occurred, even if film was kept under controlled conditions.

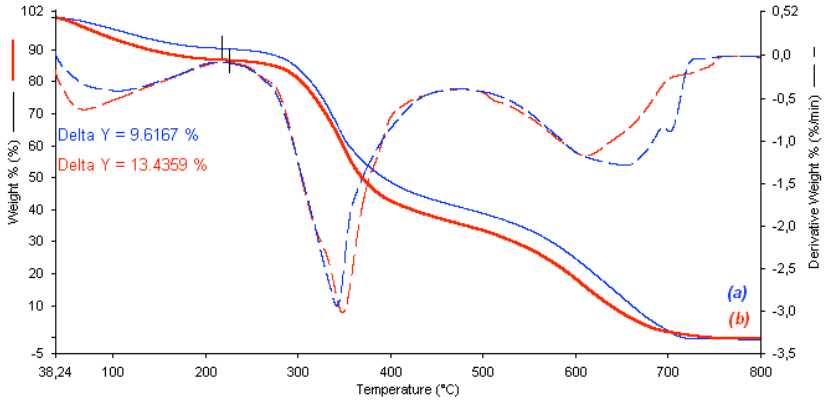

Figure 5. *Termogravimetric curves of a gelatin film after preparation (red line) and the same gelatin film, analyzed six months later (blue line).*

2.3.4 Mechanical tests

The mechanical properties of gelatin films as a function of pHs were tested under rehydrated conditions (RH at 75%). The stress–strain curves were used to evaluate the Young's modulus, E, the stress at break, σ_b, and the deformation at break, ε_b of the samples prepared at $4 \leq pH \leq 11$ (Table 3).

Table 3. Strain at break, ε_b, stress at break, σ_b, and Young's modulus, E, of rehydrated gelatin films as a function of pH.

Sample	*ε_b (%)*	*σ_b (MPa)*	*E (MPa)*
G4	270 ± 10^a	0.26 ± 0.04^a	0.13 ± 0.02^a
Gel	390 ± 60	1.3 ± 0.3	1.6 ± 0.3
G6	260 ± 30^b	1.0 ± 0.1	1.7 ± 0.3
G7	270 ± 60^c	1.3 ± 0.4	2.0 ± 0.3
G8	350 ± 20	1.6 ± 0.3	1.8 ± 0.3
G9	340 ± 60	1.6 ± 0.3	2.3 ± 0.5
G10	400 ± 60	1.7 ± 0.3	1.6 ± 0.5
G11	440 ± 40	0.33 ± 0.08^b	0.08 ± 0.01^b

Each value is the mean of ten determinations and is reported with its standard deviation.
ε_b: ^{a}G4 versus G8, G10, G11, $p<0.001$; ^{b}G6 versus G8, G10, G11, $p<0.001$; ^{c}G7 versus G11, $p<0.001$.
σ_b: ^{a}G4 versus Gel, G6, G7, G8, G9, G10, $p<0.001$; ^{b}G11 versus Gel, G6, G7, G8, G9, G10, $p<0.001$.
E: ^{a}G4 versus Gel, G6, G7, G8, G9, G10, G11, $p<0.001$; ^{b}G11 versus Gel, G6, G7, G8, G9, G10, $p<0.001$.

The values of Young's modulus and stress at break did not vary significantly for most of the samples, whereas G4 and G11 samples displayed significant lower E and σ_b values. The extensibility of the films increased at relatively high values of pH, and ε_b reached a value of 440 ± 40 at pH 11. The almost constant values of these parameters in the range of pH 5–9 were in agreement with X-ray diffraction and DSC results.
To determine how crosslinking process could affect the properties of gelatin films prepared at different pH values, three different samples were chosen: pH7, within the range where triple helix content and mechanical properties of the films are almost constant, pH4 and pH11 that are two values outside this range. Samples were crosslinked with 0.67% genipin for 24h, as described above (see paragraph 2.1.2). The mechanical and thermal

properties of crosslinked gelatin films, at different pHs, are reported in Table 4.

Table 4. Denaturation temperature, T_D, and denaturation enthalpy, ΔH_D, of air-dried crosslinked films; strain at break, ε_b, stress at break, σ_b, and Young's modulus, E, of rehydrated films.

Sample	T_D (°C)	ΔH_D (J/g)	ε_b (%)	σ_b (MPa)	E (MPa)
G4G0.67 24h	99 ± 1	15 ± 1	26 ± 4	1.3 ± 0.3	4.5 ± 0.5
G7G0.67 24h	99 ± 1	16 ± 1	21 ± 3	1.4 ± 0.2	6.0 ± 0.6
G11G0.67 24h	99 ± 1	11 ± 1	25 ± 3	0.8 ± 0.1[a]	3.5 ± 0.3[a]

σ_b: [a]G11G0.67 24h versus G4G0.67 24h, G7G0.67 24h, $p<0.001$.
E: [a]G11G0.67 24h versus G4G0.67 24h, G7G0.67 24h, $p<0.001$.

It is known that crosslinking treatment provokes a decrease in denaturation enthalpy, usually attributed to a reduction in hydrogen bonding (endothermic) and a simultaneous increase in the covalent crosslink processes (exothermic) (Bigi et al. 2001). In agreement, the values of denaturation enthalpy, ΔH_D, were significantly lower than those obtained for non-crosslinked films (cf. Table 2 and Table 4).

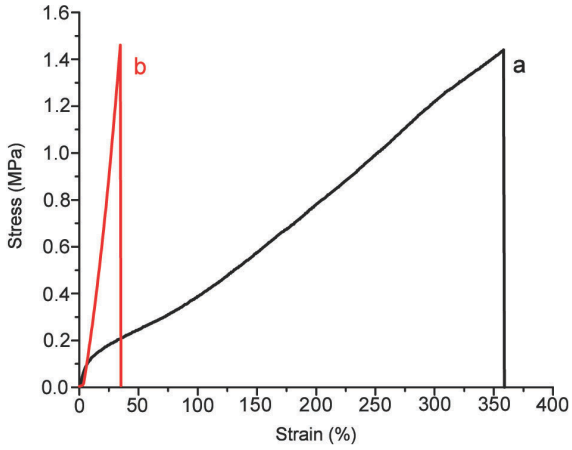

Figure 6. *Typical stress–strain curves of G7 (a) and G7G0.67 24h (b) films.*

Furthermore, crosslinking dramatically influence mechanical properties. Figure 6 reports typical stress-strain curves for G7 and G7G0.67 24h.
It is evident how genipin crosslinking caused a marked reduction in the extensibility of all the films, so that the ε_b values were slightly >20% (Table 4). The stress at break of the G7G0.67 24h films was similar to that found for G7 films, whilst the values of stress at break of the films prepared at pHs 4 and 11 increased significantly after crosslinking (cf. Table 3 and Table 4).
The values of Young's modulus, E, of crosslinked gelatin films were much greater than those recorded for non-crosslinked films. Young's modulus, E, was almost triple in the case of G7G0.67 24h films, and the increase was even greater for the G4G0.67 24h and G11G0.67 24h films.
The extent of crosslinking, calculated from the moles of free ε-amino groups per gram of gelatin (see paragraph 2.2.4), displayed a mean value of 95 ± 3%.

2.3.5 Swelling

As it known, gelatin is soluble in aqueous solution, and a few minutes of storage in physiological solution are sufficient to induce considerable swelling of the films (about 1000% after 3h). Triple helix content of gelatin influences absorption of physiological solution (Bigi et al. 2001). Figure 7 shows that the degree of swelling decreases on increasing genipin concentration, down to values of about 200%. The effect of crosslinking is remarkable even at very low genipin concentrations.

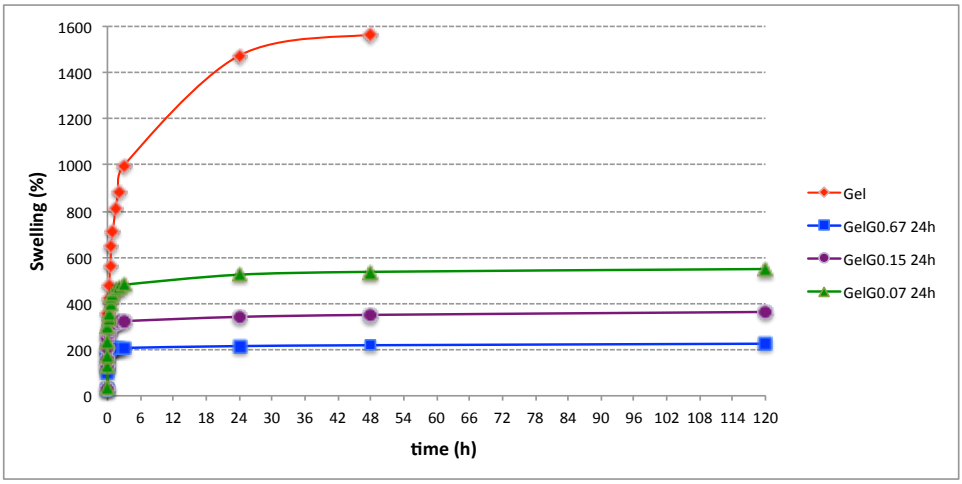

Figure 7. *Swelling curves of gelatin films (red line) and crosslinked gelatin films treated with genipin solutions at different concentrations.*

Figure 8 compares the swelling behavior of gelatin films crosslinked for different periods of time. As expected, time of crosslinking and genipin concentration displayed a synergic action on swelling.
Gelatin films crosslinked with the highest genipin concentration for 1h (GelG0.67 1h) and films treated with 0.15% genipin solution for 24h (GelG0.15 24h) showed the same swelling behavior in physiological solution. Moreover, no differences were observed when crosslinking was performed using 0.15% genipin solution for 24h (GelG0.15 24h) or by adding genipin to gelatin solution before gelling (GelG0.15in).

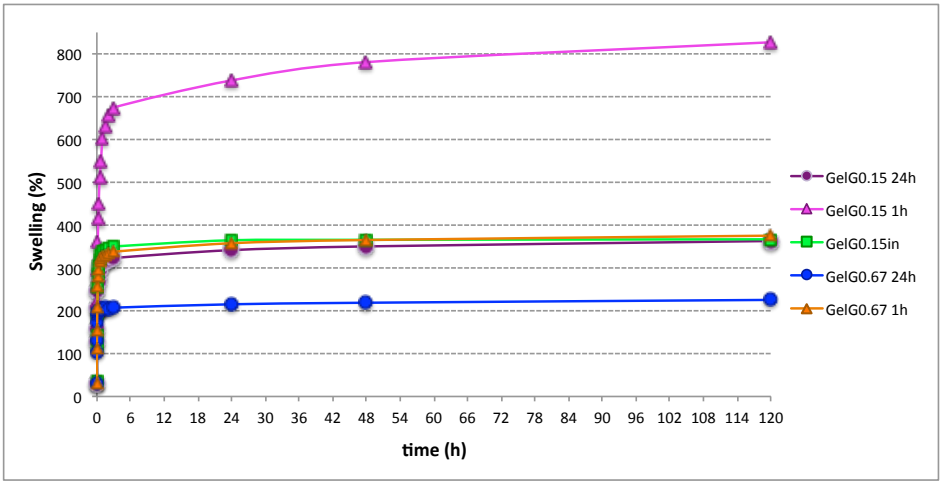

Figure 8. *Swelling curves of gelatin crosslinked at different condition.*

2.3.6 Release of gelatin

Gelatin release from films prepared under different conditions was investigated as function of the storage time in PBS solution at 37°C (Table 5). Considerable amounts of gelatin were released after 1 week from films crosslinked with the lowest genipin concentration even if crosslinking was prolonged for 24h.
In agreement with the results of swelling analysis, samples GelG0.67 1h and GelG0.15 24h released the same percentage of gelatin (about 60%) even if the release displayed by the former seemed slower during the first three weeks.
There were no appreciable differences in quantities of gelatin released from crosslinked films obtained by adding genipin in gelatin solution or by treating gelatin films for 24h with genipin solution at the same concentration.

Table 5. Gelatin release (wt%) from crosslinked films at different genipin concentrations and time of crosslinking process as a function of the storage time in PBS solution at 37°C. Each value is reported with its standard deviation.

Sample	*6h*	*1 day*	*7 days*	*14 days*	*21 days*	*28 days*	*35 days*
Gel	95.3 ± 0.9	c.d.					
GelG0.67 24h	10.3 ± 1.2	12.0 ± 0.6	16.1 ± 0.5	16.2 ± 0.3	15.4 ± 2.3	15.9 ± 1.5	15.7 ± 2.2
GelG0.15 24h	8.5 ± 1.1	12.2 ± 1.5	16.2 ± 2.5	21.2 ± 2.9	25.05 ± 6.13	57.3 ± 2.6	62.7 ± 10.0
GelG0.07 24h	16.9 ± 1.6	26.1± 0.8	62.6 ± 1.6	96.6 ± 4.4	c.d.		
GelG0.67 1h	22.2 ± 0.6	29.1 ± 1.3	44.4 ± 0.5	45.1 ± 0.8	48.3 ± 1.9	49.8 ± 5	57.6 ± 5.2
GelG0.15 1h	37.8 ± 4.9	83.7 ± 3.2	90.3 ± 2.3	91.7 ± 4.4	93.1 ± 0.5	c.d.	
GelG0.15in	23.3 ± 0.5	28.6 ± 0.5	32.3 ± 1.3	32.1 ± 3.3	35.9 ± 3.0	43.3 ± 1.6	48.2 ± 4.3

c.d. completely dissolved

2.3.7 Wettability

Wettability is the capacity of a liquid to keep contact with a solid surface through intermolecular interactions (Figure 9).

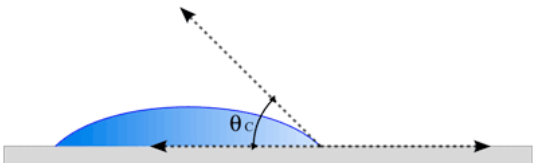

Figure 9. *Example of contact angle of a drop on an ideal surface.*

Figure 10 shows the values of contact angle, measured with a water drop at r.t., on the different samples. The data indicate that crosslinking did not significantly affect hydrophilicity of gelatin film. The mean value of contact angle was 81 ± 6.

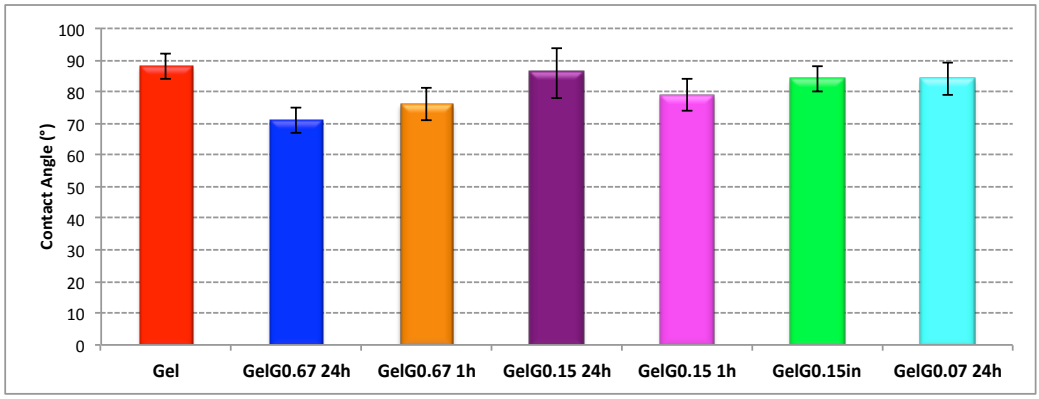

Figure 10. *Contact angle of gelatin film (red bar) and gelatin films crosslinked at different genipin concentrations and time of crosslinking. Each value is the mean of 12 determinations and is reported with its standard deviation.*

2.3.8 Cytotoxicity in vitro tests

Crosslinking can affect the biocompatibility of gelatin-based materials. Genipin is known to exhibit a lower toxicity than other crosslinking agents (Tsai et al., 2000; Sung et al., 1999). Genipin crosslinked electrospun gelatin nanofibers have been found to display good cell viability and adhesion (Panzavolta et al. 2011). However, cell behavior can be affected by morphology as well (Guarino et al., 2011). Therefore, *in vitro* tests were carried out on genipin crosslinked films (G7G0.67 24h). Proliferation of L929 fibroblast cultured for 48 h in direct contact with cross-linked gelatin films was found to be significantly greater than on CRT(−)(Table 6).

Table 6. Fibroblast proliferation and LDH measure in fibroblast culture after 48h of incubation.

48-h tests	*WST1 (450/625 nm)*	*Proliferation% / CTR (-)*	*LDH (U/L)*
G7G0.67 24h	1.820 ± 0.183[a]	148 ± 15	12.61 ± 1.28
CTR(-) (DMEM)	1.227 ± 0.079	100 ± 6	16.50 ± 1.10
CTR(+) (phenol)	0.273 ± 0.009[b]	22 ± 1	143.31 ± 31.65[c]

Mean ± SD, n = 6 replicates.
[a]*G7G0.67 24h versus CTR(−), p<0.001.*
[b]*CTR(+) versus G7G0.67 24h, CTR(−), p<0.0001.*
[c]*CTR(+) versus G7, CTR(−), p<0.0001.*

Both G7G0.67 24h and CRT(−) were significantly different from CTR(+) cells, which suffered cytotoxicity in phenol solution. LDH is a cytoplasmic enzyme that is released in the culture medium by damaged cell membranes. The LDH released in the medium by G7G0.67 24h and CTR(−) was similar, while CTR(+) values were significantly different from other groups at all experimental times.

Table 7. Qualitative morphological grading of cytotoxicity.

Grades	Reactions	Condition of cultures
0	None	No cell lysis, no reduction of cell growth, and discrete intercytoplasmatic granules.
1	Slight	Not more than 20% of the cells are round, loosely attached, and without intercytoplasmatic granules, or show changes in morphology; occasional lysed cells, slight growth inhibition.
2	Mild	Not more than 50% of the cells are round, devoid of intercytoplasmatic granules, cell lysis, and not more than 50% of growth inhibition.
3	Moderate	Not more than 70% of the cells are round and lysed, more than 50% of growth inhibition.
4	Severe	Nearly complete or complete destruction of the cell layer.

Cells were also stained with neutral red vital dye for evaluation of cell morphology. Images of neutral red stained cells on G7G0.67 24h, CTR(−), and CTR(+) were recorded after 48 h (Table 7 and Figure 11). Fibroblast on the CTR(+) group did not take up the stain, because there were no viable cells, which was also revealed by their rounded shape: the cell layer was completely destroyed. In contrast, the fibroblast cells in G7G0.67 24h and CTR(−) culture were regular, numerous, and stained well. A normal morphology, with well-defined margins of cell membranes and elongated shapes, was observed.

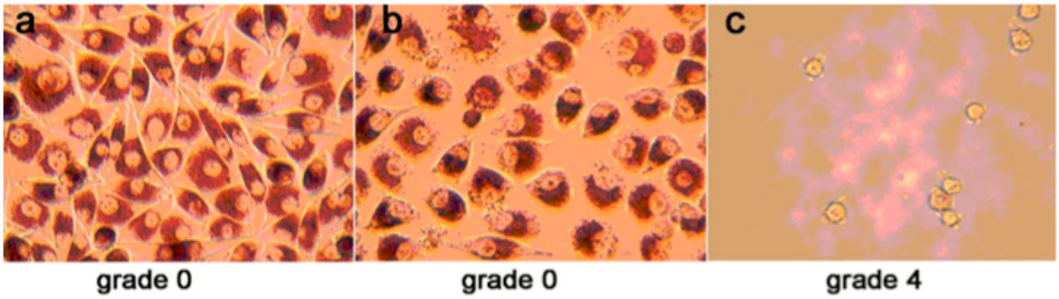

Figure 11. *Neutral red stained cells on (a) G7G0.67 24h, (b) CTR(−), and (c) CTR(+) at 48h evaluated according to Table 7 grading.*

2.4 Montmorillonite-Gelatin composite films

2.4.1 X-ray diffraction analysis

X-ray diffraction (WXRD) analysis was used to measure modifications of montmorillonite (MMT) and gelatin structure in the composite films. Figure 12 shows the XRD patterns of pristine clay (purple line) and gelatin film (grey line), overlapped.

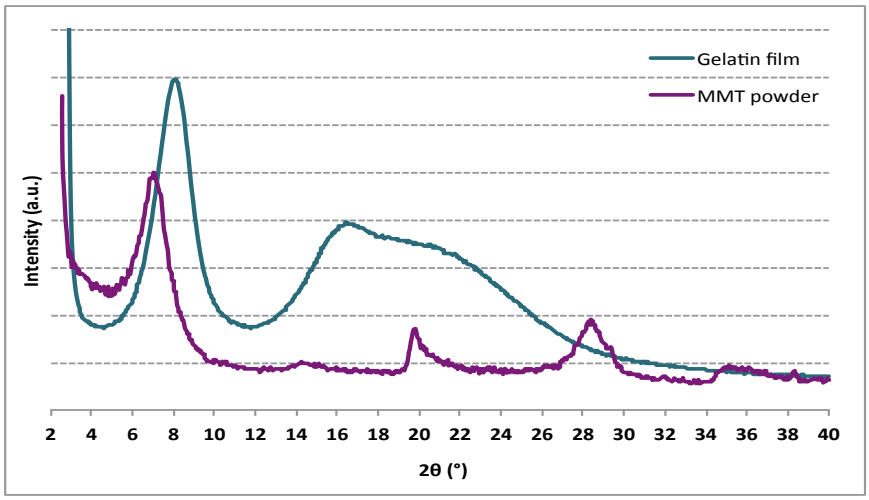

Figure 12. *X-ray diffraction patterns of gelatin film (grey line) and montmorillonite (MMT) (purple line).*

The main peak in the diffraction pattern of the MMT, at about 7° of 2θ, is attributed to the formation of the interlayer spaces by regular stacking of the silicate layers along the (001) direction (Tran et al., 2005). Peaks included in the range 15°-35° of 2θ have not been investigated in this work.
In the XRD pattern of gelatin film, the reflection at about 7.8 of 2θ, which is close to the main MMT peak, is associated to the diameter of the triple helix (see paragraph 2.3.1), whilst the broad band in the range 12°-30° of 2θ is related to peptide bonds.

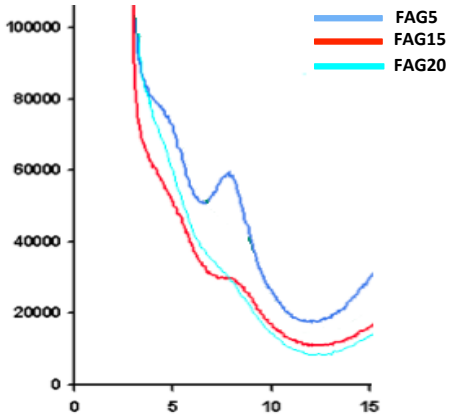

Figure 13. *X-ray diffraction patterns of gelatin films containing different MMT concentration.*

XRD patterns of composites films changed dramatically in comparison with pristine MMT and gelatin film (Figure 13). The peak of montmorillonite

shifted to lower angle (from 7° to about 4° of 2θ). Interlayer distance of MMT, calculated on these values, increases from 6.5 Å to about 8.8 Å. This change is explained with the possibility of intercalation of gelatin chains into MMT layers, which involves the increase of interlayer distance.
Measure was carried out on accurately dried composite films so the presence of structural water, which could influence the peak, is excluded. At high clay concentration, the 7°of 2θ peak is no longer appreciable, which can be ascribed to a transition from an intercalated to an exfoliated inner structure (Figure 14) (Alexandre et al., 2000). At the same time, increasing amounts of clay in gelatin films caused a gradual decrease of the relative intensity of the 1.1nm reflection, in agreement with a reduction of triple helix content. As a consequence, the renaturation level of gelatin in composite films reduced on increasing clay content.

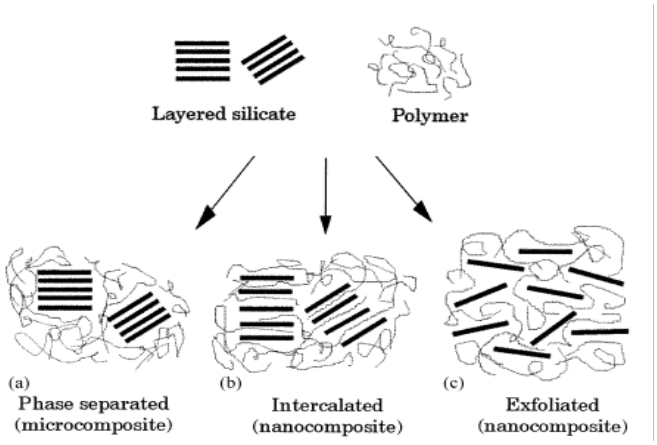

Figure 14*. Schematic representation of the three ideal interactions between gelatin and MMT.*

2.4.2 Differential Scanning Calorimetry (DSC)

The results of XRD investigation were supported by DSC analysis. The values of denaturation temperature, T_D, and denaturation enthalpy, ΔH_D, of MMT-gelatin composite films, examined in rehydrated (RH at 75%) and air-dried conditions are shown in Table 8.

Table 8. Denaturation temperature, T_D, and denaturation enthalpy, ΔH_D, of MMT-gelatin composite films examined in wet and air-dried conditions as a function of clay concentration.

	Dried samples		Wet samples	
Sample	***T_D (°C)***	***ΔH_D (J/g)***	***T_D (°C)***	***ΔH_D (J/g)***
Gel	94 ± 1	32 ± 1	36 ± 1	21 ± 1
FAG5	95 ± 1	28 ± 1	36 ± 1	14 ± 1
FAG15	94 ± 1	18 ± 1	37 ± 1	8 ± 1
FAG20	97 ± 1	17 ± 1	37 ± 1	8 ± 1

In both conditions, enthalpy values decreased on increasing MMT content in the composites. Sample FAG20 exhibited a decrease of ΔH_D of about 40% with respect to pure gelatin. As seen before (paragraph 2.3.2), the DSC

thermogram of gelatin is characterized by an endothermic peak associated to the denaturation process. The value of ΔH_D is strictly related to the triple helix content of gelatin sample. The observed decrease of ΔH_D confirms a remarkable reduction of gelatin renaturation level with the increase of MMT content. Denaturation temperature did not change as a function of MMT-gelatin films composition.

2.4.3 Mechanical tests

The mechanical properties of gelatin films were tested in dry conditions as a function of MMT content. Stress–strain curves were used to evaluate the Young's modulus, E, the stress at break, σ_b, and the deformation at break, ε_b of the samples (Table 9).

Table 9. Strain at break, ε_b, stress at break, σ_b, and Young's modulus, E, of gelatin and MMT-gelatin composite films tested in dry conditions.

Sample	*σ_b (MPa)*	*E (GPa)*	*ε_b (%)*
Gel	79 ± 9	2.1 ± 0.3	14 ± 4
FAG5	85 ± 5	1.8 ± 0.5	18 ± 4
FAG15	86 ± 9	3.7 ± 0.5	11 ± 2
FAG20	82 ± 8	4.5 ± 0.5	8 ± 2

The Young's modulus, E, increased with the amount of MMT while the deformation at break, ε_b decreased. No significant differences in the stress at break, σ_b, were observed. The increase of E as a function of clay content, demonstrated that MMT acts as reinforcement in composite films. In agreement, the Young's modulus of sample FAG20 was 4.5 GPa against 2.1 GPa of pure gelatin film.
The effect of crosslinking on gelatin-MMT composite films was tested at low genipin concentrations, namely 0.07 and 0.15%. The Young's modulus, E, the stress at break, σ_b, and the deformation at break, ε_b of crosslinked gelatin and MMT-gelatin composite films are shown in Table 10 and in Table 11. All samples have been tested in rehydrated conditions.

Table 10. Strain at break, ε_b, stress at break, σ_b, and Young's modulus, E, of gelatin and MMT-gelatin composite films, maintained at RH = 75%, crosslinked with genipin at a concentration of 0.07%.

Sample	*σ_b (MPa)*	*E (MPa)*	*ε_b (%)*
GelG0.07 24h	1.2 ± 0.2	1.3 ± 0.1	60 ± 5
FAG5 G0.07	1.34 ± 0.30	2.18 ± 0.28	54 ± 1
FAG15 G0.07	1.49 ± 0.18	3.30 ± 0.53	51 ± 5
FAG20 G0.07	0.73 ± 0.26	2.09 ± 0.14	45 ± 14

Table 11. Strain at break, ε_b, stress at break, σ_b, and Young's modulus, E, of gelatin and MMT-gelatin composite films, maintained at RH = 75%, crosslinked with genipin at a concentration of 0.15%.

Sample	σ_b *(MPa)*	*E (MPa)*	ε_b *(%)*
GelG0.15 24h	0.8 ± 0.3	1.5 ± 0.1	39 ± 8
FAG5 G0.15	1.30 ± 0.46	2.59 ± 0.37	42 ± 10
FAG15 G0.15	1.12 ± 0.34	3.75 ± 0.38	29 ± 8
FAG20 G0.15	1.11 ± 0.31	4.47 ± 0.29	36 ± 10

The results obtained with 0.15 % genipin (Table 11) put into evidence the synergic effect of crosslinking and clay reinforcement, in agreement with the high E value of sample FAG20 G0.15 (4.47 MPa). At variance, samples treated with 0.07% genipin did not show a linear behavior. By comparing samples FAG15 G0.07 and FAG20 G0.07 (Table 10), the former exhibited a Young's modulus, E, higher than the latter.

2.4.4 Swelling

Swelling of the non-crosslinked and crosslinked composite samples was tested in PBS. Figure 15, 16 and 17 compares the swelling curves of samples FAG5, FAG15 and FAG20 non-crosslinked and crosslinked with different concentrations of genipin. Swelling decreased dramatically with the concentration of crosslinking agent.

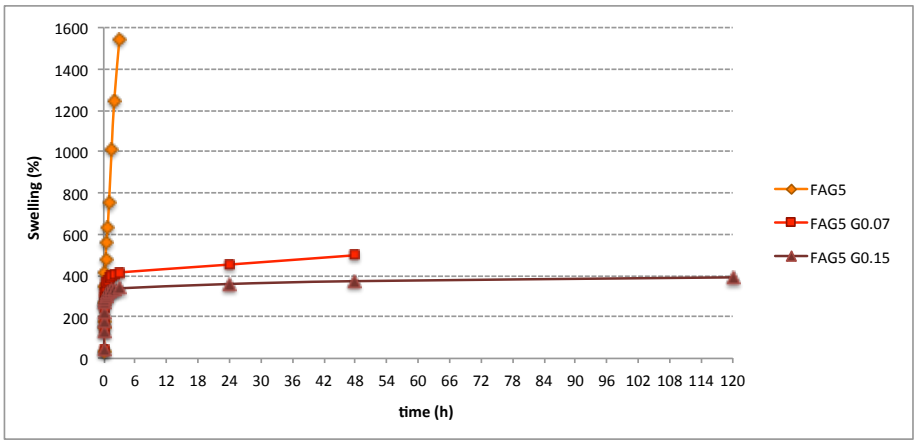

Figure 15*. MMT-gelatin composite films with 5% w/w content of clay.*

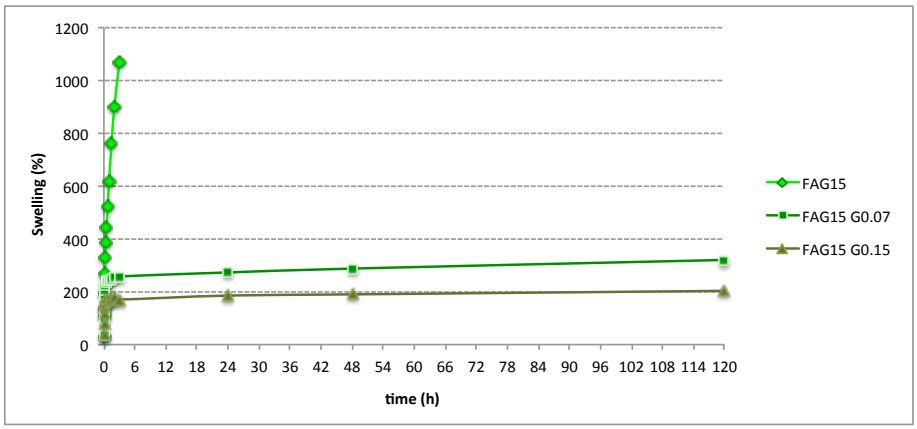

***Figure 16**. MMT-gelatin composite films with 15% w/w content of clay.*

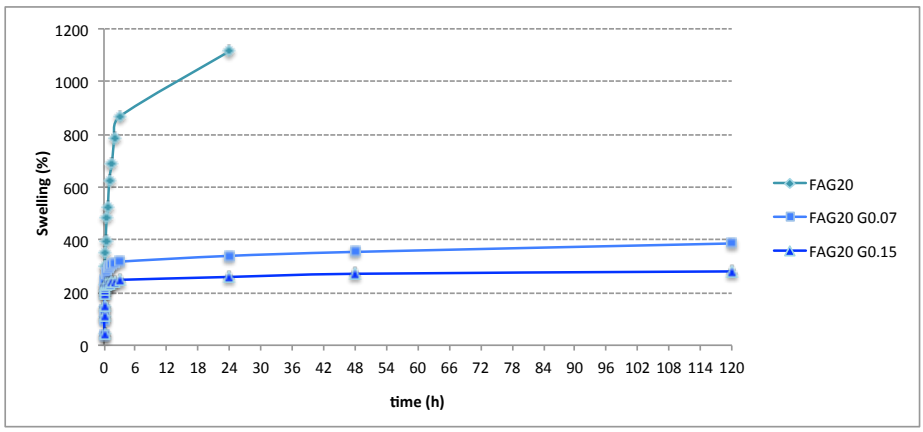

***Figure 17**. MMT-gelatin composite films with 20% w/w content of clay.*

Swelling of MMT-gelatin composite films confirmed the results of mechanical tests (see Table 9). Figure 18 shows the swelling curve of FAG20 against that of gelatin film. After the storage of samples for 24h in physiological solution, swelling of FAG20 was clearly lower (blue line) than that of pure gelatin, confirming the reinforcing action of clay (Li et al., 2003).

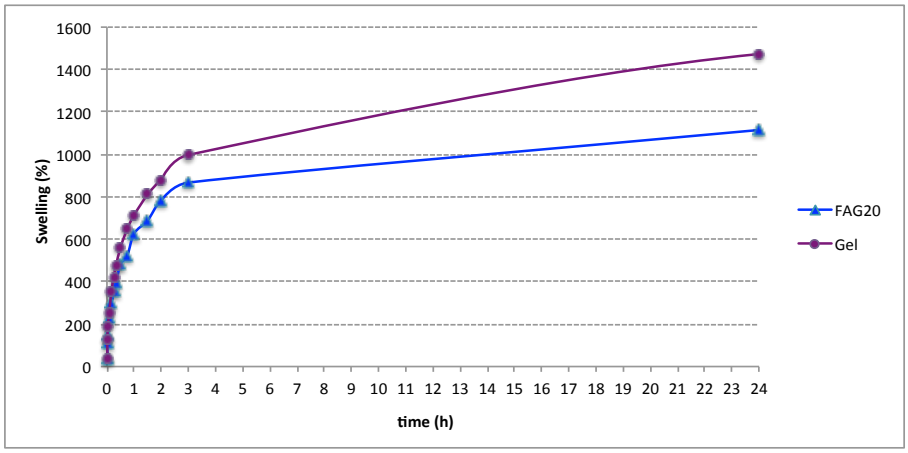

***Figure 18**. Swelling curves of gelatin and MMT-gelatin composite films containing 20% (w/w) of clay.*

2.4.5 Release of gelatin

MMT-gelatin composite films were stored in PBS solution at 37°C to investigate gelatin release as function of the storage time.
All samples containing 5% w/w of clay, dissolved completely in two weeks (Table 12). Some differences are observed, instead, in samples FAG15 and FAG20 in function of genipin concentration. Composite films crosslinked with 0.07% genipin, dissolved within three weeks, whilst, with the double genipin amount, samples kept until about one month.

Table 12. Gelatin release (wt%) from crosslinked MMT-gelatin composite films at different genipin concentration, as a function of the storage time in PBS solution at 37°C. Each value is reported with its standard deviation.

Sample	6h	1g	7gg	14gg	21gg	28gg
FAG5 G0.07	11.3 ± 1.9	21.7 ± 0.8	42.6 ± 0.2	c.d.		
FAG15 G0.07	9.7 ± 1.4	17.2 ± 1.0	51.9 ± 4.3	c.d.		
FAG20 G0.07	13.3 ± 0.6	20.9 ± 0.8	55.0 ± 4.5	75.3 ± 4.1	c.d.	
FAG5 G0.15	4.7 ± 0.6	7.3 ± 0.5	27.9 ± 0.7	c.d.		
FAG15 G0.15	3.7 ± 0.7	3.9 ± 0.8	19.4 ± 0.8	36.4 ± 12.2	85.8 ± 0.9	c.d.
FAG20 G0.15	4.2 ± 0.9	4.3 ± 0.8	23.2 ± 2.9	86.9 ± 1.8	96.8 ± 1.4	c.d.

c.d. completely dissolved

2.4.6 Wettability

The presence of montmorillonite seems to slightly influence hydrophilicity of the composite films (Figure 19). The results obtained for composite films crosslinked with 0.07 genipin showed that the value of contact angle increased on increasing MMT content. No appreciable difference, instead, could be appreciated among samples crosslinked with 0.15% of genipin.

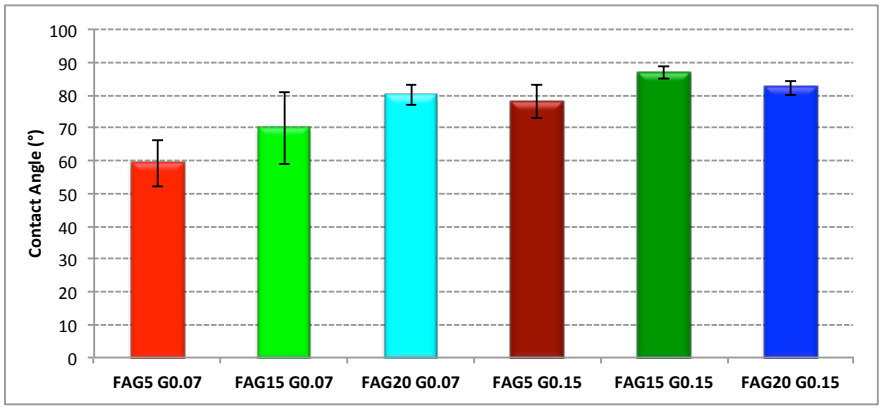

Figure 19. *Contact angle of MMT-gelatin composite films crosslinked at 0.07% and 0.15% genipin. Each value is the mean of 12 determinations and is reported with its standard deviation.*

2.4.7 Scanning electron microscopy

The microstructure of gelatin and MMT-gelatin films was observed through Scanning Electron Microscopy. All samples were previously fractured in the direction orthogonal to the surface, and oriented in such a way to observe the fractured surface.

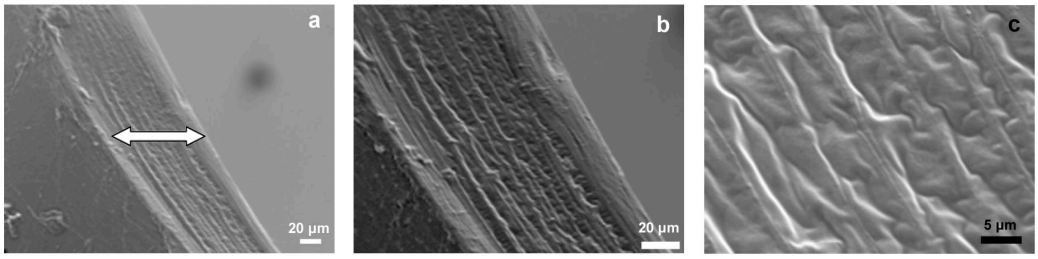

Figure 20. *SEM images of gelatin film. White arrow indicates fracture surface.*

As shown in Figure 20, the inner region of gelatin film is organized in regular layers, conversely to that one closer to the surface. This difference is due to the different time of drying of the surfaces in contact with air and Petri dishes, and along the film thickness.
Great differences in microstructure were observed between gelatin films and MMT-gelatin composite films (Figures 21, 22 and 23). The effect of clay on film morphology was evident already at low concentration (Figure 21c). Gelatin layers are no longer appreciable and the morphology inside the film was not very different from that of the surface, in agreement with a homogeneous dispersion of clay in gelatin matrix. Moreover, an organization in layer structure is visible, even if it is definitely more irregular than that of pure gelatin, especially in FAG5 (Figure 21b) and FAG15 (Figure 22b).

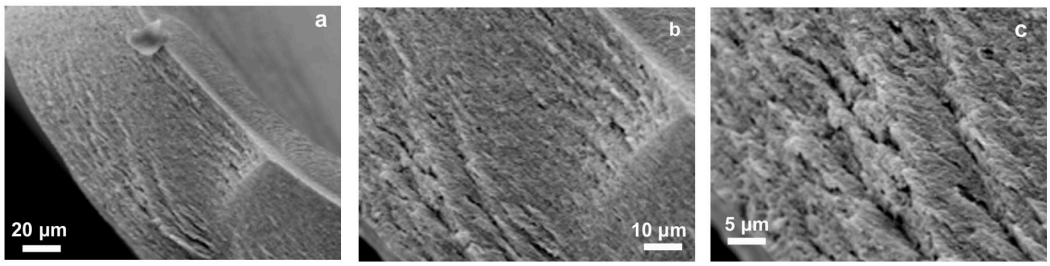

Figure 21. *SEM images of MMT-gelatin composite film, containing 5% (w/w) of clay (FAG5).*

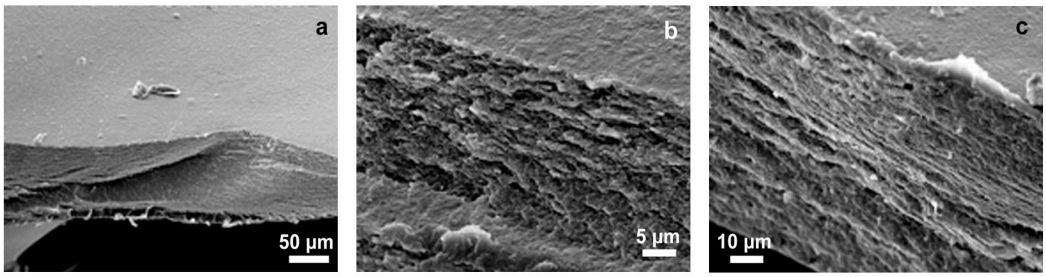

Figure 22. *SEM images of MMT-gelatin composite film, containing 15% (w/w) of clay (FAG15).*

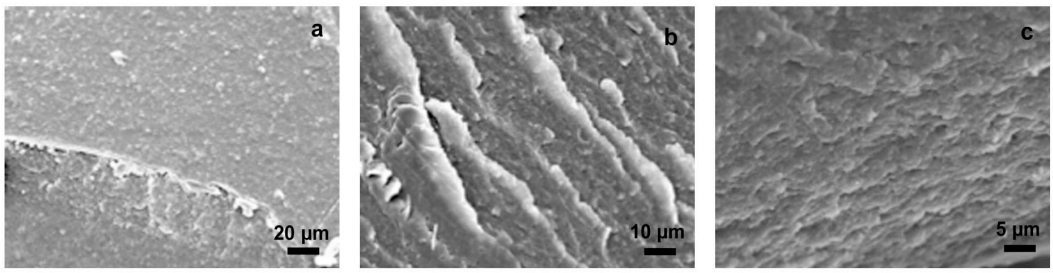

Figure 23. *SEM images of MMT-gelatin composite film, containing 20% (w/w) of clay (FAG20).*

All FAG samples were thicker than gelatin films (120-130µm), and thickness increased with increasing MMT content. The thickness of FAG5 was around 140-150µm, whilst FAG15 and FAG20 were slightly thicker (170-180µm).

Discussion

2.5 Gelatin films

As preliminary study, the influence of the pH of the film forming solution on the structural, as well as the thermal properties, of gelatin films was investigated.
Wide-angle X-ray diffraction analysis was employed to explore the renaturation level (relative triple-helix content) of the gelatin films. As matter of fact, the integrated intensity of the 1.1nm reflection can be used as a measure of the triple-helix content of gelatin (Bigi et al., 2000 and 2004; Boanini et al. 2010). In previous studies, the intensity of this reflection has been previously found to increase linearly with an increase of the Bloom index (Bigi et al., 2004) and, accordingly, with denaturation enthalpy of the different gelatins utilized for preparing the films. The results of this PhD thesis demonstrate a close relationship between the intensity of 1.1 nm reflection and the pH value of gelatin film forming solution. In particular, the integrated intensity was found to increase as pH raises up to 5, it remained almost constant over the pH range of 5–9 (from the unmodified pH of gelatin aqueous solution to the pI), and then it decreased as pH increased up to 12.
As expected, the variation of the denaturation enthalpy of dry samples with pH showed a similar trend (Figure 1).

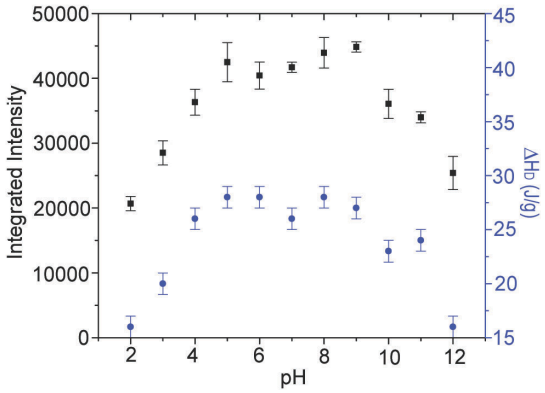

Figure 1. *Integrated intensity of the 1.1nm reflection (black squares), and ΔH_D (blue circles) values as a function of pH.*

These data indicate that the pH of the film forming solution did not significantly affect the triple-helix content of the gelatin films over the pH range of 5–9, whereas the triple-helix content decreased at higher or lower pH values. This phenomenon can be explained taking into account the process utilized for the preparation of A gelatin from pig skin: the acid process does not destroy the native collagen amide groups and, as a

consequence, gelatin molecules contain a greater number of ionizable basic than acidic groups and exhibit an isoionic point at a relatively high pH. At the isoionic point, the molecular chains contain equal positive and negative charges, which causes the maximum folding and contraction (Ward et al., 1954). As the pH changes from the pI, gelatin assumes a net negative or positive charge that causes electrostatic repulsion and unfolding of the triple-helix chains: the chains become more extended and the number of junction zones decreases leading to less rigid matrices. The isoionic (and isoelectric) point of the pigskin gelatin used in this work was pH 9, therefore, the triple-helix content of the films decreases at higher pHs. Similarly, pHs lower than 5 causes a reduction in the triple-helix content. Type A gelatin aqueous solutions display slightly acidic pH of 4.98 because of the presence of a greater number of ionizable basic groups. It follows that the pH adjustment performed in the range of 5–9 (that is from the pH of the gelatin aqueous solution to pI) is necessary to counterbalance the excess of ionizable basic groups; this does not significantly affect the triple-helix content. A different situation is observed, instead, at pH values higher than 9 and lower than 5 when major variations in the net charge occur, causing electrostatic repulsions and reduction of triple-helix content.

The Young's modulus and the stress at break did not vary significantly as a function of pH for most of the samples, whereas G4 and G11 samples displayed significant lower E and σ_b values (see paragraph 2.3.4 Table 3). The almost constant values of these parameters in the range of pH 5–9, are in agreement with the X-ray diffraction and DSC results, as well as with the previously reported constancy of dynamic storage modulus of gelatin gels in the pH range from 5 to 8.3 (Eysturskard et al, 2009).

The influence of crosslinking with the naturally occurring agent genipin on gelatin properties was investigated, in order to optimize the crosslinking procedure. The efficacy of genipin as crosslinking agent is well known from recent literature (Bigi et al., 2002; Chang et al., 2003). XRD investigation was carried out on crosslinked gelatin films, as well as during the gelling process of gelatin in presence of genipin. The results showed that crosslinking greatly influences the relative intensity of 1.1nm reflection, and therefore the renaturation process of gelatin (see paragraph 2.3.1 Figure 2 and 3).

Gelatin films were crosslinked with genipin solutions at different concentration for different periods of time: 1 and 24 hours. In both cases, and as observed before (Panzavolta et al., 2011; Bigi et al., 2002), crosslinking provoked a dramatic change in the stiffness of the gelatin films. Genipin provided covalent crosslinks which caused a marked reduction in the extensibility of all the films (see paragraph 2.3.4 Figure 6): the ε_b value recorded for sample G7G0.67 24h was about 20%, whilst it amounted to about 350% for non-crosslinked gelatin film G7. . The values of Young's modulus of the crosslinked gelatin films were much higher than those of the non-crosslinked films, while strain at break was not significantly influenced by crosslinking.

Genipin concentration and crosslinking time greatly affected swelling behavior and the percentage of gelatin release in physiological solution. Swelling was found to decrease with the increase of genipin concentration and gelatin films with tunable properties could be obtained by changing concentration and crosslinking time (see paragraph 2.3.5 Figure 7). In

agreement, release tests showed that after about one month sample GelG0.67 24h released not even 20% of gelatin (see paragraph 2.3.6) whilst gelatin films crosslinked for 24h but with the lowest genipin concentration were almost dissolved after two weeks. The denaturation enthalpy, ΔH_D, was significantly reduced with respect to the non-crosslinked films, in agreement with the reduction in hydrogen bonding (endothermic) and to a simultaneous increase in the covalent crosslinking (exothermic) processes induced by crosslinking (Bigi et al., 2001).
Preliminary *in vitro* tests revealed that fibroblast cells cultured on sample G7G0.67 24h exhibited a normal morphology, with well-defined margins of cell membranes and elongated shapes with a classification of grade 0 from the qualitative morphological grading of cytotoxicity, and indicated good cell proliferation and viability.

2.6 Montmorillonite-Gelatin composite films

In bio-mineralization processes where silica is the main deposited inorganic phase, protein-silica interactions are prevalently due to the hydrogen bonds between silanol groups present in silica and carboxyl and amine groups of polypeptides (Smitha et al., 2007). In silica belonging to clay family, the mechanisms that control assembly between polypeptides and silica layers are mainly attributed to electrostatic interactions between protein chains and clay lamellae as well as to strong van der Waals forces.
Intercalation of gelatin chains usually occurs through a mechanism of ionic exchange (Ruiz-Hitzky et al., 2005; Zheng et al., 2003). This kind of reaction is promoted when the pH of gelatin solution is below its IEP value. Amine groups are positively charged and allow the substitution of cations in mineral layers with protein chains. Intercalation, similarly to hydration, involves an increase of interlayer distance along the c-axis, as shown by means of XRD analysis (Zheng et al., 2002), as well as an improvement of mechanical properties and thermal stability of bio-nanocomposite (Zhuang et al., 2007; Zheng et al., 2007; Xu, Zheng et al., 2006). The results obtained here demonstrate that it is possible to prepare gelatin-montmorillonite composite films with tunable properties as a function of clay content.
Analysis of film fractured surface put into evidence a layered structure inside the composite films, with the layers almost parallel to film surface. The lack of aggregates on film surface, even at great magnification, indicated a good dispersion of the clay inside the composites. X-ray diffraction analysis of films at different clay content, demonstrated that MMT incorporation provokes noticeable variations of the X-ray diffraction patterns. The patterns of films at low MMT content evidenced a shift of the characteristic low-angle peak of montmorillonite from 7° of 2θ to about 4°, related to an increase of (001) layer distance from about 6.5 Å to 8.8 Å, in agreement with the introduction of gelatin chains among clay layers. On the other hand, the low-angle peak is practically absent in X-ray diffraction patterns of samples at greater clay concentration, namely FAG15 and FAG20. The lack of this peak, that is related to interlayer distance, suggests that relatively high MMT concentrations promote an exfoliated structure. The transition from an intercalated to an exfoliated MMT structure was accompanied by a decrease of the integrated intensity of 1.1nm reflection related to gelatin triple helix structure. It can be

hypothesized is that the presence of clay during gelling could interfere with, and inhibit, the concomitant partial triple helix renaturation of gelatin. In fact, the non-helical organization favors the penetration of gelatin chains among clay layers (Talibudeen et al., 1950). As a consequence, the renaturation level of gelatin in bio-nanocomposites reduces as MMT content increases.

This theory is well supported by DSC data. Thermograms of gelatin films are characterized by an endothermic peak associated with the denaturation process of the protein (see paragraph 2.3.2 Figure 4), and the denaturation enthalpy associated with this peak is strictly related to the relative amount of triple helical structure in the samples. The values of ΔH_D shown in paragraph 2.4.2 Table 8, calculated with respect to the effective amount of gelatin present in composite films, decrease as a function of clay content, both in dry state and in rehydrated conditions. On the other hand, clay did not seem to influence the thermal stability of gelatin films. Denaturation temperature T_D, in fact, did not change as a function of MMT-gelatin films composition. Despite of what previously observed (Bigi et al., 2002), the reduction of renaturation level of gelatin did not negatively influence the mechanical properties of bio-nanocomposite films. On the contrary, the values of the mechanical parameters of these films improved on increasing clay content; the Young's modulus E increased whereas the deformation at break, ε_b decreased on increasing MMT content. The observed trend confirms that clay acts as reinforcement in composite films (see paragraph 2.4.3 Table 9), in agreement with previous observations on bovine gelatin nanocomposites (Zheng et al., 2002) and with the results of swelling tests (see paragraph 2.4.4 Figure 18). The increase of the value of E at relatively high clay contents confirmed the best performance of exfoliated structure, (Chivrac et al., 2008; Rao et al., 2007). Wettability tests on gelatin-MMT composite films showed that the presence of montmorillonite slightly influence hydrophilicity of the films (see paragraph 2.4.6 Figure 19).

In the light of the good results obtained, further investigations were carried out with the aim to verify the possibility to improve the performances of gelatin-clay composite films through crosslinking with genipin. The results showed that even low concentrations of genipin, 0.07% and 0.15% w/v, can provoke a remarkable improvement of the mechanical properties of gelatin films; in particular, an increase of modulus E and an evident decrease of strain at break ε_b (see paragraph 2.4.3 Table 10 and 11) (Bigi et al., 2002).

In particular, the results obtained with 0.15 % genipin put into evidence the synergic effect of crosslinking and clay reinforcement, in agreement with the high E values of samples FAG15 G0.15 and FAG20 G0.15 (3.75 and 4.47 MPa, respectively). A further proof of the great stability of these samples was provided by the results of swelling in physiological solution at 37°C. In fact, samples FAG15 and FAG20, crosslinked with 0.15% of genipin, resisted for about almost three weeks at variance with all other samples, which dissolve within one-two weeks.

Chapter III

Foamed scaffolds enriched with calcium phosphate

Materials and Methods

3.1 Materials

The calcium solutions were prepared by dissolving $Ca(NO_3)_2 \cdot 4H_2O$ at a concentration of 18 mM (Ca solution), whereas $(NH_4)_2HPO_4$ at a concentration of 10.8 mM was used to prepare phosphate solutions (P solution). Demineralised water was always used to dissolve inorganic compounds. In both solutions, pH value was previously adjusted to 10 with ammonia.
For the preparation of the foamed scaffolds, type A gelatin (280 Bloom, Italgelatine S.p.A.) from pigskin was used.

3.1.1 Synthesis of calcium phosphates

Calcium phosphate powders were prepared from calcium and phosphate solutions by continuous fast precipitation method (Tadic et al., 2002). Ca and P solutions were stored in two glass vessels and mixed under controlled conditions: the rate of addition of the two mother solutions was regulated by a peristaltic pump (Ismatec Reglo Analog MS-4/6-160) and the temperature during the whole process was continuously maintained at the desired value. The suspension of precipitated calcium phosphate overflowed onto a Buchner funnel where water was immediately removed to prevent further crystallization. Morphology of the resulting inorganic phase is function of the temperature and the addition rate of the solutions into the reaction vessel.
At the end of the reaction, the material accumulated on the filter is removed and dried. Five different powders were obtained as a function of temperature, starting from 5°C up to 70°C, and addition rate, from 45 mL/min to 2.5 mL/min.
Samples were labelled using alphabetic letters, from the fastest reaction and lowest temperature (A - amorphous) to the highest temperature and the lowest addition rate (E - nanocrystalline).

3.1.2 Synthesis of calcium phosphate nanoparticles coated with Poly-Acrylic Acid (PAA)

The polymer-coated nanoparticles were prepared with a similar continuous fast precipitation method (Welzel et al., 2004) by mixing PAA, calcium and phosphate aqueous solutions. Two different PAA solutions, at a concentration of 2 mM and 0.2 mM, were used.
To prepare polymer-coated nanoparticles suspensions, all the solutions were simultaneously pumped in the reaction vessel for thirty seconds. Inorganic solutions were pumped both at a constant rate of 5 mL/min whilst addition rate of PAA solutions were varied from 2.5 mL/min to 20 mL/min.
Two sets of eight nanoparticles suspensions with different PAA/CaP ratio were obtained. Samples were labelled as PAA/CaP_x, where x is the PAA/CaP addition rate ratio.

3.1.3 Synthesis of crystalline hydroxyapatite

For the synthesis of crystalline hydroxyapatite (HA), 50 mL of 1.08M $Ca(NO_3)_2 \cdot 4H_2O$ solution was heated at 90 °C and 50 mL of 0.65M $(NH_4)_2HPO_4$ solution was added dropwise under stirring. The pH value of both solutions was previously adjusted to 10 with NH_4OH. After addition, calcium phosphate solution was centrifuged at 10^4 rpm for 10 min and repeatedly washed with distilled water. The product was dried at 37 °C overnight.

3.1.4 Preparation of foamed gelatin scaffolds enriched with calcium phosphates

Amorphous and nanocristalline calcium phosphate were used to prepare foamed gelatin scaffolds enriched with inorganic phase. The inorganic phase (calcium phosphates at different crystallinity or crystalline HA) was added to a 10% (w/v) gelatin solution at 55°C, at a concentration of 10% (w/v) with respect to the total volume. Foaming was obtained by maintaining the suspensions under constant stirring of about 700 rpm and temperature of 55°C, for 50 min. Then, 0.16% w/w of genipin (Wako, Japan), with respect to gelatin, was added to the reaction vessel to obtain crosslinked scaffolds. During the crosslinking process, foamed gelatin changed colour from white to azure. After that, the foams were deposited onto Petri dishes and allowed to gelify at 55°C for 2 hours. Hence, the samples were washed in 0.1 M glycine aqueous solution for 30 min, and rinsed in distilled water for 5 min. Finally, the samples were frozen in liquid N_2 for up to 10 min and then freeze-dried for 24 h at -44 °C and 0.3 mbar (Panzavolta et al., 2009).
The composite scaffolds were labelled according to their inorganic phase content: GEL_CaP_B, GEL_CaP_E and GEL_HA. Control samples of pure gelatin, labelled GEL, were prepared following the same procedure used for the composite scaffolds, without adding inorganic phase.

3.2 Methods

3.2.1 X-ray diffraction analysis

The precipitated calcium phosphate powders were studied by X-ray diffraction. XRD analysis was carried out by means of a D8 Advance, Bruker AXS powder diffractometer using CuKa radiation. Calcium phosphate were analysed in the 2θ range from 20° to 45° in transmission mode (capillary).
X-ray diffraction analysis of crystalline HA was carried out by means of a PANalytical X'Celerator powder diffractometer equipped with a monochromator in the diffracted beam. CuKα radiation was used (40 mA, 40 kV). The 2θ range was from 3° to 60° at a scanning speed of 0.75°/min.

3.2.2 Termogravimetric Analysis

Thermogravimetric analysis was carried out using a Netzsch STA 209 and was employed for quantitative analysis to detect carbonate content. The calcium phosphate samples were heated from 30°C up to 1200°C at a rate of 1°C/min, under dynamic O_2 atmosphere (50 ml/min). The samples weights were in the range 30-40 mg.

3.2.3 Elemental Analysis

Elemental analysis of the inorganic powders was utilized to investigate the calcium/phosphate ratio present in samples obtained with continuous fast precipitation method. Calcium content was detected by atomic absorption spectroscopy whilst phosphate was analysed by UV-vis spectrophotometry.

3.2.4 Dynamic Light Scattering

Dynamic light scattering (DLS) of the PAA-coated CaP nanoparticles suspensions was performed with a Malvern Zetasizer (Nano ZS, 633 nm laser; Smoluchowski method). Zeta potentials were measured with a ZetaPlus Brookhaven instrument (676 nm laser; Smoluchowski method). Measures were carried out for all the samples at different times: just after suspensions preparation, after 24h and after one week, in order to investigate stability of the suspensions in time. DLS experiments were repeated three times each with three identically prepared samples.

3.2.5 Mechanical tests

Compression tests were performed on 1×1×1 cm composite scaffolds. Stress-strain curves were recorded using an INSTRON Testing Machine 4465 equipped with a 1 kN load cell and the Series IX software package. The loading rate was 1.0 mm/min. At least six specimens were tested for each sample, and data were reported as mean and standard deviations.

3.2.6 Scanning Electron Microscopy

Morphology of calcium phosphate powders was investigated by scanning electron microscopy (SEM) with a FEI Quanta 400 ESEM instrument in high vacuum. The morphological and microstructural characterization of the porous gelatin composite scaffolds was performed using a Hitachi S- 2400 scanning electron microscope operating at 15 kV.
All the specimens were sputter-coated with gold before examination.

3.2.7 Transmission Electron Microscopy

For TEM investigations of the morphology of crystalline HA, a small amount of powder was dispersed in ethanol and submitted to ultrasonication. A drop of the calcium phosphate suspension was transferred onto holey carbon foils supported on conventional copper microgrids. A Philips CM 100 transmission electron microscope operating at 80 kV was used.

3.2.8 Cytotoxicity *in vitro* tests

In vitro tests were performed on GEL, GEL_CaP_B, GEL_CaP_E and GEL_HA scaffolds. MG-63 human osteoblast-like cells were cultured in DMEM medium (Sigma, UK) supplemented with 10% FCS, and antibiotics (100 U/ml penicillin, 100 μg/ml streptomycin). Cells were detached from culture flasks by trypsinization, and cell number and viability were checked by trypan blue dye exclusion test.
MG-63 osteoblast-like cells were plated at a density of $2x10^4$ cells/ml in 24-well plates containing six sterile (γ- ray, 25kGy) samples for each biomaterial and for each experimental time. The same concentration of cells was seeded in empty wells as the control (CTR(−)) and in a 0.5% DMEM phenol solution that is recognized to be toxic for cell culture as positive control (CTR(+)). The plate was cultured in standard conditions, at 37°C ± 0.5 with 95% humidity and 5% CO_2 for 48h.
Cell proliferation and viability were assessed by WST1 (Roche Diagnostics GmbH, Manheim, Germany) colorimetric reagent test. WST1 solution (50μL) and 450μL of medium (final dilution: 1:10) were added to the cell monolayer, and the multiwell plates were incubated at 37°C for 4h. The supernatants were quantified spectrophotometrically at 450nm with 625nm as the reference wavelength. The WST1 was recorded as optical density (OD) and correlated with the cell number. The proliferation percent relative to CTR(−) was also reported.
At the end of experimental times, the supernatant was collected from all wells and centrifuged to remove any particulates for LDH measure. A biochemical test (LDH, MeDia IVD s.r.l., Forlì, Italy, lotto F13H) was performed. A 0.033% solution of Neutral Red stain (Sigma, UK) in culture medium was added to two wells for each group for 90 min at the end of experimental times.
Only viable cells were stained in cytoplasm, while dead cells did not. The cultures were examined by microscopy for a qualitative evaluation of cell morphology, and explanatory images were selected.

Statistical analysis

Statistical evaluation of data was performed using the software package SPSS/PC+ Statistics TM 10.1 (SPSS Inc., Chicago, IL USA). The data represented the mean of six replicates and were reported as the mean ± SD at a significance level of $p<0.05$. After having verified normal distribution and homogeneity of variance, a one-way ANOVA was performed for comparison between the groups.
In addition, Scheffé's post hoc multiple comparison tests were performed to detect significant differences between groups.

Results

3.3 Calcium phosphates

3.3.1 Synthesis of calcium phosphate

The apparatus employed for the continuous fast precipitation method (Tadic et al., 2002) consists of two glass thermostated reservoirs for calcium and phosphate solutions, a peristaltic pump that regulates the solutions flow, a pH electrode to monitor reaction conditions and a Buchner funnel, in which the suspension obtained from the mix of the two solutions, overflows. After precipitation, the water is immediately removed to prevent further crystallization. The schematic set-up of the apparatus is shown in Figure 1.

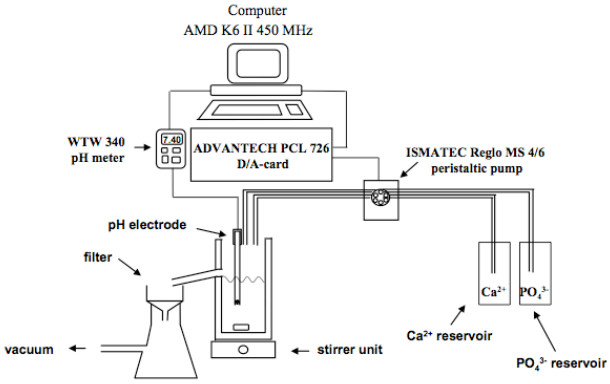

Figure 1. *Schematic set-up of the continuous crystallization apparatus (Tadic et al., 2002).*

This apparatus is able to continuously produce apatite powders under controlled conditions. Five powders were obtained, from the most amorphous A, obtained at 5°C with an addition rate of 45mL/min up to the most nanocrystalline E, at 70°C and 2.5 mL/min of addition rate. All the samples are reported in Table 1.

Table 1. Calcium phosphate powders obtained through the continuous fast precipitation method.

Sample	*T reaction (°C)*	*Addition rate (mL/min)*
A	5	45
B	r.t.	45
C	70	45
D	70	10
E	70	2.5

3.3.2 X-ray diffraction analysis

Calcium phosphate powders were investigated by wide-angle X-ray diffraction (WXRD) analysis as a function of temperature and addition rate. Samples A and B, obtained at the lowest temperatures and fastest addition, were clearly amorphous. At the highest temperature, by slowing down reaction speed, powders with more ordered structure were obtained (Figure 2). The diffraction pattern of sample E showed two very broad peaks at 26°of 2θ and 31°-34° of 2θ, that are typical for a poorly crystalline (nanocrystalline) hydroxyapatite.

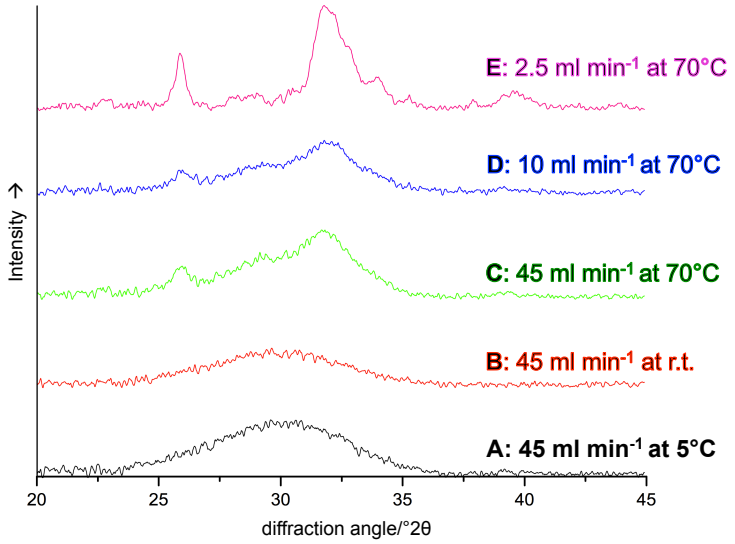

Figure 2. *X-ray diffraction patterns of CaP samples at different grade of crystallinity, obtained with the continuous fast precipitation method.*

3.3.3 Elemental Analysis

Some significant samples, with different morphology, were further analysed. Elemental analysis was utilized to investigate calcium and phosphate content in CaP powders and to evaluate their calcium/phosphate ratio.
Calcium was determined by atomic absorption spectroscopy and phosphate by spectrophotometry. The data are shown in Table 2.

Table 2. Elemental analysis of amorphous (B), scarcely crystalline (C) and nanocrystalline (E) calcium phosphate powders. Calcium was determined by atomic absorption spectroscopy and phosphate by spectrophotometry.; Ca/P ratios are also reported.

Sample	*Ca^{2+}*	*PO_4^{3-}*	*Ca/P ratio*
B	29.69	48.65	1.45
C	32.71	49.85	1.55
E	35.08	53.40	1.56

The theoretical molar ratio between calcium and phosphate in hydroxyapatite is 1.67. The experimental ratio is slightly lower than the theoretical one suggesting that the powders obtained through the method of continuous fast precipitation consists of calcium-deficient hydroxyapatite.

3.3.4 Termogravimetric Analysis

Thermogravimetric analysis was employed to determine carbonate content, which was evaluated from carbon dioxide released at temperatures higher than 500°C. The data are shown in Table 3.

Table 3. Carbonate content of the different samples evaluated from thermogravimetric analysis.

Sample	*CO_2(%)*	*CO_3^{2-}(%)*
B	1.20	1.63
C	1.13	1.54
E	1.39	1.90

3.3.5 Scanning Electron Microscopy

The microstructure of calcium phosphate powders was observed with scanning electron microscopy. In agreement with what observed by XRD analysis, the morphology of calcium phosphates clearly changed as a function of crystallinity. The amorphous sample B, exhibited a granular-shape distribution (Figure 3) whilst the sample E, which was the most nanocrystalline CaP obtained, had a structure completely different, with no presence of granules (Figure 5). An intermediate situation was observed for the sample synthesized at conditions of high temperature and high addition rate (sample C). In fact, in Figure 4, it is still possible to observe the presence of granules but they lie on a substrate very similar to that observed in nanocrystalline sample.

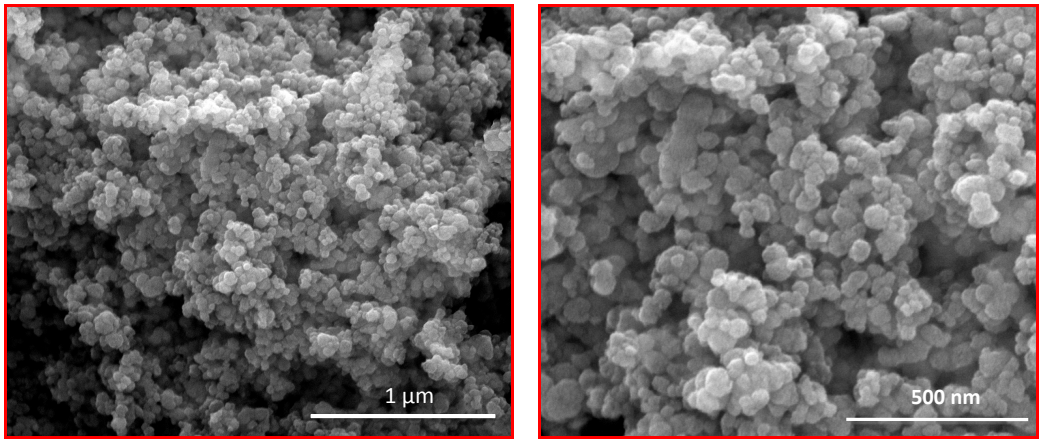

Figure 3. *SEM image of sample B, synthesized at r.t. and addition rate of 45 mL/min.*

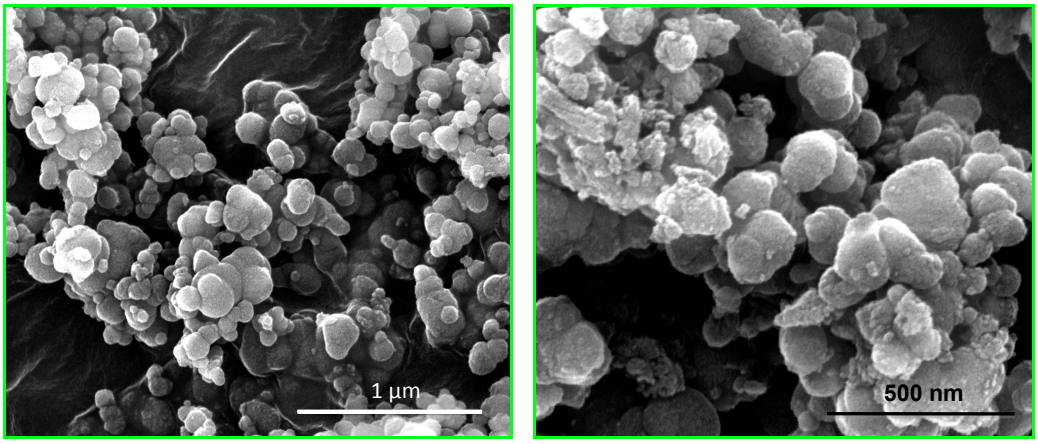

Figure 4. *SEM image of sample C, synthesized at 70°C and addition rate of 45 mL/min.*

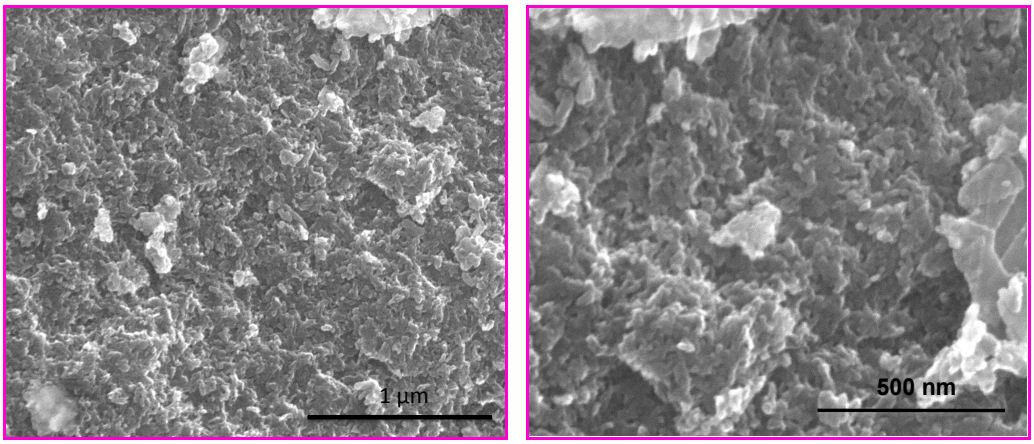

Figure 5. *SEM image of sample E, synthesized at 70°C and addition rate of 2.5 mL/min.*

3.4 Calcium phosphate nanoparticles coated with Poly-Acrylic Acid (PAA)

3.4.1 Synthesis of CaP nanoparticles coated with PAA

The continuous fast precipitation method was used also to prepare PAA-coated calcium phosphate nanoparticles. Calcium and phosphate solutions were mixed with a constant speed of 5 mL/min and the polymer solution was added with a second peristaltic pump, at a varying speed from 2.5 mL/min to 20 mL/min. Synthesis was carried out at room temperature.
The schematic set-up of crystallization and functionalization apparatus is shown in Figure 6.

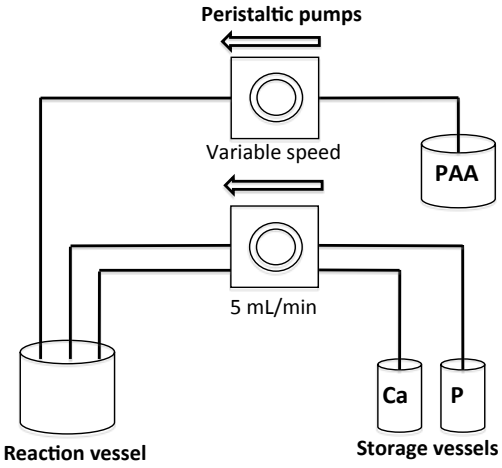

Figure 6. *Schematic set-up of the crystallization and functionalization apparatus.*

Table 4 reports the addition rates of polyacrylic acid solution used to obtain eight nanoparticles suspensions with different PAA/CaP ratio.

Table 4. PAA coated calcium phosphate nanoparticles, obtained with the continuous fast precipitation method. Addition rate of calcium and phosphate solutions are kept constant at 5 mL/min.

Sample	*Addition rate (mL/min)*
PAA/CaP_0.5	2.5
PAA/CaP_1	5
PAA/CaP_1.5	7.5
PAA/CaP_2	10
PAA/CaP_2.5	12.5
PAA/CaP_3	15
PAA/CaP_3.5	17.5
PAA/CaP_4	20

3.4.2 Dynamic Light Scattering

Dynamic light scattering (DLS) analysis was used to measure hydrodynamic diameter (Z-average) of the PAA-coated nanoparticles and their Zeta potential, whose value is related to the stability of nanoparticles suspensions (colloids).
The zeta potential indicates the degree of repulsion between adjacent particles. Colloids with high zeta potential (negative or positive) are electrically stabilized whilst colloids with low zeta potentials tend to coagulate or flocculate as outlined in the Table 4 (ASTM Standard 1985).

Table 5. Correlation between Zeta potential value and the stability of colloids.

Zeta potential (mV)	Stability behavior of the colloid
0 to ±5	Rapid coagulation/flocculation
±10 to ±30	Incipient instability
±30 to ±40	Moderate stability
±40 to ±60	Good stability
> ±61	Excellent stability

In Tables 6 the values of hydrodynamic diameter, the polydispersity index (PdI) and the Zeta Potential of CaP nanoparticles coated with 0.2mM PAA are reported.

Table 6. Dynamic light scattering data of the calcium phosphate nanoparticles coated with PAA at a concentration of 0.2mM.

Sample	*Z-average (nm)*	*PdI*	*Zeta potential (mV)*
PAA/CaP_0.5	265.7	0.250	-38.3
PAA/CaP_1	202.1	0.237	-34.9
PAA/CaP_1.5	201.9	0.267	-32.5
PAA/CaP_2	165.6	0.277	-25.9
PAA/CaP_2.5	136.0	0.270	-22.0
PAA/CaP_3	209.8	0.377	-37.7
PAA/CaP_3.5	119.6	0.393	-26.2
PAA/CaP_4	105.3	0.350	-2.05

PdI is dimensionless and indicates the validity of the values obtained with DLS analysis. A PdI value above 0.3 indicates that the measure is not good. As shown in Table 6, the samples with a high ratio PAA/CaP were less stable, probably because the excessive presence of polymer provoked an easier coagulation of nanoparticles.
As a confirmation, all the calcium phosphate samples synthetized in presence of 2 mM PAA showed a polydispersity index value behind 0.3. Moreover, values of Z-average and Zeta potential exhibit a not linear trend (data not shown). For this reasons, suspensions with 2mM PAA were not further characterized.

Stability with time of the samples 0.2mM PAA/CaP with the three lowest ratios was investigated (Figure 7). Suspensions of PAA/CaP_1 and PAA/CaP_1.5 exhibited a very constant value of the hydrodynamic diameter within a week. On the contrary, the Z-average value of the sample with the lowest PAA/CaP ratio almost doubled after one week.

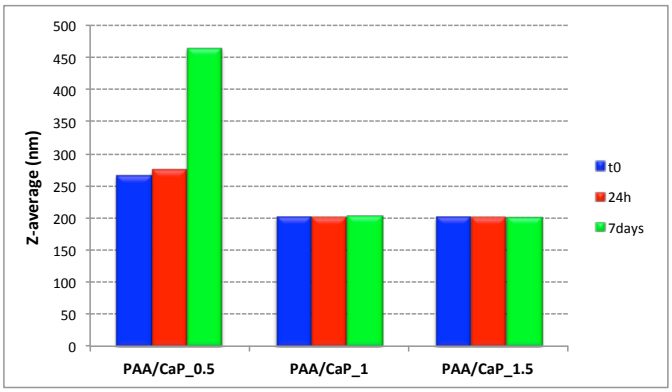

Figure 7. *Values of Z-average (nm) of the samples 0.2mM PAA/CaP with the three lowest ratios, analyzed right away (t_0), after 24h and after one week.*

In Table 7, 8 and 9 are reported the detailed DLS data for the samples 0.2mM PAA/CaP_0.5, PAA/CaP_1 and PAA/CaP_1.5, respectively. For all the samples, the values of PdI remained under 0.3 during all the week. Moreover, the values of Z-potential were all within the range of a moderate stability on the basis of Table 5.

Table 7. Stability of colloid suspension of the sample 0.2mM PAA/CaP_0.5, measured right away (t_0), after 24 h and after one week.

time	*Z-average (nm)*	*PdI*	*Zeta potential (mV)*
t_0	265.7	0.250	-38.3
24h	273.0	0.256	-35.9
7days	465.5	0.223	-34.4

Table 8. Stability of colloid suspension of the sample 0.2mM PAA/CaP_1, measured just after preparation (t_0), after 24 h and after one week.

time	*Z-average (nm)*	*PdI*	*Zeta potential (mV)*
t_0	202.1	0.237	-34.9
24h	200.6	0.254	-33.7
7days	203.6	0.245	-34.4

Table 9. Stability of colloid suspension of the sample 0.2mM PAA/CaP_1.5, measured just after preparation (t_0), after 24 h and after one week.

time	*Z-average (nm)*	*PdI*	*Zeta potential (mV)*
t_0	201.9	0.267	-32.5
24h	199.1	0.284	-37.0
7days	201.4	0.282	-24.6

3.5 Crystalline hydroxyapatite

The product prepared using a direct synthesis in aqueous solution (see paragraph 3.1.3) exhibit an X-ray diffraction pattern characteristic of crystalline hydroxyapatite (Figure 8A). In agreement, the results of TEM investigation show that the material consists of nanocrystals with a rod like shape with mean dimensions smaller than 100 nm (Figure 8B).

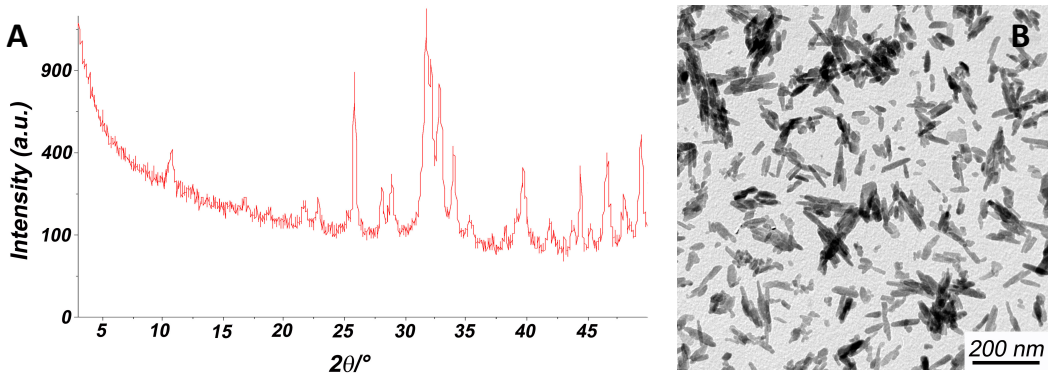

Figure 8. *(A) XRD pattern and (B) TEM image of crystalline HA.*

3.6 Foamed gelatin scaffolds enriched with calcium phosphates

Foamed gelatin scaffolds were prepared starting from 10% w/v gelatin solution. Foaming was obtained by maintaining the suspensions under constant stirring of about 700 rpm and temperature of 55°C. The change of colour from white to azure is due to the presence of the crosslinking agent genipin.
Figure 9 shows how scaffolds appear at the end of the whole process (see paragraph 3.1.4).

Figure 9. *Foamed gelatin scaffolds, crosslinked with genipin.*

3.6.1 Scanning Electron Microscopy

After morphology analysis, it is possible to observe that all the foamed gelatin scaffolds exhibited a macro and a microporosity. The morphology was very similar for all the samples. In Figures 10 and 11, SEM images of gelatin scaffold (GEL) and gelatin scaffold enriched with nanocrystalline calcium phosphate (GEL_CaP_E), respectively, are shown.

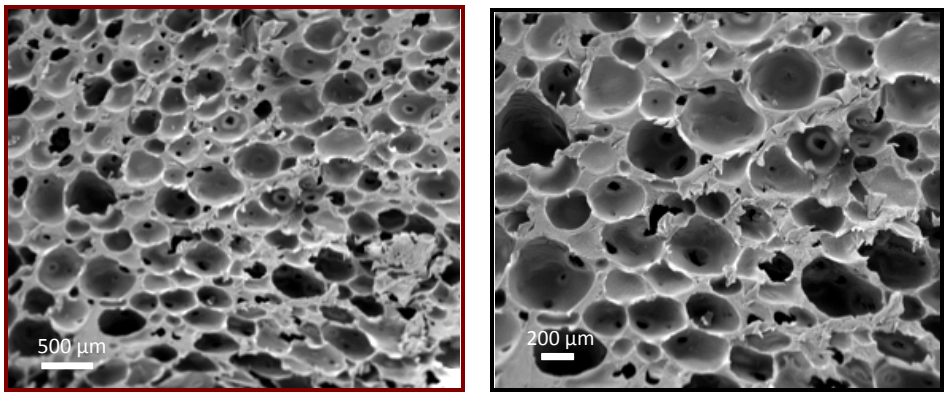

Figure 10. *SEM image of foamed gelatin scaffold (GEL)*

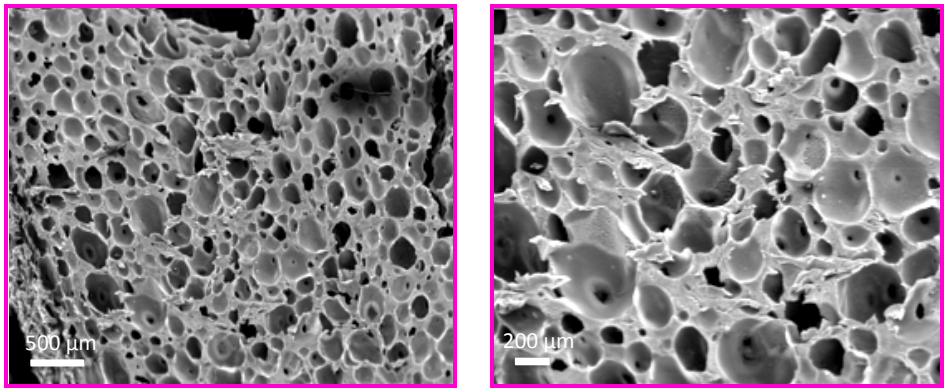

Figure 11. *Foamed gelatin scaffold with 10% of CaP nanocrystalline (GEL_CaP_E)*

Moreover, a very important aspect is the presence of a good interconnection among pores inside the scaffolds. Table 10 shows the dimensions of the average pore diameter and interconnections among pores, evaluated from morphology analysis. It is evident that the average pore diameter, as well as the interconnections, decreases as the crystallinity of the inorganic phase increases.

Table 10. Dimensions of average pore diameter and interconnections among pores of foamed gelatin scaffolds.

Sample	*Average pore diameter (µm)*	*Pore interconnection (µm)*
GEL	319 ± 132	51 ± 18
GEL_CaP_B	290 ± 128	68 ± 22
GEL_CaP_E	247 ± 99	34 ± 13
GEL_HA	192 ± 102	n.d.

3.6.2 Mechanical tests

Mechanical tests were carried out with an INSTRON Testing Machine 4465, to investigate how the presence of inorganic phase influences the mechanical properties of the composite scaffolds. The values of maximum stress, σ_{max}, and Young's modulus, E, are reported in Table 10.

Table 10. Mechanical properties of foamed gelatin scaffolds.

Sample	*σ_{max} (MPa)*	*E (MPa)*
GEL	0.17 ± 0.03	2.07 ± 0.3
GEL_CaP_B	0.08 ± 0.04	1.01 ± 0.2
GEL_CaP_E	0.20 ± 0.02	2.26 ± 0.1
GEL_HA	0.29 ± 0.03	5.14 ± 1

Sample containing amorphous calcium phosphate (GEL_CaP_B) exhibited a drop both in strain and in Young's modulus with the respect of pure gelatin scaffold. On the other hand, the presence of nanocrystalline inorganic phase provoked a slight increase of E. Crystalline HA provokes a significant increase of both mechanical parameters, in agreement with the observed reduction in pore size dimensions.

3.6.3 Cytotoxicity in vitro tests

Evaluations on interaction between osteoblast-like cells MG-63 and foamed scaffolds are reported in Table 11. There were no significant differences of cells proliferation on samples containing inorganic phase with the respect of control CTR- and sample of pure gelatin: all the percentages were greater than 70% (boundary value for the cytotoxicity). LDH values did not show significant differences as well. On the contrary, values of CTR+ were significantly different with the respect of all the samples.

Table 11. Osteblast-like cells proliferation and LDH measure in culture after 48h of incubation.

48 h-tests	*WST1 (450/625 nm)*	*Proliferation% / CTR (-) 24h*	*LDH (U/L)/WST1*
GEL	0.920 ± 0.010	87 ± 1	17.6 ± 10.6
GEL_CaP_E	0.970 ± 0.055	92 ± 5	12.1 ± 5.8
GEL_CaP_B	1.027 ± 0.116	97 ± 11	13.1 ± 9.5
GEL_HA	0.963 ± 0.024	91 ± 2	18.7 ± 1.6
CTR− (DMEM)	1.060 ± 0.043	100 ± 4	19.5 ± 3.9
CTR+ (phenol)	0.206 ± 0.003[a]	19 ± 1	104.8 ± 26.2[a]

[a]: *CTR+ vs GEL, GEL-CaP_E, GEL_CaP_B, CTR−; $p < 0.0001$*

Figure 12 shows images of Neutral Red stain of osteoblast-like cells MG-63 culture on foamed gelatin samples, and the negative and positive controls at 48h.

The numerous cells on scaffolds and negative control were well stained and exhibited a regular morphology. Cells on CTR+, instead, were clearly less than the others and did not take stain because of the loss of vitality, as confirmed by rounded shape.

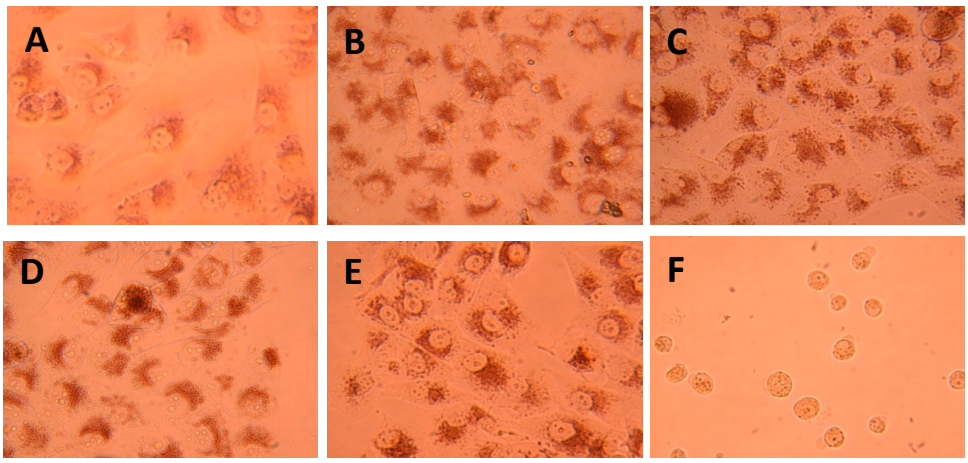

Figure 12. *Osteoblast-like cells MG-63 culture after 48h: (A) GEL, (B) GEL_HA, (C) GEL_CaP_E, (D) GEL_CaP_B, (E) CTR-, (F) CTR+. Neutral Red stain.*

Discussion

Foamed gelatin scaffolds enriched with calcium phosphates

In this PhD work, 3D gelatin scaffolds were prepared through foaming and freeze-drying. Foaming was achieved under vigorous stirring of gelatin solution enriched with calcium phosphate powders.

Calcium phosphates

Calcium phosphate (CaP) powders at different degrees of crystallinity were prepared from aqueous solutions using two different methods: the continuous fast precipitation *(constant flow method)* (Tadic et al., 2002) and the direct precipitation methods (Boanini et al., 2010).
The constant flow method allowed getting a range of samples with tunable crystallinity, from amorphous to nanocrystalline, as a function of the temperature and of the rate of solutions addition into the reaction vessel. The results of X-ray diffraction analysis showed that the degree of crystallinity of the precipitate increased on increasing temperature and on decreasing the addition rate. These data was supported by the results of elemental analysis, which showed a slight but appreciable increase of Ca/P molar ratio as crystallinity increased. The highest Ca/P ratio was however smaller than the value characteristic of hydroxyapatite (1.67) suggesting that the powders consisted of calcium-deficient hydroxyapatite.
At variance, the product synthesized using the direct precipitation method in aqueous solution exhibited a X-ray diffraction pattern characteristic of crystalline hydroxyapatite, and was constituted of nanocrystals with a rod like shape and mean dimensions smaller than 100 nm, as put into evidence by TEM investigation.
In agreement with XRD results, the morphology of the powders obtained by constant flow changed as a function of crystallinity, from granular aggregates to continuous material where it was not possible to distinguish single particles.
The continuous fast precipitation method was also used to carry on a preliminary investigation aimed to verify if PAA can be used to stabilize the nanoparticles suspensions. The results obtained by means of dynamic light scattering (DLS) on the hydrodynamic diameter (Z-average), the Zeta potential and the polydispersity index (PdI) of the polymer-coated nanoparticles suspensions indicated that the colloidal suspensions at low PAA/CaP ratios exhibited a good stability even over time, at variance with the data obtained at relatively high PAA concentrations.

Foamed scaffolds

The experimental conditions utilized in this work, which involve foaming gelatin solutions containing calcium phosphates at different degree of crystallinity, gelling and then freeze–drying the composites, allowed to prepare porous 3D scaffolds, which properties can be modulated by varying the composition.

All the scaffolds exhibited a macro and a microporosity. As expected, pure gelatin scaffolds showed good interconnectivity and average pore dimensions of the order of 300 μm, well above the minimum pore size of about 100 μm suggested for significant bone growth (Vallet-Regí, 2008). Connectivity, as well as average pore size, decreased in calcium phosphate containing scaffold. In particular, the values of these parameters were observed to decrease as the crystallinity of the inorganic phase increased.

In agreement with the observed reduction of pore size dimensions, the presence of nanocrystalline and crystalline inorganic phase provoked an improvement of the mechanical properties of the composites. The best values of maximum stress, σ_{max}, and Young's modulus, E, of the samples submitted to compression tests were obtained for the scaffolds enriched with crystalline HA prepared by direct precipitation.

Osteoblast-like cells MG-63 response to 3D scaffolds was evaluated in comparison with negative and positive control (CTR). The results did not show significant differences in cell proliferation of composite samples with the respect to control CTR- and pure gelatin scaffolds. All the percentages, in fact, were greater than the boundary value for the cytotoxicity. The cells on scaffolds and negative control appeared well stained and exhibited a regular morphology, when treated with the Neutral Red stain, at variance with those on CTR+.

Chapter IV

Electrospun scaffolds

Materials and Methods

4.1 Materials

4.1.1 Electrospun scaffolds preparation

All the mats were prepared using type A gelatin (280 Bloom, Italgelatine S.p.A.) from porcine skin.

Electrospun fibers from gelatin and gelatin–genipin solutions

Gelatin, at a concentration of 30% (w/v), was dissolved in 60/40 acetic acid/double distilled water (v/v). This solution was stirred at 50°C for 60 min and then electrospun. The samples obtained from this solution were labelled G.
To prepare mats labelled GG, 30% (w/v) gelatin was dissolved in 60/30/10 acetic acid/double distilled water/0.75M phosphate buffered saline solution (PBS) at pH 7.4 (v/v). This solution was stirred too at 50°C for 60 min. To a volume of 10mL, 60 mg of genipin (Wako, Japan), dissolved in 0.5 ml of ethanol, were added. About 30 min after genipin addition, the mixture was electrospun.

Co-electrospun fibers from gelatin and poly(L-lactic acid) solutions

Poly(L-Lactic acid), PLLA (Lacea H.100-E, Mw = $8.4x10^4$g/mol, PDI = 1.7) was used.
PLLA was dissolved in 65/35 dichloromethane/dimethylformamide (v/v) at a concentration of 13% (w/v) and stirred for 2h at room temperature. Gelatin was dissolved in 60/40 acetic acid/distilled water (v/v) at a concentration of 30% (w/v) and stirred for 60 min at 50°C. These solutions were electrospun with opportune conditions to obtain composite scaffolds of different composition labelled GEL, PLLA30GEL70, PLLA50GEL50, PLLA70GEL30 and PLLA.

4.1.2 Electrospun non-woven mat fabrication

The electrospinning apparatus, made in house, is composed of a high voltage power supply (Spellman SL 50 P 10/CE/230), two syringe pumps (KD

Scientific 200 and 100 series) and glass syringes containing polymer solutions, each connected to a stainless steel blunt-ended needle (inner diameter 0.84 mm).
As collector, a grounded circular copper collector (diameter 5 cm) or a grounded aluminum rotating mandrel (12 cm length, 5 cm diameter, rotational speed 2.1 m/s) were used.
To prepare G and GG nanofibrous scaffolds, gelatin and gelatin-genipin solutions were individually dispensed from a glass syringe, through a Teflon tube to the needle, placed vertical to the circular copper collecting plate. For both solutions, the electrospun conditions were: applied voltage 15 kV, needle to collector distance 15 cm, solution flow rate 0.005 ml min^{-1} controlled by a syringe pump (KD Scientific 200 series), at room temperature (RT) and a relative humidity (RH) of 42±3%.
Composite scaffolds were fabricated by co-electrospinning PLLA and gelatin solutions, whose feed rates were independently controlled by the two syringe pumps. Polymer solutions were dispensed from two glass syringes through a Teflon tube to the needles that were positioned at opposite sides of the aluminum rotating collecting drum. Needle-to-collector distance was fixed at 15cm. Scaffolds containing different amounts of PLLA and gelatin (nominal PLLA/gelatin weight ratio: 0/100, 30/70, 50/50, 70/30, 100/0) were fabricated by properly changing the feed rate of the two polymer solutions. All electrospun mats were kept under vacuum over P_2O_5 at RT overnight in order to remove residual solvents.

4.1.3 Crosslinking of electrospun mats with genipin

All electrospun mats were fixed to plastic rings (CellCrown™ 12, Scaffdex) and crosslinked with the naturally occurring agent genipin (Bigi et al., 2002). Three different crosslinking methods were used.
In *method A*, GG mats were soaked in 5%, 7% or 11% (w/v) genipin solution in ethanol, at a temperature of 37°C, for 7 days. Then the mats were dried overnight at 37°C, rinsed in ethanol and dried again. Crosslinked samples were labelled GG_XA, were X is the concentration of genipin. In *method B*, GG scaffolds were soaked in 5% (w/v) genipin solution in ethanol for 7 days at 37°C. Subsequently mats were dried overnight at 45°C, then rinsed in ethanol and dried again. The crosslinked samples were labelled GG_5B. *Method C* was applied to both scaffolds G and GG. Mats were soaked in 5% (w/v) genipin solution in ethanol for either 3 or 7 days at 37°C. Afterwards, they were rinsed in 0.1M PBS at pH 7.4, dried overnight at 37°C, then rinsed in ethanol and dried again. Crosslinked samples were labelled as G_5CYd and GG_5CYd, where Y indicates the duration, expressed in days, of crosslinking process (Panzavolta et al., 2011).
Composite gelatin-PLLA scaffolds (see paragraph 4.1.1) were crosslinked, using *method C*.

4.1.4 Scaffolds Mineralization

In vitro mineralization tests were performed using a slightly supersaturated CaP solution (Bigi et al., 2005). The reagent grade chemical $CaCl_2 \cdot 2H_2O$ was dissolved in double distilled water and buffered at pH 7.2 with Hepes (Ca solution). The reagent grade chemicals $Na_3PO_4 \cdot 12H_2O$, and $NaHCO_3$ were dissolved in double distilled water and buffered at pH 7.2 with Hepes (P solution). Ca/P supersaturated calcifying solution was freshly prepared by mixing equal volumes of the Ca and the P solutions at 37°C. Mineralization was performed by immersion of the crosslinked scaffolds, fixed to plastic rings (CellCrowns™ 12, Scaffdex), in CaP calcifying solution at 37°C for 6h, with solution refreshment after 3h. Mineralized samples were accurately rinsed in double distilled water, and dried at 37 °C overnight.

4.1.5 Preparation of gelatin films

In order to verify the effect of the electrospinning solution on gelatin, gelatin films were prepared from solutions at 30% (w/v) gelatin concentration in double distilled water or in 60/40 acetic acid/double distilled water (v/v), at 50°C for 60min. Films were obtained on the bottom of Petri dishes (diameter 6 cm) after water evaporation at RT from 10 ml of gelatin solution (Bigi et al., 1998). The same solutions, after dilution at 1:20, were used to prepare films for Fourier transform infrared (FTIR) analysis.

4.2 Methods

4.2.1 X-ray diffraction analysis

High-angle X-ray diffraction patterns were recorded on a flat camera with a sample-to-film distance of 60 mm using Ni-filtered CuK radiation. The diffraction analysis was carried out by means of a PANalytical X'Celerator powder diffractometer using CuKa radiation (40 mA, 40 KV). Scaffolds were analysed in the 2θ range from 5° to 25° in transmission mode, with a step size of 0.1° and a time per step of 700 s.

4.2.2 Infrared absorption analysis

FTIR analysis of as-spun mats and gelatin films were carried out using a Perkin Elmer model 682 and a Nicolet 380 FT-IR. Furthermore, composite PLLA-gelatin electrospun mats were dissolved in TFE (20 mg in 0.5 ml) and few drops of solution were casted on KBr disk that was dried for 30 min prior to FTIR analysis. All spectra were collected in the range 4000–400 cm^{-1}, with 32 scans and at 4 cm^{-1} resolution.

4.2.3 Morphological investigation

Morphological investigation of the samples was performed using a Philips XL-20 and a Hitachi S-2400 scanning electron microscopes. The samples were sputter-coated with gold prior to examination. The distribution of fiber diameters was determined by the measurement of a number of fibers (100–250) using acquisition and image analysis software (EDAX Genesis) and the results are given as the average diameter ± standard deviation.
Single factor analysis of variance (ANOVA) was employed to assess statistical significance of the results. $P<0.001$ was considered statistically significant.
In order to confirm the presence and interspersion of the two different fiber population in gelatin/PLLA scaffolds, and to verify the spatial distribution of gelatin and PLLA fibers, the polymeric solutions were stained with two fluorescence dyes: Rhodamine B was added to PLLA fibers at a concentration of 0,01% w/w and FITC was added to gelatin fibers at a concentration of 0,1% w/w. Nikon Eclipse Ti microscope with A1R confocal laser system (CLSM) was used to obtain images of fluorescent fibers in as-spun electrospun mats.

4.2.4 Mechanical properties

Tensile stress-strain measurements were carried out on electrospun scaffolds using an Instron Testing Machine 4465 and the Series IX software package.
Eight rectangular specimens cut from each mat (5x20 mm, thickness 0.012–0.017 mm) were stretched in the dry state, using a crosshead speed of 0.5 mm/min. Average specimen thickness was determined by using a digital micrometer and a scanning electron microscopy.
The Young's modulus E, the strain at break ε_b and the stress at break σ_b of the strips were measured in static mode and the data were given as the average value ± standard deviation. Single factor analysis of variance (ANOVA) was employed to assess statistical significance of the results. $P<0.001$ was considered statistically significant.

4.2.5 Crosslinking degree

The extent of crosslinking of gelatin scaffolds was determined by an UV assay of the non-crosslinked ε-amino groups before and after reacting with genipin (Bubnis and Ofner, 1992).
Following reaction with 0.5% trinitrobenzensulfonic acid (TNBS), gelatin mats were hydrolyzed with 6M HCl. A volume of 5mL of the hydrolyzate was diluted with 5mL of water and then extracted with ethyl ether. A 5mL aliquot of the aqueous phase was removed from each sample and heated for 15 min in a hot water bath cooled at room temperature and diluted with 15mL of water. The absorbance of the diluted solution was measured at 346 nm in a Kontron Uvikon 931 spectrophotometer against a blank. The relationship between absorbance and moles of ε-amino groups per gram of gelatin was:

$$moles\ \varepsilon - \text{amino groups}/_{g\ gelatin} = \frac{2 \cdot Absorbance \cdot 0.02\ L}{1.46 \cdot 10^4 \cdot b \cdot x}$$

where $1.46 \cdot 10^4$ L/mol·cm is the molar absorptivity of TNP-lys, b is the cell path length in centimetre and x is the sample weight in grams.

4.2.6 *In vitro* tests

Before cells seeding all electrospun mats were fixed to plastic rings (CellCrown™ 12, Scaffdex), and sterilized by immersion in 85% ethanol for 15 min, then 70% ethanol for 15 min, followed by three rinses with PBS plus 2% penicillin/streptomycin (Euroclone), 0.2% amphotericin B (Sigma). Scaffolds were kept in this solution overnight under UV irradiation (230 V at 50 Hz). The next day the PBS solution was removed and the scaffolds were pre-wetted in complete culture medium. When 80% confluence was reached the cells were trypsinized (0.05% Trysin–EDTA, Sigma), centrifuged and suspended again in medium.

Cell seeding and culture on G and GG scaffolds

Vascular wall mesenchymal stem cells (VW-MSCs), isolated from human femoral arteries (Pasquinelli et al., 2010), were used to assess the biocompatibility of G and GG electrospun nanofibrous scaffolds.
VW-MSCs were propagated in Dulbecco's modified Eagle's medium (DMEM) containing 4.5 g/l glucose supplemented with 10% fetal bovine serum (FBS), 2mM L-glutamine and 100 U/ml penicillin/streptomycin at 37°C in 5% CO_2.
Cells were seeded ($2x10^4$) onto the scaffolds and cultured under standard culture conditions (37°C, 5% CO_2) for 7 days before being processed for SEM analysis.

Cell seeding and culture on gelatin-PLLA composite scaffolds

A normal human primary chondrocyte culture derived from the human knee articular cartilage (NHAC-kn, Clonetics™ Cell System, Lonza Milano s.r.l., BG, I), was used for the experiment on electrospun gelatin-PLLA composite scaffolds and cells were expanded in monolayer cultures, using Chondrocyte Growth Medium (CGM, containing FBS 5%, gentamicin sulfate-amphotericin B 0.1%, bFGF-B 0.5%, R3-IGF-1 0.2%, insulin 0.2%, transferrin 0.1%).
When all cells reached 70-80% confluence, they were detached from culture flasks by trypsinization, and centrifuged; cell number and viability were checked with Trypan Blue dye exclusion test (Sigma, UK). Chondrocytes (cell suspension of $2.5x10^5$ cells/ml) were seeded as pellet of concentrated cells on six samples of each type of the gelatin-PLLA composite scaffolds (see paragraph 4.1.1). A differentiating medium to activate chondrocytes (Chondrocyte Differentiation Medium (CGM supplemented with TGFβ-1 0.5%, R3-IGF-1 0.2%, insulin 0.2%, transferrin 0.2% and ascorbic acid 2.5%) was used. Cells were cultured under standard culture conditions (37°C, 5% CO_2) from 7 up to 14 days. The same concentration of cells was also seeded

on polystyrene of the culture plate as control (CTR).

Cell proliferation, viability and bioactivity on gelatin-PLLA composite scaffolds

At baseline conditions, at 7 and at 14 days WST1 test was performed to assess cell proliferation and viability on gelatin-PLLA composite scaffolds. 100µl of WST1 (tetrazolium salt) and 900µl of fresh culture medium were added at every well and cultures were incubated at 37°C for further 4h. Tetrazolium salt is transformed to formazan by reductase of mitochondrial respiratory chain, active in viable cells only. Supernatants were measured by spectrophotometer at 450/625nm. Results were reported as optical density (OD) and values directly correlate with cell number. At 24h LDH activity (Lactate dehydrogenase, Roche, D) was measured in supernatant to assess cytotoxicity. Supernatant was also collected at 7 and at 14 days for the evaluation of most common markers of chondrocyte differentiation: CPII (Collagen type II, USCN Life Science, China), AGC (Aggrecan, USCN Life Science, China), CTSB (Cathepsin B, Abnova, Taiwan).

Cell morphology

Samples of each material, at the end of the experiment, were processed for SEM analysis. Briefly, samples were fixed in 2.5% buffered glutaraldehyde overnight at 4 °C, washed with 0.15M or 0.01M PBS at pH 7.4, and post-fixed with 1% osmic acid for 15 min at RT. After being washed in double distilled water for 15 min the samples were dehydrated in increasing concentrations of ethanol (i.e. 70%, 96% and 100% for 15 min each), dried in a 1:1 solution of absolute ethanol and hesamethyldisilazane (HMDS) (Fluka) for 30 min and dried in pure HMDS. Nanofibrous scaffolds were mounted using adhesive tape on stubs and prior to examination coated with a 10 nm thick layer of gold or palladium in a sputtering device (Balzers Union). Samples were observed with a Philips XL-20 microscope or with Hitachi S-2400 scanning electron microscope at 15 keV.

Statistical analysis

Statistical evaluation of data was performed using the software package SPSS/PC+ Statistics TM 10.1 (SPSS Inc., Chicago, IL USA). Data were reported as mean ± standard deviations (SD) of triplicate at a significance level of $p<0.05$. After having verified normal distribution and homogeneity of variance, a one-way ANOVA was done for comparison between groups. The Scheffé's post hoc multiple comparison tests were performed to detect significant differences between groups.

Results

4.3 Gelatin and Gelatin–Genipin electrospun fibers

4.3.1 As-electrospun nanofibers

Gelatin and gelatin-genipin solutions were individually dispensed from a glass syringe and electrospun to produce G and GG scaffolds, respectively (see paragraph 4.1.2). The electrospinning apparatus, made in house, used to prepare samples is shown in Figure 1.

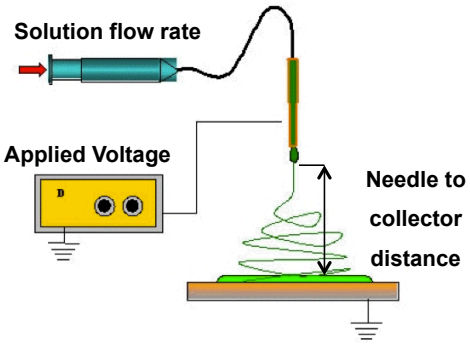

Figure 1. *Schematic representation of an electrospinning apparatus composed of a high voltage power supply, a glass syringe, containing polymer solutions, connected to a stainless steel blunt-ended needle and a collector.*

Figure 2a shows a SEM image of gelatin nanofibers (G) electrospun from a solution of acetic acid/water. The randomly collected fibers are free of bead defects and display a relatively uniform diameter distribution.

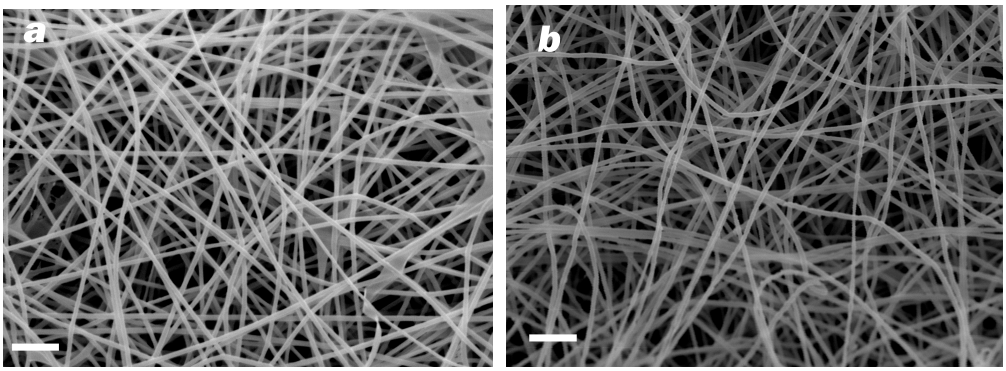

Figure 2. *SEM images of as-electrospun (a) G and (b) GG mats. Bars: 5 μm.*

The numerous attempts to optimize crosslinking of these gelatin mats did not provide completely satisfactory results. The slightly modified composition obtained by addition of a small amount of genipin in ethanol to the electrospinning solution resulted in improvement of crosslinking and, as a consequence, of the properties of scaffolds. The SEM image of a gelatin–genipin (GG) electrospun scaffold (Figure 2b) shows that fibers were defect free and very regular. The fiber mean diameter was similar to that of G nanofibers, as reported in Table 1.

Table 1. Nanofiber diameters of as-electrospun and crosslinked mats (mean values ± standard deviations are reported).

Sample	Fiber diameter (nm)
G	440 ± 50
GG	460 ± 60
GG_5A	600 ± 120[a,b]
GG_7A	980 ± 180
GG_11A	940 ± 130
GG_5B	810 ± 180
G_5C7d	740 ± 120[a]
GG_5C7d	990 ± 130[c]

a GG_5A vs G, GG, G_5C7d vs G, GG ($P < 0.001$).
b GG_5A vs GG_7A, GG_11A, GG_5B ($P < 0.001$).
c GG_5C7d vs GG_5B, GG_5A, G_5C7d ($P < 0.001$).

Possible gelatin structural modifications due to the electrospinning process were investigated through FTIR and XRD analyses of the electrospun scaffolds, as well as of the gelatin and gelatin–genipin films.

4.3.2 Infrared absorption analysis

FTIR spectra of gelatin films prepared from aqueous solution (blue line) and from acetic acid/water solution (green line), together with the spectra of G and GG electrospun scaffolds (red and black line, respectively) are shown in Figure 3. All spectra show several absorption bands corresponding to amide A, I, II and III (Hashim et al., 2010). The spectrum of the film prepared from gelatin–genipin in acetic acid/water is similar to that reported in Figure 3 (data not shown). With respect to the other spectra, that one recorded from the film prepared from gelatin aqueous solution displays a relatively high intensity for the 1234 cm^{-1} band in the amide III region. Moreover, the spectrum of the GG scaffold, and even more that of the G scaffold, are less resolved with respect to those of the films.

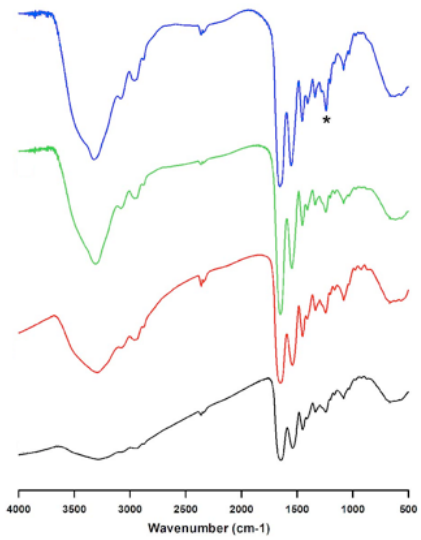

Figure 3. *FTIR absorption spectra of gelatin films prepared from aqueous (blue line) and acetic acid/water (green line) solutions, compared with the spectra of as-electrospun G (red line) and GG (black line) mats. *1234 cm^{-1} band.*

4.3.3 X-ray diffraction analysis

Figure 4 compares the wide angle X-ray diffraction pattern of a gelatin film prepared from an aqueous solution (blue line) with that of a film prepared from an acetic acid/water solution (green line), and with that recorded from a GG electrospun scaffold (red line). The pattern of the gelatin film from aqueous solution shows two diffraction reflections: the first corresponds to a periodicity of about 1.1nm and is related to the diameter of the triple helix; the second corresponds to a periodicity of about 0.45nm and has been ascribed to the distance between adjacent polypeptide strands (Okuyama et al., 2008; Gioffrè et al., 2011). The patterns of gelatin film from acetic acid/water solution and GG mats patterns are much less defined and show only the second broad peak.

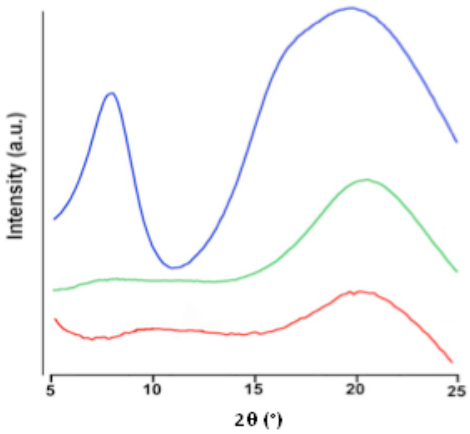

Figure 4. *XRD diffraction patterns of gelatin films prepared from aqueous (blue line) and acetic acid/water (green line) solutions, compared with the pattern of as-electrospun GG mat (red line).*

4.3.4 Optimization of the crosslinking conditions

The addition of genipin to the electrospinning solution did not prevent solubilization of the electrospun scaffolds when exposed to water. Therefore, the mats were submitted to further crosslinking treatments with genipin, with three different methods (Method A, B and C). Moreover, possible morphological modifications of the crosslinked nanofibers upon water exposure were investigated through SEM analysis of the mats air-dried at 37°C after immersion in water for 30 min.

Table 2. Crosslinking conditions used for the different samples.

Sample	Genipin conc. % (w/v)	Crosslinking time (days)	Immersion in PBS	T (°C) of drying
GG_5A	5	7	✗	37
GG_7A	7	7	✗	37
GG_11A	11	7	✗	37
GG_5B	5	7	✗	45
G_5C3d	5	3	✓	37
GG5C3d	5	3	✓	37
G_5C7d	5	7	✓	37
GG_5C7d	5	7	✓	37

Method A

Some of the GG mats were soaked in genipin solutions at different concentrations at 37°C for 7 days. Genipin concentrations in ethanol of 5%, 7% and 11% (w/v) were tested (Table 2). Figure 5a-5c shows SEM images of the GG mats crosslinked with increasing genipin concentrations. The mean fiber diameters were significantly greater than those of the as-electrospun fibers, and increased at relatively high genipin concentration (Table 1). In the images recorded after scaffold immersion in water (Figure 5e–5g) the fibers show a drastic morphology change with many junction zones fused together.

Method B

The influence of air-drying temperature was tested on GG mats crosslinked with 5% genipin. In particular, the samples were dried overnight at 45°C instead of 37°C as in method A (Table 2). The images recorded before and after water exposure (Figure 5d and 5h) show that the increase of the drying temperature did not prevent fiber fusion after water exposure.

Method C

Method C introduced a further step in the crosslinking procedure, which is rinsing the mats in 0.1M PBS, pH7.4, before air-drying. The method was tested on mats soaked in 5% w/v genipin for two different periods of time, 3 and 7 days (Table 2). The fibers in the mat GG_5C3d after rinsing in water appear fused together at most contact points (data not shown). Figure 6

shows the morphology of the GG_5C7d fibers (a) before and (c) after exposure to water. It is evident that soaking in genipin for 7 days followed by rinsing in PBS yielded samples able to retain the morphology of the individual nanofibers after exposure to water, as enhanced in the detail shown in the inset to Figure 6c.
Figure 6b and 6d reports the SEM images of G_5C7d before and after rinsing in water. Figure 6d shows that even the fibers electrospun from gelatin solution in the absence of genipin retained their morphology after rinsing in water, although in this case parts of the junction zones appeared fused together.

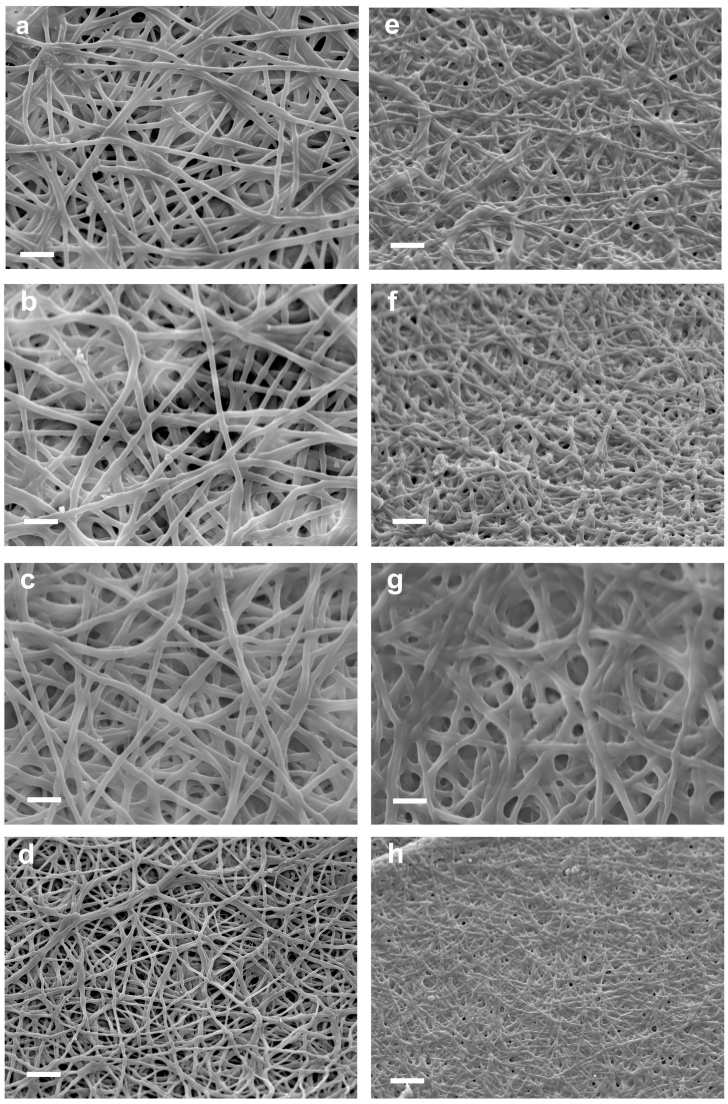

Figure 5. *SEM images of GG mats crosslinked according to method A (a)–(c) before and (e)–(g) after rinsing in water; (a, e) 5%, (b, f) 7% and (c, g) 11% genipin solution. The images of GG mats crosslinked according to method B (d) before and (h) after rinsing in water are also reported.*
Bars: (a)–(c), (e)–(g), 5 μm and (d, h), 10 μm.

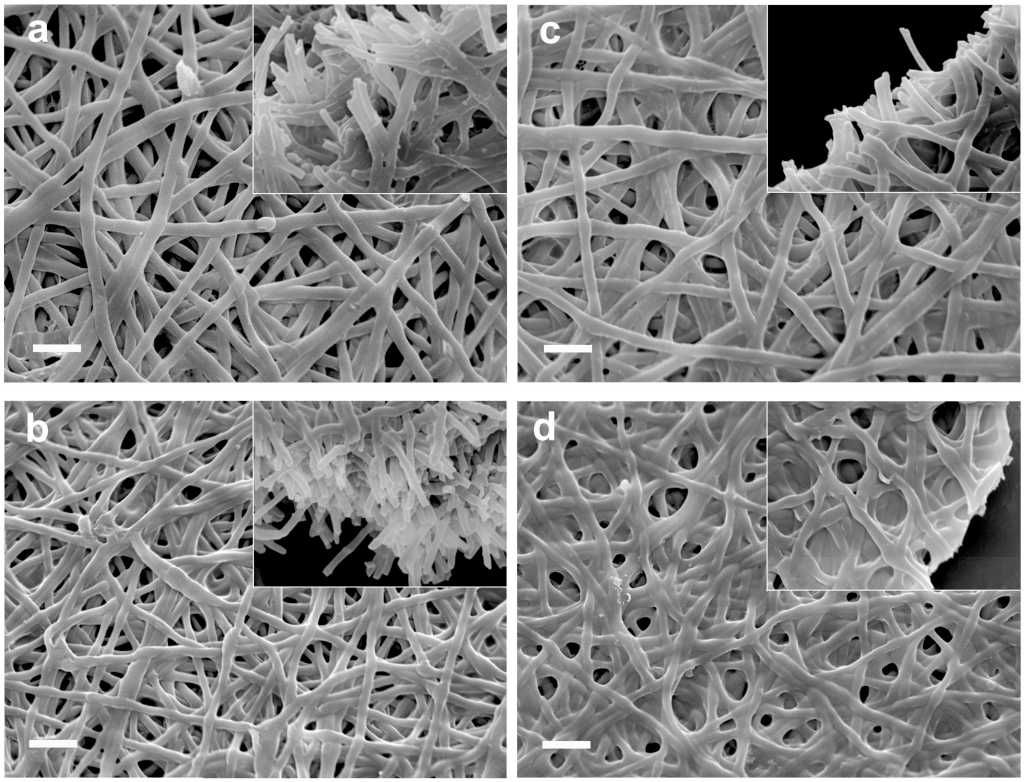

Figure 6. *SEM images of (a, c) GG and (b, d) G mats crosslinked according to method C; (a, b) before and (c, d) after rinsing in water. The insets report a view of a mat edge. Bars: 5 μm.*

The morphological characterization of both G_5 and GG_5 scaffolds indicate that the conditions utilized in the method C gave the best results in terms of stabilization of the mats against water solubilization. As a consequence, this procedure was selected as the best method to crosslink electrospun gelatin scaffolds with genipin. Sample GG_5C7d, as well as G_5C7d as a control sample, were submitted to further characterization.

4.3.5 Degree of cross-linking and stability in solution

The extent of cross-linking of the scaffolds prepared according to method C was calculated from the moles of free ε-amino groups per gram of gelatin (Bubnis et al., 1992). The results indicated that GG_5C7d and G_5C7d exhibited 92 ± 5% cross-linking, whereas the value determined for the as-electrospun GG nanofibers was 15 ± 5%. The stability of these scaffolds was tested investigating fiber morphology modifications after immersion in cell culture medium (DMEM) for 7 days. The SEM images reported in Figure 7a and 7b show no undesired alteration of the nanofibers, which exhibited only a slight reduction in their mean diameter with respect to that measured before immersion (see Table 1). The mean diameters of G_5C7d and GG_5C7d after 7days in DMEM were 720 ± 80 and 840 ± 150 nm, respectively.

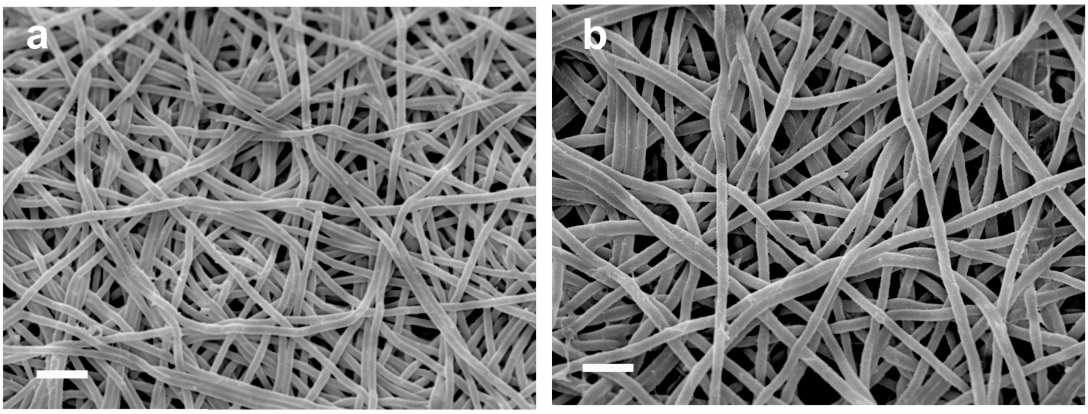

Figure 7. *SEM images of (a) G_5C7d and (b) GG_5C7d after immersion of 7 days in DMEM. Bars: 5 μm.*

4.3.6 Mechanical tests

Typical tensile stress–strain curves recorded from G and GG samples before and after crosslinking are reported in Figure 8. A dramatic modification of the mechanical behavior induced by the presence of genipin is evident in the as-electrospun mats. The stress–strain curves recorded from the different samples have been used to evaluate the Young's modulus E, the stress at break σ_b and the deformation at break ε_b of the scaffolds. The mean values are reported in Table 3.

Table 3. Strain at break (ε_b), stress at break (σ_b), and Young's modulus (E) of as-electrospun and cross-linked mats (each value is the mean of 10 determinations reported with the standard deviation).

Sample	*ε_b (%)*	*σ_b (MPa)*	*E (MPa)*
G	37 ± 5[a]	6 ± 0.6[c]	240 ± 30[e]
GG	3.2 ± 0.5	3.8 ± 0.6	194 ± 20
G_5C7d	5.5 ± 0.3[b]	22 ± 4[d]	820 ± 100[f]
GG_5C7d	3.5 ± 0.2	20.9 ± 0.4[d]	990 ± 40[f,g]

a G vs GG, G_5C7d, GG_5C7d ($P < 0.001$).
b G_5C7d vs GG_5C7d ($P < 0.001$).
c G vs GG($P < 0.001$).
d G_5C7d vs G, GG; GG_5C7d vs G, GG ($P < 0.001$).
e G vs GG ($P<0.001$).
f G_5C7d vs G, GG; GG_5C7d vs G, GG ($P < 0.001$).
g GG_5C7d vs G_5C7d ($P < 0.001$).

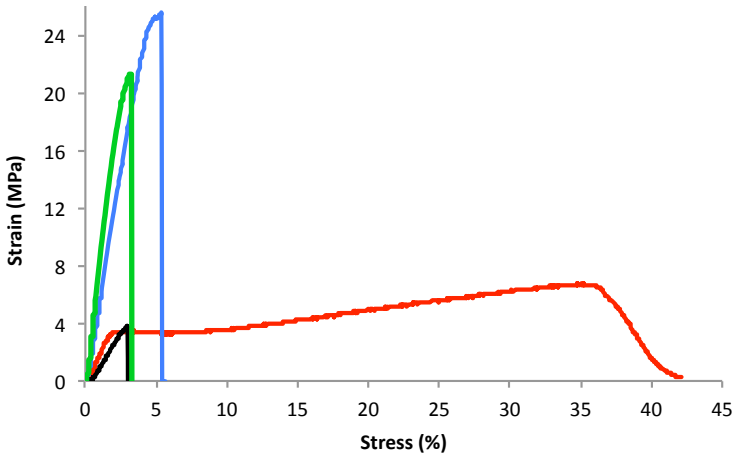

Figure 8. *Typical stress–strain curves recorded from as-electrospun (a) G and (b) GG mats and from cross-linked (c) G_5C7d and (d) GG_5C7d mats.*

4.3.7 *In vitro* tests

The viability of VW-MSCs cultured on G and GG electrospun mats after 7 days culture was preliminarily assessed by SEM analysis. VW-MSCs are vital in both types of scaffolds and they retain the native mesenchymal spindle-shaped morphology, as shown in Figure 9a and 9b for G_5C7d. No differences in terms of cell adhesion and morphology were observed between the two types of mats.

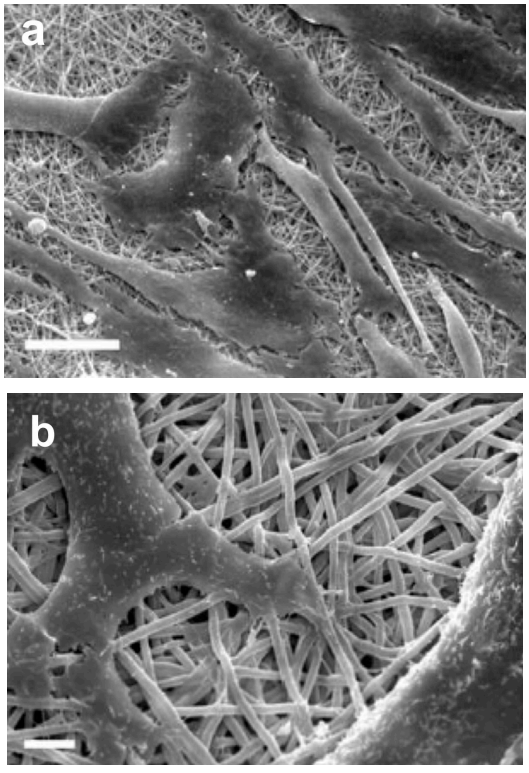

Figure 9. *SEM images of VW-MSCs grown on G_5C7d for 7 days. Bars: (a) 50 µm and (b) 5 µm.*

4.4 Gelatin-Poly(L-Lactic Acid) co-electrospun fibers

4.4.1 As-electrospun nanofibers

Composite scaffolds were fabricated by co-electrospinning PLLA and gelatin solutions, dispensed from two glass syringes through a Teflon tube to the needles, which were positioned at opposite sides of the aluminum rotating collecting drum (see paragraph 4.1.2). In Figure 10, the apparatus for PLLA and gelatin co-electrospinning process is shown.

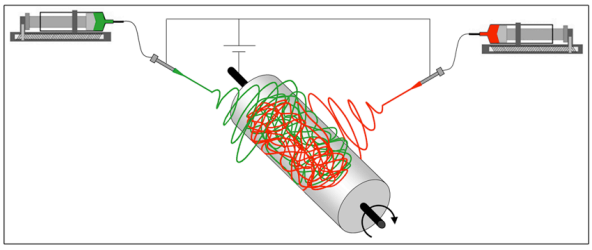

Figure 10. *Diagram of PLLA and gelatin co-electrospinning process.*

Scaffolds containing different amounts of PLLA and gelatin (nominal PLLA/gelatin weight ratio: 0/100, 30/70, 50/50, 70/30, 100/0) were fabricated by properly changing the feed rate of the two polymer solutions (Table 4).

Table 4. Electrospinning process parameters used for scaffold fabrication. To prepare composite scaffold, a voltage value of 15-20 kV and a drum speed of 2.1 m/s were used. Needle-to-collector distance was 5 cm.

Sample	*Gelatin feed ratio (ml/min)*	*PLLA feed ratio (ml/min)*
GEL	0.005	-
PLLA30GEL70	0.01	0.01
PLLA50GEL50	0.012	0.005
PLLA70GEL30	0.0215	0.004
PLLA	-	0.015

Nanofibrous scaffolds of the two plain polymers, PLLA and gelatin, were composed of bead-free and randomly arranged fibers, with similar morphology and similar diameter distribution: PLLA fiber diameter of 560±140 nm and gelatin fiber diameter of 500±90 nm. The similar morphology of PLLA and gelatin fibers prevented to distinguish them in the composite mats by SEM observations (SEM images not shown).
For this reason fluorescence dyes were added to the two polymeric solutions to demonstrate the presence of the two different fiber populations within the scaffold, through CLSM analysis (Figure 11).

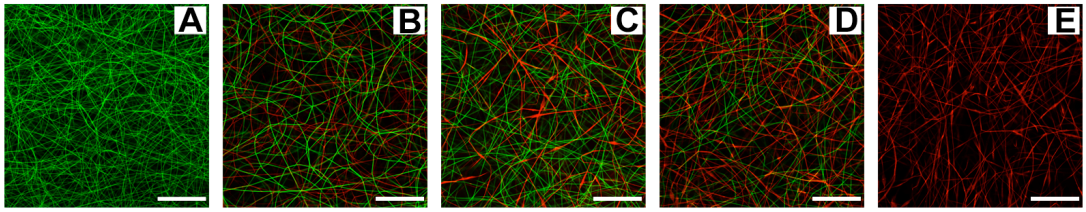

Figure 11. *CLSM images of as-electrospun mat A) GEL, B) PLLA30GEL70, C) PLLA50GEL50, D) PLLA70GEL30 and E) PLLA. Scale bars: 50 μm.*

The gradual change of colour from green (scaffold of pure gelatin) to red (scaffold of pure PLLA) provided evidence of the variation of scaffold chemical composition according to solution feed rates and demonstrated that the fibers could be successfully interspersed by co-electrospinning.

4.4.2 Infrared absorption analysis

Qualitative evaluation of PLLA and gelatin content in the electrospun scaffolds was performed through FTIR analysis of mats dissolved in TFE (Figure 12).

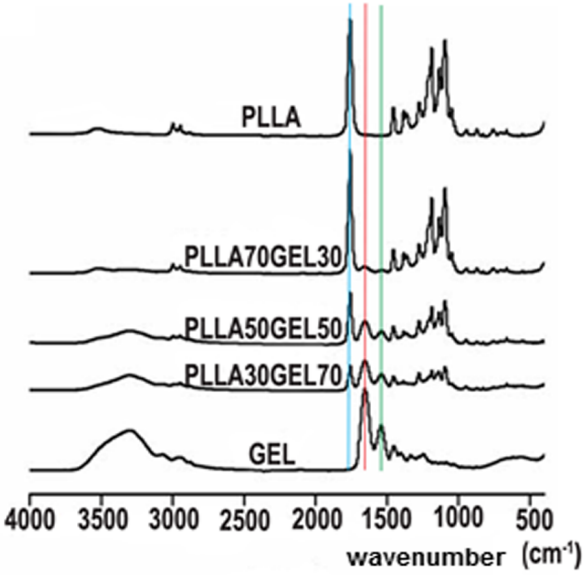

Figure 12. *FTIR spectra of co-electrospun PLLA-gelatin mats dissolved in TFE.*

It is worth noticing that additional FTIR analysis performed on as-spun mats showed the same bands as those reported for the mat dissolved in TFE (see paragraph 4.3.2). The characteristic PLLA band, corresponding to the C=O stretching, was located at 1760 cm^{-1} (azure line) whereas gelatin showed Amide I (C=O double stretching mode) and Amide II (deformation of N–H bonds and C–H stretching) bands at 1651 cm^{-1} (red line) and 1537 cm^{-1} (green line), respectively (Bergo and Sobral, 2012; Hashim et al., 2010). In composite electrospun scaffolds the intensity of the band at 1760 cm^{-1} decreased with decreasing PLLA feed rate and, concomitantly, the characteristic bands of gelatin increased, consistently with the expected chemical composition of the electrospun scaffolds.

4.4.3 Crosslinking of co-electrospun mats with genipin

Figure 13 shows SEM images and respective photographs of crosslinked scaffolds. Fiber morphology and fiber diameter distribution of pure PLLA scaffold did not appear to be significantly modified by the crosslinking treatment (average fiber diameter change from 560±140nm to 480±100nm), whereas the average fiber diameter of pure gelatin scaffolds slightly increased: 750±120nm vs. 500±90nm of the non-crosslinked scaffold (see Table 1).

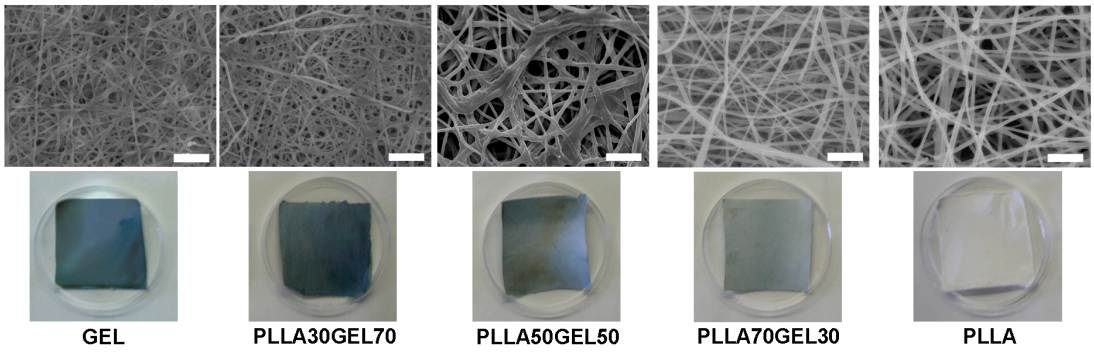

Figure 13. *SEM images and photographs of crosslinked mats. (Scale bars: 10 μm).*

As illustrated in the photographs reported in Figure 13, after crosslinking gelatin containing scaffolds took up a blue coloration, whose intensity variation was consistent with gelatin content of the scaffolds (Touyama and Takeda et al., 1994; Touyama and Inoue et al., 1994). No coloration was observed for PLLA scaffolds.

4.4.4 Mechanical tests

The stress–strain curves recorded from crosslinked scaffolds have been used to evaluate the Young's modulus E, the stress at break σ_b, and the deformation at break ε_b of the scaffolds. The mean values are reported in Table 5. The elastic modulus E, and the stress at break σ_b, of the crosslinked scaffolds are also reported in Figure 14.

Table 5. Strain at break (ε_b), stress at break (σ_b), and Young's modulus (E) of crosslinked PPLA-gelatin composite scaffolds.

Sample	*ε_b (%)*	*σ_b (MPa)*	*E (MPa)*
GEL	5.5 ± 0.3	22 ± 4	820 ± 100
PLLA30GEL70	31 ± 12	14 ± 2	621 ± 76
PLLA50GEL50	20 ± 9	7.4 ± 0.9	334 ± 50
PLLA70GEL30	27 ± 12	6.0 ± 0.3	253 ± 13
PLLA	57 ± 12	3.4 ± 0.2	130 ± 10

Among the crosslinked scaffolds, pure gelatin scaffold was the most rigid and fragile one, with the highest value of elastic modulus E, the highest stress at break σ_b, and the lowest strain at break ε_b.
Conversely, pure PLLA scaffold displayed the lowest values of E and σ_b and the highest ε_b. Tensile properties of composites scaffolds were intermediate between those of the pure components and they were function of the ratio of PLLA to gelatin. These findings are consistent with previous works (Chen et al., 2012; Detta et al., 2010; Li et al., 2005) and show that combining fiber components with different mechanical properties through co-electrospinning influences the scaffold tensile properties, which vary as a function of composition.

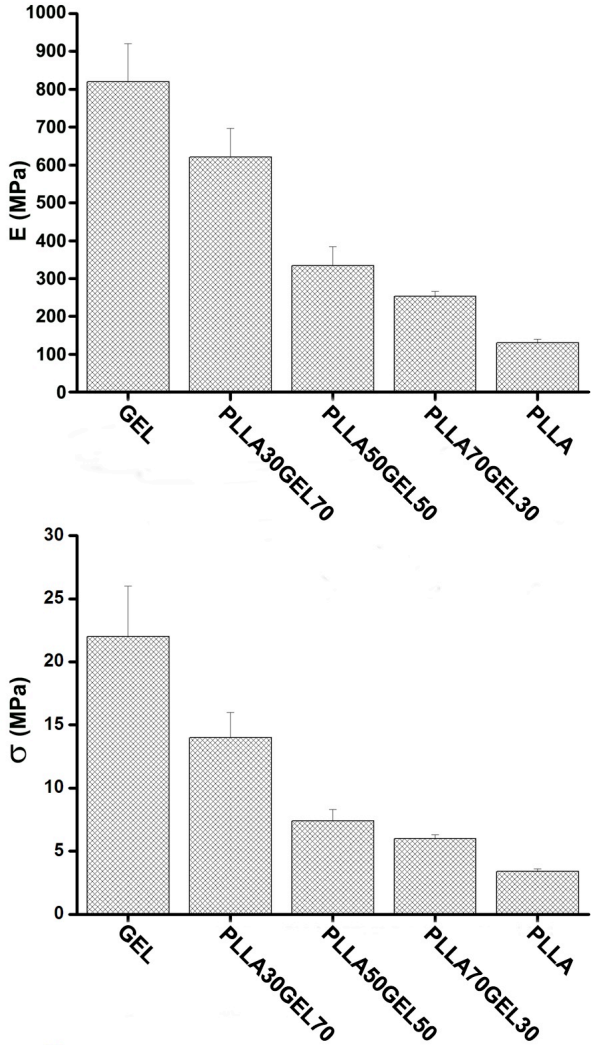

Figure 14. *Tensile moduli (E), stress at break (σ_b) and strain at break (ε_b) of composite electrospun scaffolds and pure PLLA and gelatin mats after crosslinking treatment.*

4.4.5 *In vitro* tests

Cell proliferation, viability and bioactivity

WST1 assay was used to measure cell proliferation and viability. Chondrocytes seeded on composite scaffolds were viable and proliferated from baseline conditions (mean of seeded cells $2.5x10^5$/ml: WST1 0.783±0.088) to 7 and 14 days, as shown in Figure 15A. At 7 days no differences were observed among all groups, while at 14 days chondrocytes cultured on PLLA50GEL50, and PLLA70GEL30 showed significant WST1 higher values than GEL, PLLA30GEL70, PLLA, and CTR. PLLA values were significantly greater than PLLA30GEL70 values at 14 days. LDH levels in cell culture supernatant were measured to evaluate cytotoxic effect on chondrocytes cultured on PLLA, GEL and their composites up to 24 hours. No differences of LDH values were found between experimental groups and CTR, demonstrating that no membrane damage affected cell cultures (Table 6).

Table 6. LDH measurement at 24h on GEL, PLLA30GEL70, PLLA50GEL50, PLLA70GEL30, PLLA culture. CTR– (medium) and CTR+ (phenol solution 0.5% in medium) were added for LDH evaluation. No differences were found among groups and CTR–, while CTR+ showed a highly significant difference.

Measure	*GEL*	*PLLA30GEL70*	*PLLA50GEL50*	*PLLA70GEL30*	*PLLA*	*CTR–*	*CTR+*
LDH	0.95±0.08	0.91±0.11	0.97±0.04	0.85±0.07	0.89±0.07	0.92±0.01	1.87±0.10
p	0.551	0.776	0.088	0.063	0.313		<0.0001

Common markers of chondrocytes differentiation and activity were evaluated after 7 and 14 days of culture on the different scaffolds, to assess cell bioactivity. The concentrations of Cathepsin B (CTSB), collagen type II (COLL II), and Aggrecan (AGC) produced by chondrocytes are reported in Figure 5B-D. At 7 days no differences were found among groups for all studied parameters. CTSB level (Figure 15B) significantly decreased from 7 to 14 days in all experimental groups; CTSB value decreased also in CTR group, but it did not reached a significant lower value. At 14 days COLL II production (Figure 15C) was significantly higher in PLLA50GEL50 and PLLA70GEL30 in comparison with CTR group. As shown in Figure 15D, AGC synthesis in GEL, PLLA, and in all PLLA/GEL composites at 14 days was greater than CTR, even if with different level of significativity. Besides, PLLA70GEL30 was higher when compared also to GEL, PLLA30GEL70, and PLLA.

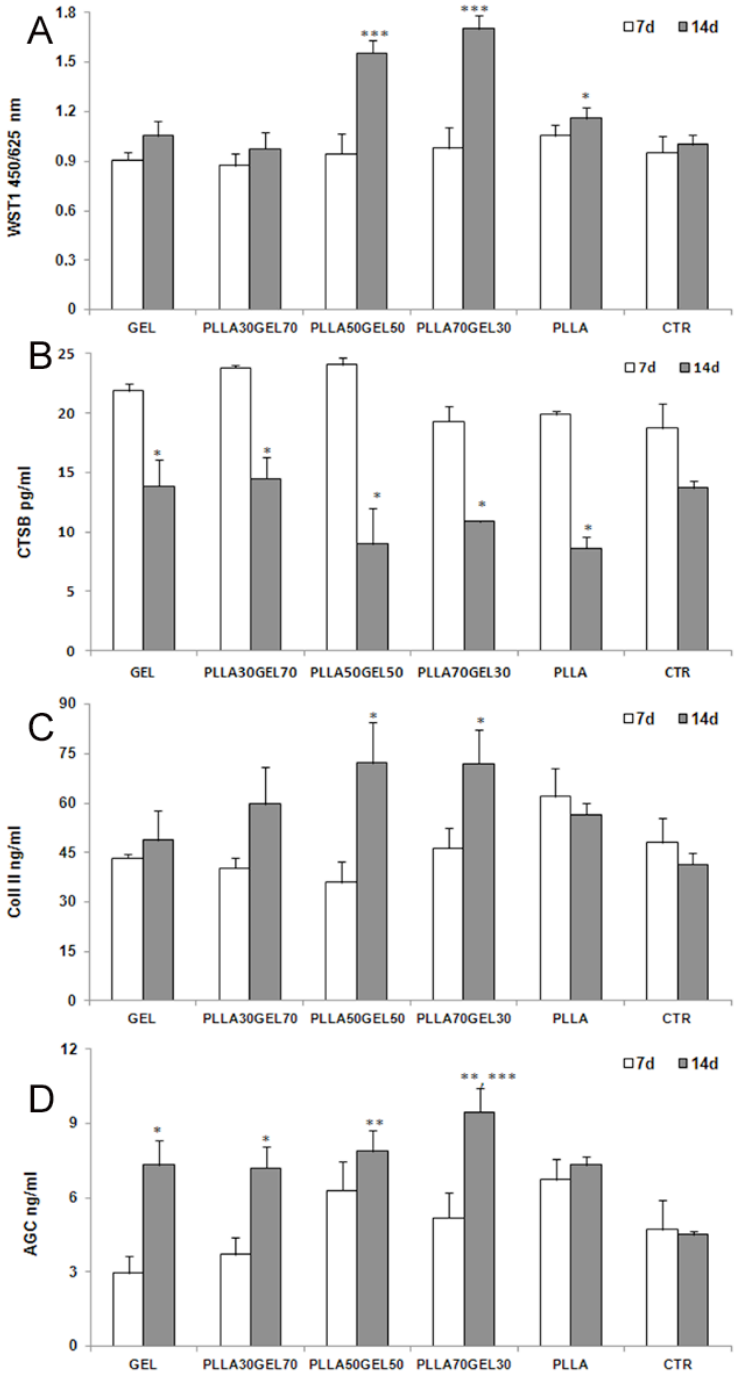

Figure 15. *Cell proliferation and bioactivity of chondrocytes cultured on GEL, PLLA30GEL70, PLLA50GEL50, PLLA70GEL30, PLLA and CTR for 7 (white bar) and 14 (grey bar) days. (* p<0.05; ** p<0.005; *** p<0.0005).*

A) WST1. 14 days: PLLA50GEL50, PLLA70GEL30, vs GEL, PLLA30GEL70, PLLA, CTR (p<0.0005); PLLA vs PLLA30GEL70 (p<0.05);

B) CTSB. GEL, PLLA30GEL70, PLLA50GEL50, PLLA70GEL30, PLLA: 7 vs 14 days (p<0.05);

C) COLL II. 14 days: PLLA50GEL50, PLLA70GEL30 vs CTR (p<0.05);

D) AGC. 14 days: GEL, PLLA30GEL70 vs PLLA70GEL30, CTR (p<0.05); PLLA50GEL50 vs CTR (p<0.005); PLLA70GEL30 vs PLLA (p<0.005), CTR (p<0.0005).

Cell morphology

SEM imaging was performed to evaluate morphology of human chondrocytes grown on the different scaffolds after 7 days of culture. The cells were observed to attach and spread on all the surfaces, independently from the scaffold composition. They generally appeared well flattened and rich of filopodia, as it can be observed in Figure 16A and 16B for PLLA50GEL50 and PLLA70GEL30 scaffold respectively. Moreover, chondrocytes were seen to penetrate into the scaffolds, within the polymer fibers, as shown in the representative Figure 16C for PLLA scaffold.

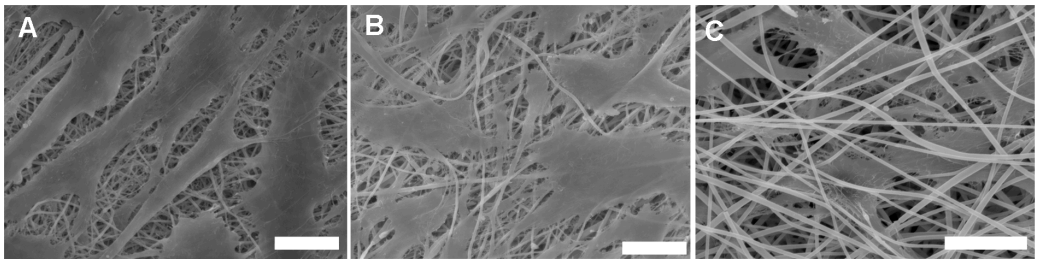

Figure 16. *SEM images of human chondrocytes grown on electrospun scaffolds: (A) PLLA50GEL50, (B) PLLA70GEL30, (C) PLLA. (Scale bars: 20 µm).*

4.4.6 Scaffolds Mineralization

Immersion of the scaffolds into the calcifying CaP solution (Bigi et al., 2005) provoked the deposition of a uniform mineralized layer onto all the scaffolds. No significant differences were observed among the different samples. Figures 17A and 17B show representative SEM images of PLLA30GEL70 and PLLA scaffold respectively. The deposits consisted of almost spherical aggregates with mean diameter of 1-2 µm. Moreover, single gelatin and PLLA fibers appeared covered with a mineralized layer (Figure 17A-17B). The EDX spectra recorded on the mineralized fibers surface of PLLA30GEL70 scaffold (Figure 17C) indicate a Ca/P molar ratio of 1.45, coherent with the presence of poorly crystalline apatite.

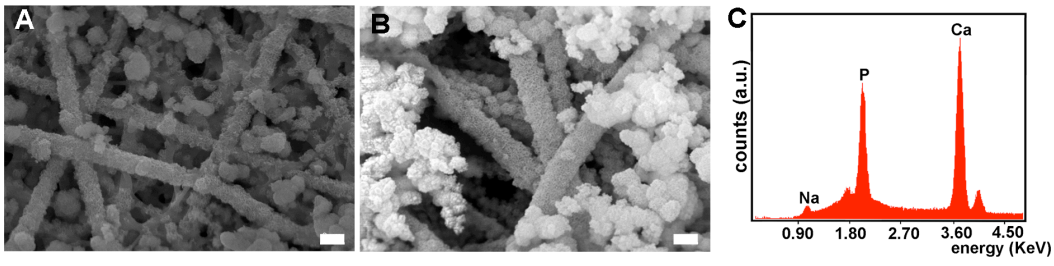

Figure 17. *SEM images of mineralized electrospun PLLA30GEL70 (a), PLLA (b) and EDX spectra of PLLA30GEL70 scaffold (c). (Scale bars: 2 µm).*

Discussion

4.5 Gelatin and Gelatin–Genipin electrospun fibers

The results of this study allowed, first of all, the optimization of the crosslinking conditions for electrospun gelatin nanofibers with genipin. Genipin was chosen because of its better biocompatibility and lower cytotoxicity compared with other crosslinking agents (Tsai et al., 2000) as well as for its crosslinking efficiency. Genipin-fixed tissues were reported to exhibit similar resistance to enzymatic degradation of glutaraldehyde-fixed tissue (Sung et al., 1998; Huang et al., 1998). Previous attempts to crosslink gelatin fibers using genipin in water/ethanol solution provoked remarkable modifications of the original fiber morphology, which was attributed to slow crosslinking kinetics compared with the rate of gelatin dissolution (Sisson et al., 2009). A novel method recently proposed incorporation of genipin within gelatin nanofibers during electrospinning and demonstrated crosslinking of the fibers thus obtained (Ko et al., 2010). However, upon water contact modification of the fiber morphology was observed.

In this PhD thesis, in order to prevent dissolution of the mats upon water contact, several tests with a number of different conditions were carried out, but most attempts performed on electrospun gelatin scaffolds (G) were unsuccessful. At variance, addition of a small amount of genipin to the electrospinning solution (GG) improved the results remarkably, without substantial modification of the initial fiber morphology (see paragraph 4.3.1, Figure 2a and 2b).

The G and GG mats did not display significant structural differences. In fact, the FTIR spectra of the GG and G mats were quite similar and showed the characteristic amide bands. The amide A band is associated with the N–H stretching mode and amide I arises from the carbonyl C=O double stretching mode, whereas amide II has been ascribed to the deformation of N–H bonds and C–H stretching and amide III corresponds to vibration in the plane of C–N and N–H groups of bound amide or vibration of CH_2 (Hashim et al., 2010; Bergo and Sobral, 2012).

The reduced intensity of the absorption bands in the amide I and II regions, and even more in the amide III region, of the FTIR spectra of gelatin with respect to collagen has been associated with the loss of triple helix content during gelatin extraction (Muyonga et al., 2004). The present results indicate that in comparison with those of gelatin films (see paragraph 4.3.2, Figure 3), the FTIR spectra of the electrospun samples displayed a broadening of the bands, most likely because of the porous surface of the scaffolds, with respect to the smooth surface of the films.

Moreover, gelatin films prepared from aqueous solution exhibited a relative higher intensity of the absorption band at 1234 cm^{-1} in the amide III region

than the other samples, in agreement with a relatively higher content of triple helix structure. The similarity between the relative intensity of these bands in the spectra of acetic acid/water gelatin film and electrospun mats indicated that the reduction in structural order was due to the treatment with acetic acid and not to the electrospinning process. Accordingly, X-ray diffraction data indicated that the reflection at about 1.1 nm, characteristic of the triple helix structure (Okuyama et al., 2008), could be appreciated in the pattern of gelatin films obtained from aqueous solution (see paragraph 4.3.3, Figure 4) but not in the patterns from films, as well as electrospun nanofibers, prepared from acetic acid/water solutions. It must be concluded that acetic acid, as previously reported for formic acid (Ki et al., 2005), prevented the partial renaturation of gelatin that occurs during gelling from aqueous solution and implies a partial rearrangement of its structure from random coil to triple helix (Ross-Murphy et al., 1992).
Crosslinking greatly affected the mechanical properties of the scaffolds. The strain at break of as-spun GG mats, in fact, assumed a mean value significantly smaller that that measured on as-spun G mats and a remarkable modification of the stress–strain curve was also evident. After crosslinking according to method C, the stress at break and the Young's modulus of the G and GG mats increased remarkably and the strain at break of the G scaffolds decreased significantly.
Genipin addition to the electrospinning solution does not prevent scaffold solubilization upon water exposure, but it improves the results of further crosslinking reaction. Treatment with genipin for 7 days at 37 °C (method A) provides much better water resistance of GG electrospun nanofibers, even if their morphology still appears affected by water contact. Genipin crosslinking also induces a significant increase in the mean diameter of the nanofibers, in agreement with the data in the literature (Ko et al., 2010) . An increase in the temperature of crosslinking (method B) was verified to induce only minor variations, whereas the results obtained on the samples crosslinked using the C method demonstrated that rinsing in PBS solution before air drying is a key factor in stabilization of the scaffolds, most probably because the ionic strength of PBS reduces gelatin swelling (Veis, 1964). Crosslinked GG mats retain their morphology after water exposure, and the morphology of crosslinked G mats also appears only slightly affected by water (see paragraph 4.3.4 Figures 5 and 6). The nanofibers of both kinds of mats maintain a straight morphology and are not fused together after 1 week immersion in DMEM. In fact, the morphology does not appear to be altered even when VW-MSCs were cultured on the mats for 7 days. Moreover, SEM analysis of cell morphology and adhesion confirms that G and GG in the form of electrospun fiber mats are both biocompatible and able to support VW-MSCs spreading and adhesion (see paragraph 4.3.7 Figure 9).

4.6 Gelatin-poly(L-lactic acid) co-electrospun fibers

The study of PLLA-gelatin co-electrospun scaffolds demonstrated that co-electrospinning is a promising and versatile technique to obtain composite scaffolds with hybrid properties (Baker et al., 2008), as well as continuously graded scaffolds for interfacial tissue engineering applications in the

orthopaedic field (Samavedi et al., 2011; Ladd et al., 2011). The term "co-electrospinning" refers to spinning of two polymers from two distinct spinnerets as well as the polymer blending approach where two different materials are electrospun from the same solution through a single spinneret. The first one, as demonstrates this work, offers several advantages, such as the possibility to incorporate in the same scaffold, selected amounts of polymer fibers with different chemical-physical and mechanical properties. In particular, the present study represents the first attempt of co-electrospinning PLLA and gelatin, thus obtaining a biosynthetic scaffold that combines the good mechanical properties and mechanical integrity of the synthetic PLLA polymer, with the very good biocompatibility and better cellular interaction of the natural gelatin polymer. Optimization of fabrication conditions of composite PLLA/GEL scaffolds allowed getting a uniform interspersion of the two polymer nanofibers, as confirmed by CLSM results.

A qualitative evidence of gradual change of scaffold composition was provided by FT-IR measurements (see paragraph 4.4.2 Figure 12) and by visually comparing the intensity of the blue-coloured scaffolds after genipin crosslinking (see paragraph 4.4.3 Figure 13). These results demonstrated the possibility to modulate, in a controlled and predictable way, the relative amount of the two polymeric components in the scaffold and therefore scaffold chemical composition.

Preventing the dissolution of gelatin fibers in aqueous solutions through crosslinking was a mandatory issue. The low toxicity agent genipin was used to maintain the original good nanofiber morphology after exposure to cells culture medium, as well as to water. PLLA fiber morphology was not affected by genipin crosslinking that, instead, induced an increase of the average diameter of gelatin nanofibers in agreement with earlier data (see paragraph 4.3.1 Table 1).

Stress-strain measurements were performed on crosslinked scaffolds to explore the relationship between scaffold composition and tensile properties. Pure gelatin scaffold after crosslinking was highly rigid and brittle, whereas the PLLA scaffold showed a lower tensile modulus and higher elongation at break with respect to gelatin. It was previously found that combination of two individual fiber components with dissimilar mechanical properties, through co- electrospinning, influences the composite scaffold mechanics, and samples display properties of both fiber components (Samavedi et al., 2011; Chen et al., 2012; Detta et al., 2010; Li et al., 2005).

In agreement with these findings the tensile properties of the composite scaffolds were found to be intermediate between those of the pure PLLA and gelatin components and, even more interesting, the values of Young modulus and stress at break were found to decrease on increasing PLLA content of the composite, as is shown in paragraph 4.4.4 Figure 14.

Cell culture studies were performed to assess biological response to the composite scaffolds. Chondrocytes seeded on composite scaffolds showed good viability and proliferation rate. CTSB is considered a marker of chondrocytes differentiation, because its level was found to decrease when cells are differentiated (Baici et al., 1988). COLL II and AGS are the major components of articular cartilage extracellular matrix, synthesized by chondrocytes. Therefore, in addition to support chondrocytes growth, the electrospun composite scaffolds promoted their differentiation, as stated by

CTSB reduced level in all experimental groups. Additionally, the composites PLLA50GEL50, PLLA70GEL30 seemed to be the two best compositions, able to enhance significantly not only cell proliferation, but also both COLL II and AGS production. In agreement, SEM images of chondrocytes grown on the two above mentioned scaffolds showed cells with a flattened and spreading morphology (see paragraph 4.4.5 Figure 16).
The evidence of cell infiltration into the scaffolds (see Figure 16C as an example) was of great interest in view of the possible application of the scaffolds for tissue engineering constructs. All results on chondrocytes growth and differentiation markers indicate that the scaffolds are suitable for cartilage tissue engineering application.
Furthermore, electrospun scaffolds obtained from PLLA/gelatin blends were previously proposed also for bone tissue repair (Andric et al., 2011; Cai et al., 2011), and the capability of the scaffolds to promote apatite deposition was tested through immersion in simulated body fluid (SBF), a solution with an ionic composition similar to that of blood plasma. In particular, in order to accelerate mineralization, 5xSBF and 10xSBF solutions were usually utilized onto electrospun scaffolds of PLLA/gelatin blends (Andric et al., 2011; Cai et al., 2011). Herein, a slightly supersaturated calcium phosphate solution (CaP) characterized by a very simple composition and buffered with Hepes was employed (Bigi et al., 2005). Although the degree of supersaturation of the CaP solution is very low in comparison with those of 5xSBF and 10xSBF, it was previously shown that CaP deposits a uniform coating of nanocrystalline apatite on metallic substrates in a few hours (Bigi et al., 2007). Preliminary mineralization study on the composite scaffolds demonstrated the deposition of a uniform mineralized layer onto all scaffolds. The deposits were composed of almost spherical aggregates of poorly crystalline apatite, as revealed by EDX measurements (see paragraph 4.4.6 Figure 17). Single PLLA and gelatin fibers were completely covered by a mineralized layer. These results confirms that the composite PLLA/GEL scaffolds are able to promote mineralization from slightly supersaturated solutions and that osteoconductivity can be easily enhanced though incorporation of a mineral phase, while maintaining the fibrous structure of the scaffold.

Conclusions

This PhD work was aimed to design, develop, and characterize gelatin-based scaffolds, for the repair of defects in the muscle-skeletal system.
Gelatin films prepared with the *solvent casting method* were utilized to study the effect of pH and of crosslinking on the structure and stability of the protein. The results indicated that pH values of the casting solution higher than the isoelectric point of the protein, as well as lower than the unmodified pH of gelatin solution, provoke a considerable reduction of the triple-helix content, as well as of the thermal stability and mechanical properties of the films. Moreover, further modulations of gelatin swelling, stability and mechanical parameters can be obtained through variation of crosslinking conditions with the naturally occurring agent genipin.
Reinforcement of gelatin films was achieved by adding montmorillonite (MMT) to the composition of the films. The results of the X-ray diffraction investigation suggest that the nanocomposite films at low MMT concentration display an intercalated structure, with gelatin chains interspersed between MMT layers. On increasing clay content, the intercalated structure changes to an exfoliated one, in agreement with the observed improvement of the mechanical properties, in spite of the simultaneous decrease of the renaturation level of gelatin. Treatment with genipin allowed verifying the synergic effect of the crosslinker and MMT on the mechanical performances of MMT/gelatin nanocomposites.
Using the *electrospinning* technique, in this PhD work it was developed a successful method to prepare electrospun gelatin nanofibrous scaffolds able to preserve their original morphology after exposure to water. The procedure involves electrospinning an acetic acid/water solution containing gelatin and a small amount of genipin, followed by further cross-linking of the as-electrospun mats with genipin, and it provides bead-free electrospun gelatin nanofibers. The crosslinked mats display interesting and tunable mechanical properties; moreover, the use of genipin allows to combine crosslinking efficiency with low toxicity, as shown by the good results of preliminary *in vitro* tests.
Co-electrospinning technique was successfully used to prepare poly(L-lactic acid) (PLLA)/gelatin nanofibrous scaffolds, in order to improve mechanical and degradation properties, as well as biological properties, of the composite scaffolds in comparison with individual components. As demonstrated in this work, this technique can be suitably utilized to modify, under controlled condition, the relative amounts of interspersed PLLA and gelatin fibers in biosynthetic scaffolds. The tensile mechanical properties of the composite scaffolds vary as a function of PLLA relative content and are intermediate between those of the pure PLLA and gelatin mats. Results on chondrocytes growth and differentiation markers indicated that the scaffolds are suitable for cartilage tissue engineering application, with PLLA50GEL50 and PLLA70GEL30 providing the best cellular response. Moreover, the results of mineralization experiments suggest that scaffolds potential applications could be extended even to bone interface tissue engineering.
3D porous scaffolds were prepared with the *freeze-drying method*. The procedure allowed obtaining scaffolds with high connectivity, good porosity and pore size distribution, which should promote bone growth. The

composite scaffolds were prepared using inorganic phases synthetized through two different approaches: continuous fast method and direct precipitation. The continuous fast method provided calcium phosphates with tunable crystallinity, whereas direct precipitation yielded crystalline hydroxyapatite. The different morphology and structure of the calcium phosphates influenced the properties of the 3D scaffolds. In particular, a significant decrease in mean pore size and pores interconnections was observed on increasing crystallinity of the inorganic phase. Furthermore, the presence of nanocrystalline and crystalline inorganic phase provoked an improvement of the mechanical properties of the composites. The results of *in vitro* tests showed a good cell response, without significative differences in cell proliferation of composite samples with the respect to control CTR- and pure gelatin scaffolds, suggesting that these 3D composite scaffolds could be successfully used for applications in bone tissue regeneration.

Bibliography

Achet D, He XW. Determination of the renaturation level in gelatin films. Polymer, 1995; 36: 787–791.

Aewsiri T, Benjakul S, Visessanguan W, Tanaka M. Chemical compositions and functional properties of gelatin from pre-cooked tuna fin.
Int J Food Sci Tech 2008; 43: 685-693.

Akao T, Kobashi K, Aburada M. Enzymatic studies on the animal and intestinal bacterial metabolism of geniposide.
Biol Pharm Bull 1994; 17: 1573–1576.

Alexandre M, Dubois P, Polymer-layered silicate nanocomposites: preparation, properties and uses of a new class of materials.
Mater Sci Eng 2000; 28: 1-63.

Andric T, Wright LD, Freeman JW. Rapid mineralization of electrospun scaffolds for bone tissue engineering.
J Biomat Sci-Polym E 2001; 22: 1535-1550.

ASTM Standard D4187-82, Zeta potential of colloids in water and wastewater.
ASTM 1985.

Badii F, Howell NK. Fish gelatin: structure, gelling properties and interaction with egg albumen proteins.
Food Hydrocolloid 2006; 20: 630-640.

Bae HJ, Park HJ, Hong SI, Byun YJ, Darby DO, Kimmel RM, Whiteside WS. Effect of clay content, homogenization RPM, pH, and ultrasonication on mechanical and barrier properties of fish gelatin/montmorillonite nanocomposite films.
Food Sci Technol-Leb 2009; 42: 1179–1186.

Baici A, Lang A, Horler R, Knopfel M. Cathepsin B as a marker of the dedifferentiated chondrocyte phenotype.
Ann Rheum Dis 1988; 47: 684-691.

Baker BM, Gee AO, Metter RB, Nathan AS, Marklein RA, Burdick JA, Mauck RL. The potential to improve cell infiltration in composite fiber-aligned electrospun scaffolds by the selective removal of sacrificial fibers. Biomaterials 2008; 29: 2348-2358.

Bear RS. Long X-Ray diffraction spacings of collagen.
J Am Chem Soc 1942; 64: 727.

Bergo P, Sobral PJA. Effects of plasticizer on physical properties of pigskin gelatin films.
Food Hydrocolloid 2012; 21: 1285-1289.

Berisio R, Vitagliano L, Mazzarella L, Zagari A. Crystal structure of the collagen triple helix model $[(Pro\text{-}Pro\text{-}Gly)_{10}]_3$.
Protein Sci 2002; 11: 262-270.

Bertoni E, Bigi A, Falini G, Panzavolta S, Roveri N. Hydroxyapatite/ polyacrylic acid nanocrystals.
J Mater Chem 1999; 9: 779–782.

Bigi A, Boanini E, Bracci B, Facchini A, Panzavolta S, Segatti F, Sturba L. Nanocrystalline hydroxyapatite coatings on titanium: a new fast biomimetic method.
Biomaterials 2005; 26: 4085-4089.

Bigi A, Borghi M, Cojazzi G, Fichera AM, Panzavolta S, Roveri N. Structural and mechanical properties of crosslinked drawn gelatin films.
J Therm Anal Calorim 2000; 61: 451-459.

Bigi A, Bracci B, Cojazzi G, Panzavolta S, Roveri N. Drawn gelatin films with improved mechanical properties.
Biomaterials 1998; 19: 2335-2340.

Bigi A, Cojazzi G, Panzavolta S, Roveri N, Rubini K. Mechanical and thermal properties of gelatin films at different degrees of glutaraldehyde crosslinking.
Biomaterials 2001; 22: 763-768.

Bigi A, Cojazzi G, Panzavolta S, Roveri N, Rubini K. Stabilization of gelatin films by crosslinking with genipin.
Biomaterials 2002; 23: 4827-4832.

Bigi A, Nicoli-Aldini N, Bracci B, Zavan B, Boanini E, Sbaiz F, Panzavolta S, Zorzato G, Giardino R, Facchini A, Abatangelo G, Cortivo R. In vitro culture of mesenchymal cells onto nanocrystalline hydroxyapatite-coated $Ti_{13}Nb_{13}Zr$ alloy.
J Biomed Mater Res Part A 2007; 82A: 213-221.

Bigi A, Panzavolta S, Rubini K. Relationship between triple helix content and mechanical properties of gelatin films.
Biomaterials 2004; 25: 5675-5680.

Boanini E, Gazzano M, Bigi A. Ionic substitutions in calcium phosphates synthesized at low temperature.
Acta Biomater 2010; 6: 1882–1894.

Boanini E, Rubini K, Panzavolta S, Bigi A. Chemico-physical characterization of gelatin films modified with oxidized alginate.
Acta Biomater 2010; 6: 383-388.

Bonderer LJ, Studart AR, Gauckler LJ. Bioinspired design and assembly of platelet reinforced polymer films.
Science 2008; 319: 1069-1073.

Bubnis WA, Ofner CM. The determination of ε-amino groups in soluble and poorly soluble proteinaceous materials by a spectrophotometric method using trinitrobenzenesulfonic acid.
Anal Biochem 1992; 207: 129-133.

Butler MF, NG YF, Pudney PDA. Mechanism and kinetics of the cross-linking reaction between biopolymers containing primary amine groups and genipin.
J Polym Sci Pol Chem 2003; 41: 3941-3953.

Cai Q, Xu Q, Feng Q, Cao X, Yang X, Deng X. Biomineralization of electrospun poly(l-lactic acid)/gelatin composite fibrous scaffold by using a supersaturated simulated body fluid with continuous CO_2 bubbling.
Appl Surf Sci 2011; 257: 10109-10118.

Cancedda R, Giannoni P, Mastrogiacomo M. A tissue engineering approach to bone repair in large animal models and in clinical practice.
Biomaterials 2007; 28: 4240–4250.

Chang WH, Chang Y, Lai PH, Sung HW. A genipin-crosslinked gelatin membrane as wound-dressing material: in vitro and in vivo studies.
J Biomat Sci-Polym E 2003; 14: 481-495.

Chen Z, Cao L, Wang L, Zhu H, Jiang H. Effect of fiber structure on the properties of the electrospun hybrid membranes composed of poly(ε-caprolactone) and gelatin.
J Appl Polym Sci 2012; 127: 4225-4232.

Chen H, Ouyang W, Lawuyi B, Prakash S. Genipin cross-linked alginate-chitosan microcapsules: membrane characterization of optimization of cross-linking reaction.
Biomacromolecules 2006; 7: 2091-2098.

Chivrac F, Pollet E, Schmutz M, Avérous L. New approach to elaborate exfoliated starch-based nano-biocomposites.
Biomacromolecules 2008; 9: 896-900.

Cohen NP, Foster RJ, Mow VC, Composition and dynamics of articular cartilage: structure, function, and maintaining healthy state.
J Orthop Sport Phys 1998; 28: 203-215.

Dai CA, Liu MW. *The effect of crystallinity and aging enthalpy on the mechanical properties of gelatin films.*
Mat Sci Eng A-Struct 2006; 423: 121-127.

Darder M, Colilla M, Ruiz-Hitzky E. Biopolymer-Clay Nanocomposites Based on Chitosan Intercalated in Montmorillonite.
Chem Mater 2003; 15: 3774-3780.

Detta N, Errico C, Dinucci D, Puppi D, Clarke D, Reilly G, Chiellini F. Novel electrospun polyurethane/gelatin composite meshes for vascular grafts.
J Mater Sci-Mater Med 2010; 21: 1761-1769.

Djagny KB, Wang Z, Xu S. Gelatin: A valuable protein for food and pharmaceutical industries.
Crit Rev Food Sci 2001; 14: 481-492.

Djerassi C, Gray JD, Kincl FA. Naturally occurring Oxygen Heterocyclics. IX. Isolation and characterization of genipin.
J Org Chem 1960; 25: 2174-2177.

Djerassi C, Nakano T, James AN, Zalkow LH, Einsenbraun EJ, Shoolery JN. Terpenoids XLVII. The Structure of Genipin.
J Org Chem 1961; 26: 1192-1206.

Dorozhkin SV. Nanodimensional and Nanocrystalline Calcium Orthophosphates.
Am J of Biomed Eng 2012; 2: 48-97.

Ellis DO, McGavin S. The structure of collagen—An X-ray study.
J Ultra Mol Struct R 1970; 32: 191-211.

Eysturskard J, Haug IJ, Ulset AS, Draget KI. Mechanical properties of mammalian and fish gelatins based on their weight average molecular weight and molecular weight distribution.
Food Hydrocolloid 2009; 23: 2315–2321.

Fratzl P, Weinkamer R, Nature's hierarchical materials.
Prog Mater Sci 2007; 52: 1263–1334.

Fujikawa S, Yokota T, Koga K, Kumada J. The continuous hydrolysis of geniposide to genipin using immobilized β-glucosidase on calcium alginate gel.
Biotechnol Lett 1987; 9: 697–702.

Garlotta D. A literature review of poly(lactic acid).
J Polym Environ 2001; 9: 63-84.

Gilsenan PM, Ross-Murphy SB. Rheological characterization of gelatins from mammalian and marine sources.
Food Hydrocolloid 2006; 14: 191-195.

Gioffrè M, Torricelli P, Panzavolta S, Rubini K, Bigi A. Role of pH on stability and mechanical properties of gelatin films.
J Bioact Compat Polym 2011; 27: 67–77.

Gornall JL, Terentjev EM. Helix-coil transition of gelatin: helical morphology and stability.
Soft Matter 2008; 4: 544-549.

Gualandi C, Soccio M, Saino E, Focarete ML, Lotti N, Munari A, Moroni L, Visai L. Easily synthesized novel biodegradable copolyesters with adjustable properties for biomedical applications.
Soft Matter 2012; 8: 5466-5476.

Guarino V, Alvarez-Perez M, Cirillo V, Ambrosio L. HMSC interaction with PCL and PCL/gelatin platforms: a comparative study on films and electrospun membranes.
J Bioact Compat Polym 2011; 26: 144–160.

Guillot PV, Cui W, Fisk NM, Polak DJ. Stem cell differentiation and expansion for clinical applications of tissue engineering.
J Cell Mol Med 2007; 11: 935-944.

Guo L, Colby RH, Lusignan CP, Howe AM. Physical gelation of gelatin studied with rheo-optics.
Macromolecules 2003; 36: 10009-10020.

Hashim DM, Che Man YB, Norakasha R, Shuhaimi M, Salmah Y, Syahariza ZA. Potential use of Fourier transform infrared spectroscopy for differentiation of bovine and porcine gelatins.
Food Chem 2010; 118: 856–860.

Hataka T, Sato H, Watanabe Y, Matsumoto M. Effect of storage temperature on the physicochemical properties of soft gelatin capsule shells.
Chem Pharm Bull 1994; 42: 1496-1500.

Henton DE, Gruber P, Lunt J, Randall J. Polylactic Acid Technology.
Natural Fibers, Biopolymers, and Biocomposites. CRC Press 2005; 527-577.

http://www.gelatine.org

http://en.wikipedia.org/wiki/Ballistic_gelatin

Huang LL, Sung HW, Tsai CC, Huang DM. Biocompatibility study of a biological tissue fixed with a naturally occurring crosslinking reagent.
J Biomed Mater Res 1998; 42: 568–576.
Inkinen S, Hakkarainen M, Albertsson AC, Södergard A. From lactic acid to poly(lactic acid) (PLA): characterization and analysis of PLA and its precursors.
Biomacromolecules 2011; 12: 523–532.

Katti KS, Katti DR. Relationship of Swelling and Swelling Pressure on Silica-Water Interactions in Montmorillonite.
Langmuir 2006; 22: 532-537.

Ki CS, Baek DH, Gang KD, Lee KH, Um IC, Park YH. Characterization of gelatin nanofiber prepared from gelatin–formic acid solution.
Polymer 2005; 46: 5094–5102.

Kivirikko KI. Collagen biosynthesis: a mini-review cluster.
Matrix Biol 1998; 16: 355-356.

Ko J, Yin HY, An J, Chung D, Kim JH, Lee S.B., Pyun DG. Characterization of cross-linked gelatin nanofibers through electrospinning.
Macromol Res 2010; 18: 137–143.

Kozlov PV. The structure and properties of solid gelatin and the principles of their modification.
Polymer 1983; 24: 651-666.

Kretlow JD, Mikos AG. From material to tissue: biomaterial development, scaffold fabrication, and tissue engineering.
J Am Inst Chem Eng 2008; 54: 3048-3067.

Ladd MR, Lee SJ, Stitzel JD, Atala A, Yoo JJ. Co-electrospun dual scaffolding system with potential for muscle-tendon junction tissue engineering. Biomaterials 2011; 32: 1549-1559

Langer R, Vacanti J.P. Tissue Engineering
Science 1993; 260: 920-926.

Lee SW, Lim JM, Bhoo SH, Paik YS, Hahn TR. Colorimetric determination of amino acids using genipin from Gardenia jasminoides.
Anal Chim Acta 2003; 480: 267-274.

Li M, Guo Y, Wei Y, MacDiarmid AG, Lelkes PI. Electrospinning polyaniline-contained gelatin nanofibers for tissue engineering applications. Biomaterials 2005; 27: 2705-2715.

Li P, Zheng JP, Ma YL, De Yao K, Gelatin/Montmorillonite Hybrid Nanocomposite II. Swelling Behavior.
J Appl Polym Sci 2003; 88: 322–326.

Liu Q, de Wijn JR, van Blitterswijk CA. Nano-apatite/polymer composites: mechanical and physicochemical characteristics.
Biomaterials 1997; 18: 1263-1270.

Lunt J. Large-scale production, properties and commercial applications of polylactic acid polymers.
Polym Degrad Stabil 1998; 59: 145-152.

Ma PX. Biomimetic materials for tissue engineering.
Adv Drug Deliv Rev 2008; 60: 184-198.

Mackie AR, Gunning AP, Ridout MJ, Morris VJ. Gelation of gelatin observation in the bulk and at the air-water interface.
Biopolymers 1998; 46: 245–252.

Malafaya PB, Silva GA, Reis RL. Natural-origin polymers as carriers and scaffolds for biomolecules and cell delivery in tissue engineering applications.
Adv Drug Deliv Rev 2007; 59: 207-233.

Mann S., Biomineralization. Principles and concepts in bioinorganic materials chemistry. Oxford: Oxford University Press 2001.

Mano JF, Silva GA, Azevedo HS, Malafaya PB, Sousa RA, Silva SS, Boesel LF, Oliveira JM, Santos TC, Marques AP, Neves NM, Reis RL. Natural origin biodegradable systems in tissue engineering and regenerative medicine: present status and some moving trends.
J R Soc Interface 2007; 4: 999–1030.

Martucci JF, Vázquez A, Ruseckaite RA. Nanocomposites based on gelatin and montmorillonite: Morphological and thermal studies.
J Therm Anal Calorim 2007; 89: 117–122.

Meyers MA, Chen PY, Yu-Min Lin A, Seki Y. Biological materials: Structure and mechanical properties.
Prog Mater Sci 2008; 53: 1–206.

Mi FL. Synthesis and characterization of a novel chitosan-gelatin bioconjugate with fluorescence emission.
Biomacromolecules 2005; 6: 975-987.

Mi FL, Sung HW, Shyu SS, Su CC, Peng CK. Synthesis and characterization of biodegradable TPP/Genipin co-crosslinked chitosan gel beads.
Polymer 2003; 44: 6521-6530.

Middleton JC, Tipton AJ. Synthetic biodegradable polymers as orthopedic devices.
Biomaterials 2000; 21: 2335-2346.

Miller A. Biochemistry of collagen. New York, Plenum Press 1976.

Muyonga JH, Cole CGB, Duodu KG. Extraction and physic-chemical characterization of Nile perch (Lates niloticus) skin and bone gelatin.
Food Hydrocolloid 2004; 18: 581-592.

Nerem RM. Tissue engineering in the USA.
Med Biol Eng Comput 1992; 30: CE8-CE12.

Nickerson MT, Farnworth R, Wagar E, Hodge SM, Rousseau D, Paulson AT. Some physical and microstructural properties of genipin-crosslinked gelatin-maltodextrin hydrogels.
Int J Biol Macromol 2006; 38: 40-44.

Okuyama K. Revisiting the molecular structure of collagen connective tissue. Connect Tissue Res 2008; 49: 299–310.

Owen SC, Shoichet MS. Design of three-dimensional biomimetic scaffolds.
J Biomed Mater Res A 2010; 94A: 1321–1331.

Paik YS, Lee CM, Cho MH, Hahn TR. Physical stability of the blue pigments formed from geniposide of Gardenia fruits: effects of pH, temperature and light.
J Agr Food Chem 2001; 49: 430-432.

Panzavolta S, Fini M, Nicoletti A, Bracci B, Rubini K, Giardino R, Bigi A. Porous composite scaffolds based on gelatin and partially hydrolyzed α-tricalcium phosphate.
Acta Biomater 2009; 5: 636–643.

Panzavolta S, Gioffrè M, Focarete ML, Gualandi C, Foroni L, Bigi A. Electrospun gelatin nanofibers: optimization of genipin crosslinking to preserve fiber morphology after exposure to water.
Acta Biomater 2011; 7: 1702–1709.

Panzavolta S, Torricelli P, Amadori S, Parrilli A, Rubini K, della Bella E, Fini M, Bigi A. 3D interconnected porous biomimetic scaffolds: in vitro cell response.
J Biomed Mat Res: Part A – *in press.*

Park JE, Lee JY, Kim HG, Hahn TR, Paik YS. Isolation and characterization of water-soluble intermediates of blue pigments transformed from geniposide of Gardenia jasminoides.
J Agr Food Chem 2002; 50: 6511-6514.

Pasquinelli G, Pacilli A, Alviano F, Foroni L, Ricci F, Valente S, Orrico C, Lanzoni G, Buzzi M, Tazzari PL, Pagliaro P, Stella A, Bagnara AS. Multidistrict human mesenchymal vascular cells: pluripotency and stemness characteristics.
Cytotherapy 2010; 12: 275-287.

Pezron I, Djabourov M, Bosio L, Leblond J. X-ray-diffraction of gelatin fibers in the dry and swollen states.
J Polym Sci Pol Phys 1990; 28: 1823-1839.

Place ES, Evans ND, Stevens MM. Complexity in biomaterials for tissue engineering.
Nature Mater 2009; 8: 457-470.

Rao YQ. Gelatine Clay. Nanocomposites of Improved Properties.
Polymer 2007; 48: 5369-5375.

Ray SS, Bousmina M. Biodegradable polymers and their layered silicate nanocomposites: In greening the 21st century materials world.
Prog Mater Sci 2005; 50: 962–1079.

Ross-Murphy SB. Structure and rheology of gelatin gels: recent progress.
Polymer 1992; 33: 2622–2627.

Ruiz-Hitzky E, Darder M, Aranda P. Functional biopolymer nanocomposites based on layered solids.
J Mater Chem 2005; 15: 3650–3662.

Samavedi S, Olsen H.C, Guelcher SA, Goldstein AS, Whittington AR. Fabrication of a model continuously graded co-electrospun mesh for regeneration of the ligament-bone interface.
Acta Biomater 2011; 7: 4131-4138.

Shanmugam G, Polavarapu PL. Structural transition during thermal denaturation of collagen in the solution and film states.
Chirality 2009; 21: 152-159.

Shchipunov Y, Ivanova N, Silant'ev V. Bionanocomposites formed by in situ charged chitosan with clay.
Green Chem 2009; 11: 1758–1761.

Smitha S, Mukundan P, Pillai PK, Warrier KGK. Silica–gelatin bio-hybrid and transparent nano-coatings through sol-gel technique.
Mater Chem Phys 2007; 103: 318–322.

Sionkowska A. Current research on the blends of natural and synthetic polymers as new biomaterials: Review.
Prog Polym Sci 2011; 36: 1254–1276.

Sionkowska A, Kaminska A., Thermal helix-coil transition in UV irradiated collagen from rat tail tendon.
Int J Biol Macromol 1999; 24: 337-340.

Sisson K, Zhang C, Farach-Carson MC, Chase DB, Rabolt JF. Evaluation of crosslinking methods for electrospun gelatin on cell growth and viability.
Biomacromolecules 2009; 10: 1675–1680.

Stainsby G. Recent advances in gelatin and glue research. London, New York, Paris, Los Angeles: Pergamon Press 1958.

Sun F, Zhou H, Lee J. Various preparation methods of highly porous hydroxyapatite/polymer nanoscale biocomposites for bone regeneration.
Acta Biomater 2011; 7: 3813–3828.

Sundelacruz S, Kaplan DL. Stem cell- and scaffold-based tissue engineering approaches to osteochondral regenerative medicine.
Semin Cell Dev Biol 2009; 20: 646–655.

Sung HW, Huang DM, Chang WH, Huang LL, Tsai CC, Liang IL. Gelatin-derived bioadhesives for closing skin wounds: an in vivo study.
J Biomater Sci-Polym E 1999; 10: 751–771.

Sung HW, Huang RN, Huang LLH, Tsai CC. In vitro evaluation of cytotoxicity of a naturally occurring cross-linking reagent for biological tissue fixation.
J Biomater Sci-Polym E 1999; 10: 63–78.

Sung HW, Huang RN, Huang L.H, Tsai CC, Chiu CT. Feasibility study of a natural cross-linking reagent for biological tissue fixation.
J Biomed Mater Res 1998; 42: 560–567.

Tabata Y, Ikada Y. Protein release from gelatin matrices.
Adv Drug Deliver Rev 1998; 31: 287-301.

Tadic D, Peters F, Epple M. Continuous synthesis of amorphous carbonated apatites.
Biomaterials 2002; 23: 2553–2559.

Talibudeen O. Interlamellar adsorption of protein monolayers on pure montmorillonoid clays.
Nature 1950; 166: 236–236.

Talibudeen O., Complex formation between montmorillonoid clays and amino-acids and proteins.
Trans Faraday Soc 1955; 51: 582–590.

Temenoff JS, Mikos AG. Review: tissue engineering for regeneration of articular cartilage.
Biomaterials 2000; 21: 431-440.
Tiktopulo EI, Kajava AV. Denaturation of type I collagen fibrils is an endothermic process accompanied by a noticeable change in the partial heat capacity.
Biochemistry 1998; 37: 8147-8152.

Torricelli P, Gioffrè M, Fiorani A, Panzavolta S, Gualandi C, Focarete ML, Bigi A. Co-electrospun gelatin-poly(L-lactic acid) scaffolds: modulation of mechanical properties and chondrocytes response as a function of composition.
Acta Biomater - *in press*

Touyama R, Inoue K, Takeda Y, Yatsuzuca M, Ikumoto T, Moritome N, Shingu T, Yokoi T, Inouye H. Studies on the blue pigments produced from genipin and methylamine. II. On the formation mechanism of brownish-red intermediates leading to the blue pigment formation.
Chem Pharm Bull 1994; 42: 1571-1578.

Touyama R, Takeda Y, Inoue K, Kawamura I, Yatsuzuca M, Ikumoto T, Shingu T, Yokoi T, Inouye H. Studies on the blue pigments produced from genipin and methylamine. I. Structures of the brownish-red intermediates leading to the blue pigments.
Chem Pharm Bull 1994; 42: 668-673.

Tran NH, Dennis GR, Milev AS, Kannangara GSK, Wilson MA, Lamb RN. Interactions of sodium montmorillonite with poly(acrylic acid).
J Colloid Interf Sci 2005; 290: 392–396.

Tsai CC, Huang RN, Sung HW, Liang HC. In vitro evaluation of the genotoxicity of a naturally occurring crosslinking agent (genipin) for biologic tissue fixation.
J Biomed Mater Res 2000; 52: 58–65.

U.N.C.O.T.A.D. - United Nations Conference On Trade And Development, Market brief in the European Union for selected natural ingredients derived from native species. Genipa americana (Jagua ,huito).
BioTrade Facilitation Program –BTFP 2005.

Usuki A, Kojima Y, Kawasumi M, Okada A, Fukushima Y, Kurauchi T, Kamigaito O. Synthesis of nylon 6-clay hybrid.
J Mater Res 1993; 8: 1179-1184.

Vallet-Regí M. Current trends on porous inorganic materials for biomedical applications. Editorial.
Chem Eng J 2008; 137: 1–3.

Vallet-Regí M, González-Calbet JM. Calcium phosphates as substitution of bone tissues.
Prog Solid State Ch 2004; 32: 1–31.

van den Bosch E, Gielens C. Gelatin degradation at elevated temperature.
Int J Biol Macromol 2003; 32: 129-138.

Veis A. The macromolecular chemistry of gelatin. New York, London: Accademic Press 1964.

Viidik A, Vuust J. Biology of Collagen. Academic Press 1980.

Visser CE, Voute ABE, Oosting J, Boon ME, Kok LP. Microwave irradiation and cross-linking of collagen.
Biomaterials 1992; 13: 34-37.

Wang M.C., Pins G.D., Silver F.H., Collagen fibres with improved strength for the repair of soft tissue injuries.
Biomaterials 1994; 15: 507-512.

Ward AG. The physical properties of gelatin solutions and gels.
Br J Appl Phys 1954; 5: 85–90.

Weadock KS, Miller EJ, Bellincampi LD, Zawadsky JP, Dunn MG. Physical cross-linking of collagen fibers - comparison of ultraviolet-irradiation and dehydrothermal treatment.
J Biomed Mater Res 1995; 29: 1373-1379.

Weiner S, Wagner HD. The material bone: structure-mechanical function relations.
Annu Rev Mater Sci 1998; 28: 271–298.

Welzel T, Meyer-Zaika W, Epple M. Continuous preparation of functionalised calcium phosphate nanoparticles with adjustable crystallinity.
Chem Commun 2004; 1204–1205.

Willie BM, Petersen A, Schmidt-Bleek K, Cipitria A, Mehta M, Strube P, Lienau J, Wildemann B, Fratzlbc P, Duda G. Designing biomimetic scaffolds for bone regeneration: why aim for a copy of mature tissue properties if nature uses a different approach?
Soft Matter 2010; 6: 4976–4987.

Xu Y, Ren X, Hanna MA. Chitosan/clay nanocomposite film preparation and characterization.
J Appl Polym Sci 2006; 99: 1684–1691.

Xu SW, Zheng JP, Tong L, De Yao K. Interaction of functional groups of gelatin and montmorillonite in nanocomposite.
J Appl Polym Sci 2006; 101: 1556–1561.

Yang H, Wang Y, Zhou P, Regenstein JM. Effects of alkaline and acid pretreatment on the physical properties and nanostructures of the gelatin from channel catfish skins.
Food Hydrocolloid 2008; 22: 1541-1550.

Yao HB, Fang HY, Tan ZH, Wu LH, Yu SH. Biologically inspired, strong, transparent and functional layered organic–inorganic hybrid films.
Angew Chem Int Edit 2010; 122: 2186 –2191.

Yao CH, Liu BS, Chang CJ, Hsu SH, Chen YS. Preparation of networks of gelatin and genipin as degradable biomaterials.
Mater Chem Phys 2004; 83: 204-208.

Young S, Wong M, Tabata Y, Mikos AG. Gelatin as delivery vehicle for the controlled release of bioactive molecules.
J Control Release 2005; 109: 256- 274.

Zheng JP, Li P, Ma YL, De Yao K. Gelatin/montmorillonite hybrid nanocomposite. I. Preparation and properties.
J Appl Polym Sci 2002; 86: 1189–1194.

Zheng JP, Wang CZ, Wang XX, Wang HY, Zhuang H, De Yao K. Preparation of biomimetic three-dimensional gelatin/montmorillonite–chitosan scaffold for tissue engineering.
React Funct Polym 2007; 67: 780–788.

Zheng JP, Xi LF, Zhang HL, Yao KD. Correlation between reaction environment and intercalation effect in the synthesis of gelatin/montmorillonite hybrid nanocomposite.
J Mater Sci Lett 2003; 22: 1179– 1181.

Zhuang H, Zheng JP, Gao H, De Yao K. In vitro biodegradation and biocompatibility of gelatin/montmorillonite-chitosan intercalated nanocomposite.
J Mater Sci-Mater Med 2007; 18: 951–957.